

NODC, ACCESSION 7600732 (MODE-1)

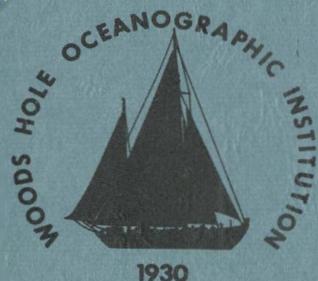
WHOI-74-46

and 7600778

(NOT MODE)

C:2:11

Woods Hole Oceanographic Institution



IMPORTANT

THIS MATERIAL IS A PART OF THE DATA/ DOCUMENTATION OF THE MODE-1 DATA SET. DO NOT REMOVE, DISPOSE OF, OR GIVE THIS MATERIAL AWAY WITHOUT THE PRIOR APPROVAL OF THE NODC DATA SERVICES DIVISION, OCEANOGRAPHIC SERVICES BRANCH, D761. THANK YOU.

THE DESIGN AND PERFORMANCE OF A FREE-FALL ELECTRO-MAGNETIC VELOCITY PROFILER (EMVP)

By
Thomas B. Sanford, Robert G. Drever,
and John H. Dunlap

July 1974

TECHNICAL REPORT

*Prepared for the Office of Naval Research
under Contract N00014-66-CO241; NR 083-004.*

*Approved for public release; distribution
unlimited.*

WHOI-74-46

GC
57.2
.W6
NO. 74-46

THE DESIGN AND PERFORMANCE OF A FREE-FALL
ELECTRO-MAGNETIC VELOCITY PROFILER (EMVP)

By

Thomas B. Sanford, Robert G. Drever,

and John H. Dunlap

WOODS HOLE OCEANOGRAPHIC INSTITUTION
Woods Hole, Massachusetts 02543

July 1974


TECHNICAL REPORT

*Prepared for the Office of Naval Research
under Contract N00014-66-CO241; NR 083-004.*

*Reproduction in whole or in part is permitted
for any purpose of the United States Government.
In citing this manuscript in a bibliography, the
reference should be followed by the phrase:
UNPUBLISHED MANUSCRIPT.*

*Approved for public release; distribution
unlimited.*

Approved for Distribution


L. Valentine Worthington, Chairman
Department of Physical Oceanography

Abstract

The principles of operation, the construction and the performance are described for a free-fall Electro-Magnetic Velocity Profiler (EMVP). The device measures and records weak electric currents produced by the motion of the sea through the geomagnetic field. The electric current measurements as a function of depth are interpreted in terms of the depth variable, horizontal velocity field. A complete velocity profile in 6000 m of water is achieved in about $1\frac{1}{2}$ hours with an accuracy of about 1 cm/s at a vertical resolution of 10 m. In addition to velocity, temperature, electrical conductivity and pressure are recorded once per second for a vertical resolution of about 1 m. The velocity and density data are processed at sea immediately after the drop. Real-time acoustic telemetry is used to monitor performance during a drop and to navigate the ship relative to the free instrument. The EMVP has been used extensively (171 drops) in several experiments including MODE-1.

Acknowledgements

Many people have made contributions to the instrumentation and analysis system described in this report. Foremost among these are Arthur Bartlett and Edward Denton. We are deeply indebted to them for their careful and conscientious efforts during the construction and operation of the instrumentation. We are also grateful for the advice from a number of colleagues, particularly A. J. Williams III, who made a number of suggestions during the design phase and participated in the first sea tests of the digital EMVP. We wish to acknowledge that Neil Brown suggested the concept for the oscillating amplifiers and that Richard Koehler designed the tape recorder interface, the precision time and acoustic pinger boards. Thomas B. Aldrich and Kenneth Doherty made many design suggestions while making drawings of the mechanical parts.

We wish to acknowledge the assistance of Kevin Leaman and Joyce Stratton with data processing.

Personnel of the Information Processing Center at the W.H.O.I. have been of considerable help to us. Mary Hunt and Roger Goldsmith have developed programs to read our data tapes and to plot the velocity profiles. Ken Peal organized the arrangement and installation of the shipboard computer system which Chris Polloni and Tom Crook maintained at sea.

The cooperation and skill of the officers and crew of the W.H.O.I. vessels have contributed much to the success of our sea operations as evidenced by more than 250 instrument recoveries.

Kevin Leaman, Nelson Hogg, and Gerard Martineau read a draft of this report and suggested many improvements and corrections.

We wish to thank John Swallow, Frank Malone, Ted Pochapsky, and Tom Rossby for providing data used in method intercomparisons.

The financial support and encouragement of the Office of Naval Research is gratefully acknowledged.

Section V.	Instrument Analysis and Instrument Performance	91
Section VI.	Launch and Recovery Procedures	109
References		113

Table of Contents

	<u>Page No.</u>
Abstract	i
Acknowledgements	ii
List of Figures	v
List of Tables	viii
Section I. Introduction	1
Section II. The Design and Construction of Present EMVP	23
Section III. Response of Instrument to Electric Currents and Relative Velocity	43
Section IV. Data Analysis	54
Section V. Error Analysis and Instrument Performance	71
Section VI. Launch and Recovery Procedures	109
References	113

List of Figures

		<u>Page No.</u>
Fig. I-1	First EMVP 1969-1971	6
Fig. I-2	Drop 10 Gulf-Stream Up and Down Profiles	7
Fig. I-3	Comparison of Simultaneous Velocity Profiles Obtained by Tracking a Falling Float (Dots: Rossby) and by the First EMVP (Solid: EM).	8
Fig. I-4	Second EMVP (1971) about to be Launched	10
Fig. I-5	Series of EMVP Profiles Taken at Site J (36°N, 70°W)	11
Fig. I-6	Comparison of Velocity Profiles Taken 1/2 Inertial Period Apart	11
Fig. I-7	Difference between Simultaneous Velocity Profiles Taken by Two Instruments Separated by 100 m	12
Fig. I-8	Velocity Profiles Taken 1/2 Inertial Period Apart at Four Locations along a Line Passing from Smooth to Rough Bottom Topography	13
Fig. I-9	Examples of Simultaneous Velocity Profiles Taken at Separate Locations	14
Fig. I-10	Electric Network Analog of Motional Induction in the Deep Sea	17
Fig. II-1	Bottom Contact (Left) and Mid-Depth Pressure (Right) Releases and Safety Links of Corrodible Magnesium	25
Fig. II-2	Radio and Xenon Flasher Units Mounted on Flexible Frame on Sensor End Cage	27
Fig. II-3	Two Sets of Electrode Blocks, Salt-bridge Arms and Electrical Cables	29

List of Figures (Contd.)

	<u>Page No.</u>
Fig. II-4 Detail of Electrode Block Construction	31
Fig. II-5 Arrangement and Orientation of Electrode Arms and Compass Coil	33
Fig. II-6 Arrangement of Circuit Boards and Components within Electronics Rack	35
Fig. II-7 Block Diagram of Electronics	37
Fig. II-8 Record of Acoustic Telemetry pulses. Upper Panel was Recorded at One Sweep per Second. Lower Panel was Recorded at Five Sweeps per Second	41
Fig. III-1 Prolate Spheroidal Coordinates	45
Fig. IV-1 Plot of Raw Data on E1, E2, and CC Channels and of First Difference of Pressure (DP) as the Instrument Nears the Sea Surface for Drop 226	55
Fig. IV-2 List of Velocity Profile Values for Drop 202 as Computed by Shipboard Computer System	66
Fig. IV-3 Plot of North Component of the Velocity Profile for Drop 202 as Produced by Shipboard Computer System	67
Fig. IV-4 Listing of Velocity and Density Profile for Drop 202 as Computed by PROFEQ (Salinity and Density Values in Error Due to Broken Liner in Conductivity Sensor)	69
Fig. IV-5 Plot of East and North Velocity Components for Drop 202 as Produced by PROFEQ	70

List of Figures (Contd.)

		<u>Page No.</u>
Fig. V-1	Electrode Offset Due to Step Change in Ambient Temperature	73
Fig. V-2	Noise on E1 and E2 Preamplifier Channels	77
Fig. V-3	Gain and Phase Response of Band-Pass Amplifiers	78
Fig. V-4	Relative Phase Difference between E1 and CC Band-Pass Filters (PHBIASE1 and PHSLOPE1 Refer to Intercept and Slope of β_1 - β_C versus Period in the Operating Range)	79
Fig. V-5	Comparison of EMVP and Acoustic Float Velocity Profiles	96
Fig. V-6	Comparison of EMVP Profiles (solid) and Velocity Values at Several Depths Determined from Tracking Swallow Floats (dots)	98
Fig. V-7	Profiles of Velocity Differences between E1 and E2 Profiles	99
Fig. V-8	Profiles of the Velocity Differences between Up and Down Profiles	102
Fig. V-9	Two Velocity Profiles Taken Simultaneously in Time at 100 Horizontal Separation	104
Fig. V-10	Profiles of the Velocity Difference Measured between 213D and 214D	105

List of TablesPage No.

Table IV-1 Definitions of γ_1 and γ_2 57

Table IV-2 Definitions of ψ_1 and ψ_2 60

Table V-1 Solar-Diurnal Variations 85

Table V-2 Magnetic Storm Variations 85

Table V-3 Error Summary 93

Table V-4 E1 Minus E2 Statistics 100

Table V-5 Up Minus Down Statistics 103

Table V-6 213D Minus 214D Statistics 106

SECTION I

Introduction

A new observational technique has been developed for measuring relative velocity profiles in the deep sea. The method is based on the measurement and interpretation of weak electric fields generated by the motion of the water through the geomagnetic field. Horizontally spaced electrodes mounted on a freely-falling probe are used to sense variations of the motionally induced electric fields as a function of depth. These data provide a profile of variations of horizontal velocity relative to an unknown constant velocity independent of depth. A relative velocity profile with vertical resolution of 10 m and standard error of about 1 cm/s is obtained in 1 1/2 hours in water depth of 6000 m. The method is self-contained and mobile since not dependent upon special radio or acoustical navigation systems.

The development of the instrumentation described in this report followed analytical studies into electromagnetic induction as applied to the open ocean (Sanford, 1971). The analysis showed how measurements of the electric current density (\vec{J}), electric field (\vec{E}) and magnetic induction (\vec{B}) in the sea could be utilized. In particular, it was shown that measurements of \vec{J}/σ reveal the depth dependent or baroclinic portion of a current. That is, the profiles which could be measured would be of relative velocity showing how currents changed with depth, but not of absolute velocity. Even

though the technique was insensitive to the vertically-averaged or barotropic velocity, the prospect of detecting shear in the baroclinic field justified the development of an instrument to measure the motional electric field as a function of depth.

The Electro-Magnetic Velocity Profiler or EMVP, in concept and use, is unlike a conventional current meter. Velocity data are customarily obtained directly from methods such as moored current meters, neutrally-buoyant floats or drogues. These methods emphasize measurements for long periods of the flow at one level. In contrast, a velocity profile determines the structure at, essentially, all levels at one time.

Any velocity profiling method, being a new observational approach, may only gradually become accepted or appreciated widely in the oceanographic community. One additional hurdle the EMVP faces results from the concept of its operation. Unlike a method depending on the direct action of the velocity field or a sensor such as on a current meter or transport float (Richardson and Schmitz, 1965), the EMVP depends on induced or indirect actions. Certainly, the almost instinctive understanding we have for direct-action sensors like rotors or displacement is not evident when it comes to motional induction and the EMVP. The characteristic of indirect response to the velocity field is the source of both the strength and weakness of the E-M method. It is susceptible to undesirable influences but it is also capable of providing information not otherwise available. The first nearly continuous profiles of current, are of speed variation in the water relative to the motion of the probe.

obtainable. However, the utility of any method depends critically on its use. Playing to its strength an EMVP can be used effectively as a mobile, real-time survey tool or when detailed vertical structure is required. It can complement other methods by providing additional data but it is not well suited for some tasks such as collecting a long time series of data. It is only fair to recognize that with any measurement technique there exist advantages and liabilities. That a measurement is direct does not assure it is free of significant errors. It is clearly nonsense to discount any method, even an indirect one, on any basis but a critical evaluation of its performance. This report seeks to provide such a critical evaluation of the latest EMVP.

Previous Velocity Profile Measurements

The distribution of current through the deep-sea water column has been measured in a number of ways. Bowden (1954) summarized the direct observations of subsurface velocities in the deep ocean. These meager data were obtained largely from current meters lowered from anchored ships. The other common sources of deep current observations were based on dynamic computations involving the spatial distribution of density and on the tracking of surface markers attached to deep drogues.

The bathypitotometer (Malkus, 1953) which recorded dynamic pressure on a lowered probe suggested the presence of vertical structure to the deep currents. These data, probably the first nearly continuous profiles of current, are of speed variation in the water relative to the motion of the probe.

Currents at a few depths have been monitored for long periods of time with drogues, Swallow floats (Swallow, 1955) and moored recording current meters (Richardson et al, 1963).

Brief measurements of current at a few depths have been obtained using transport floats (Richardson and Schmitz, 1965) and inclinometer-compass instrumented moored cables (McNary, 1968).

Considerably more detailed velocity profiles have been reported using current meters lowered at the end of or along a cable. Siedler and Krause (1964) used a bottom-mounted winch to raise and lower a current meter while Plaisted and Richardson (1970) lowered a current meter from a tracked free buoy. Constrained to move along a cable of fixed length and stable catenary, the current meter of Düing and Johnson (1972) measured vertical structure of ocean currents.

Both Pochapsky and Malone (1972) and Rossby (1969) have observed vertical shear of currents by tracking a free-fall acoustic probe as it was carried by the currents.

The above listing is not complete; many attempts have been made to measure currents as a function of depth. However, the references cited represent the major efforts presently known. Other approaches, such as that of Mangelsdorf (1962), using vertical electric fields, have not been used extensively.

Velocity profiles, particularly those from lowered current meters and acoustically tracked floats, have shown unexpectedly large velocity structure. Just as early continuous

profiles of temperature and salinity demonstrated the existence of large variability with depth, the velocity profiles were found to contain more structure than anticipated. Not only was the deep water energetic and variable in time but also quite changeable with depth. Gradually, a new perception of the structure and an understanding of the dynamics of deep sea currents are emerging due to these and more recent measurements.

Some Data

A look at some data seems to be a good way to motivate the later discussions of construction and performance details. Our first measurements were taken in the Gulf Stream by the instrument shown in Figure I-1. A detailed description of this instrument and its operation is given by Drever and Sanford (1970). The measured current amplitudes on down and up profiles are compared in Figure I-2. We were quite heartened that the strong near surface expression of the Gulf Stream could be resolved. The agreement between deep water features on down and up profiles was a great bonus. These data clearly showed that the method could measure features with an uncertainty of only a few cm/s.

The next important set of observations occurred in May 1971 near Bermuda. Direct verification that the method was indeed sensing velocity variations was obtained in an experiment in which T. Rossby measured velocity profiles using acoustic tracking. Figure I-3 shows comparisons of two nearly simultaneous profile measurements. The agreement is generally

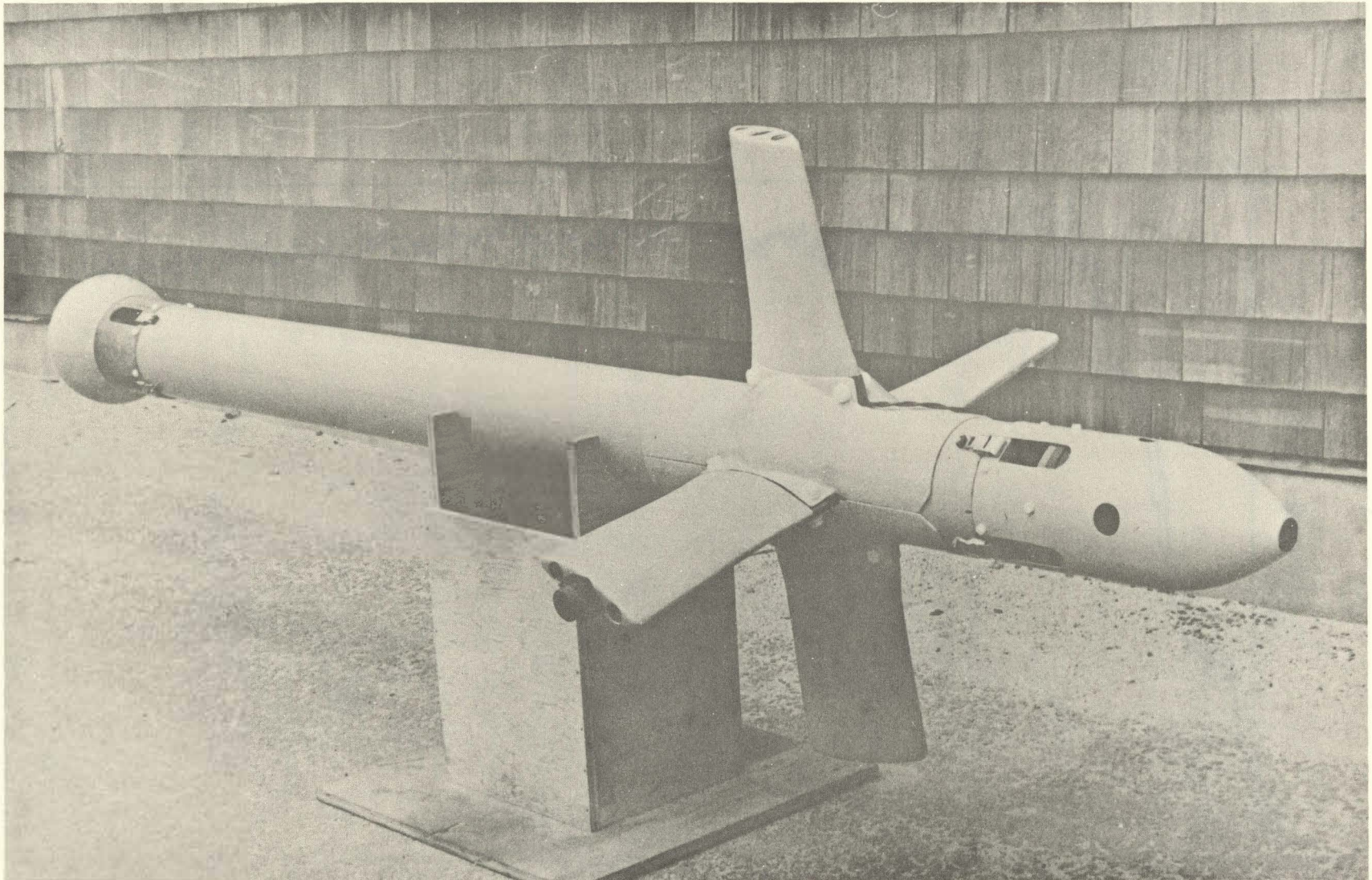


Figure I-1. First EMVP 1969-1971

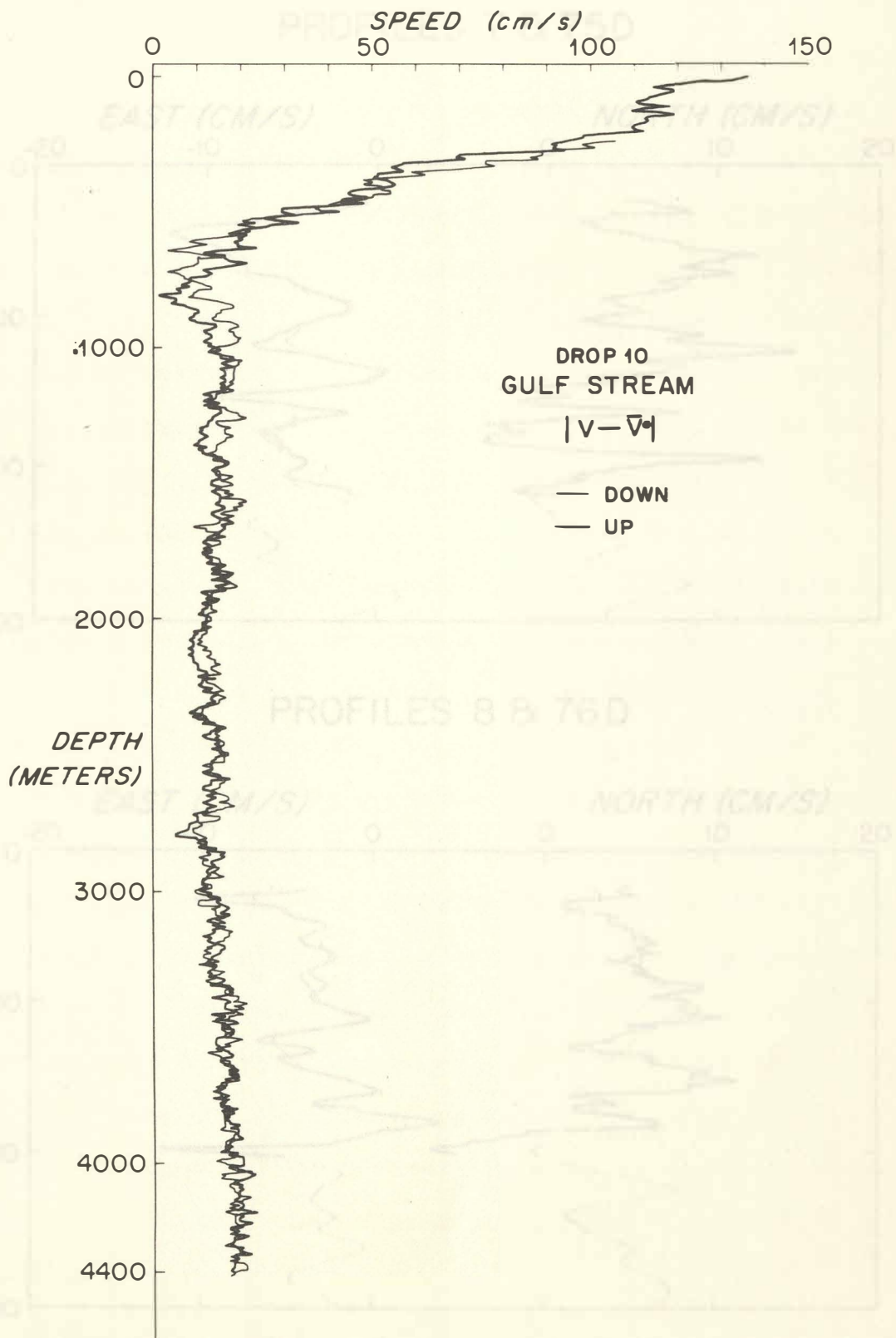
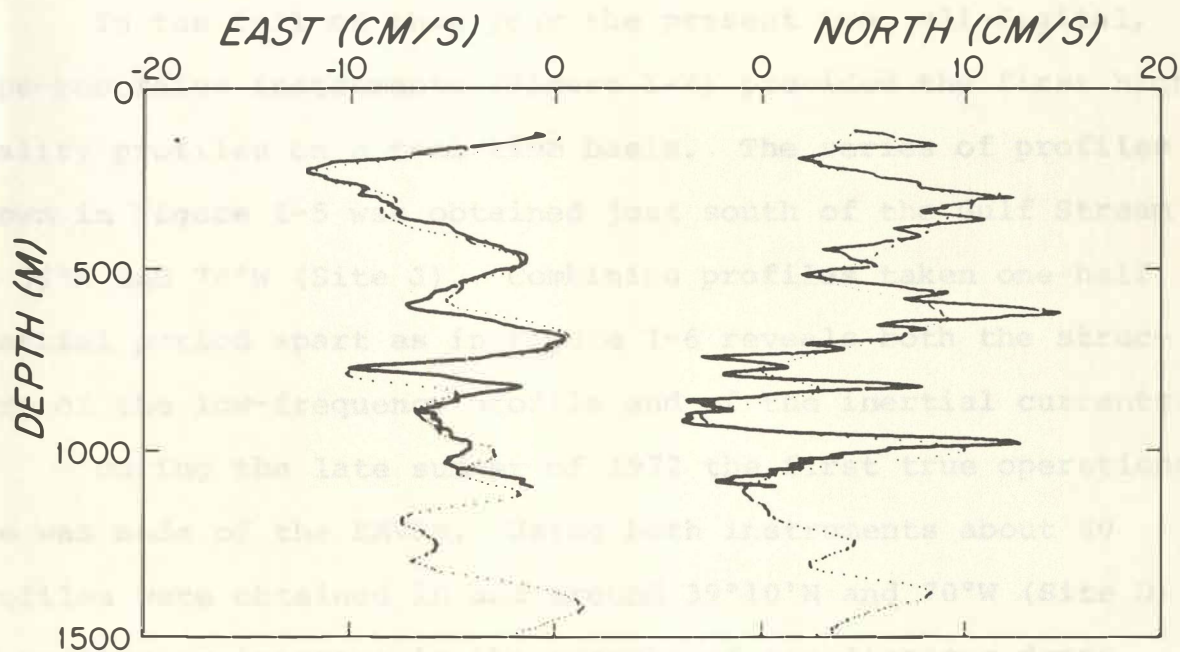


Figure I-2. Drop 10 Gulf-Stream Up and Down Profiles

PROFILES 7 & 75D



PROFILES 8 & 76D

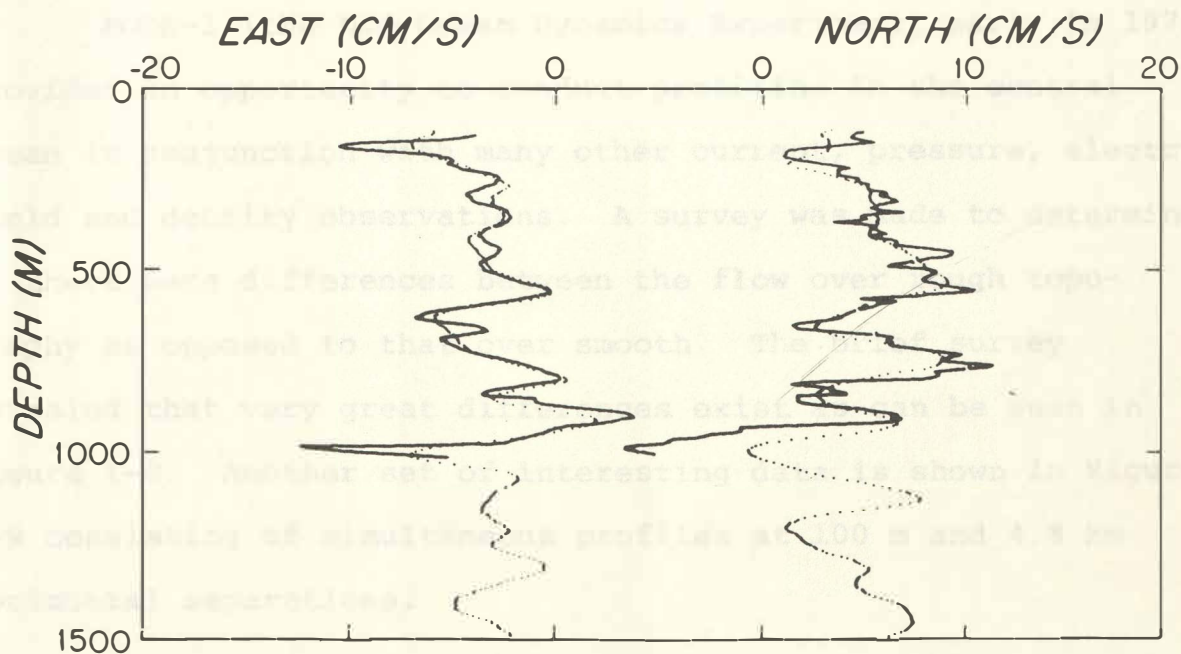


Figure I-3. Comparison of Simultaneous Velocity Profiles Obtained by Tracking a Falling Float (Dots: Rossby) and by the First EMVP (Solid: EM).

within the expected uncertainties of each method (1-2 cm/s). The north component of the E-M profile is more variable due to uncertainties in the compensation for the vertical fall speed.

In the fall of that year the present two, all-digital, tape-recording instruments (Figure I-4) provided the first high-quality profiles on a real-time basis. The series of profiles shown in Figure I-5 was obtained just south of the Gulf Stream at 36°N and 70°W (Site J). Combining profiles taken one-half inertial period apart as in Figure I-6 reveals both the structure of the low-frequency profile and of the inertial currents.

During the late summer of 1972 the first true operational use was made of the EMVPs. Using both instruments about 80 profiles were obtained in and around $39^{\circ}10'\text{N}$ and 70°W (Site D). Of particular interest is the example of simultaneous drops about 100 m apart shown in Figure I-7. The RMS difference is typically 1 cm/s.

MODE-1 (the Mid-Ocean Dynamics Experiment) early in 1973 provided an opportunity to conduct profiling in the central ocean in conjunction with many other current, pressure, electric field and density observations. A survey was made to determine if there were differences between the flow over rough topography as opposed to that over smooth. The brief survey revealed that very great differences exist as can be seen in Figure I-8. Another set of interesting data is shown in Figure I-9 consisting of simultaneous profiles at 100 m and 4.8 km horizontal separations.

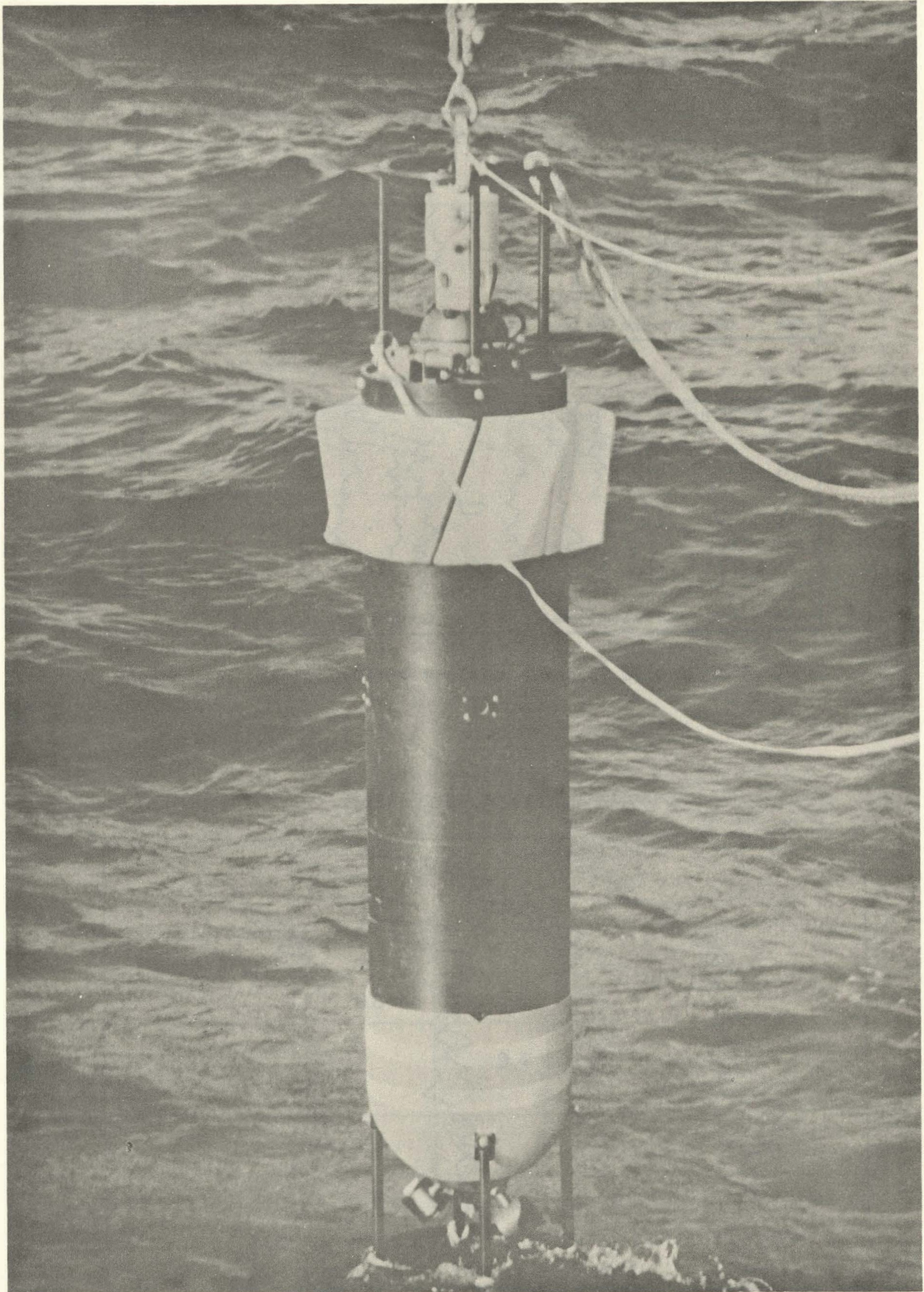


Figure I-4. Second EMVP (1971) about to be Launched

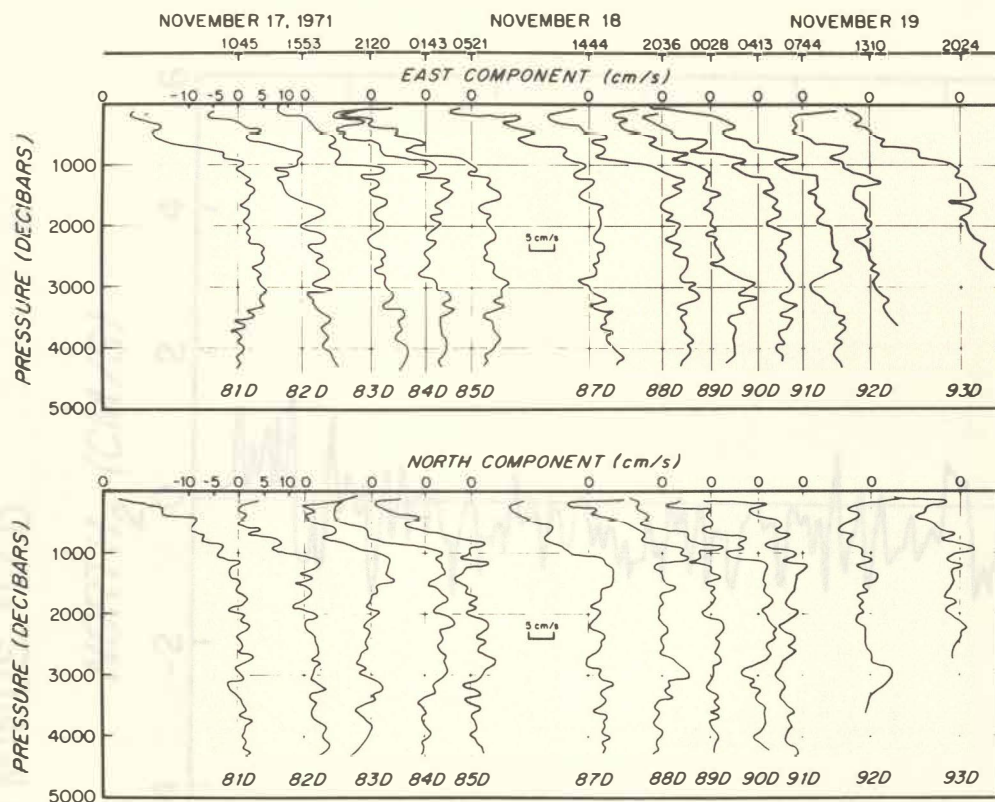


Figure I-5. Series of EMVP Profiles Taken at Site J (36°N , 70°W)

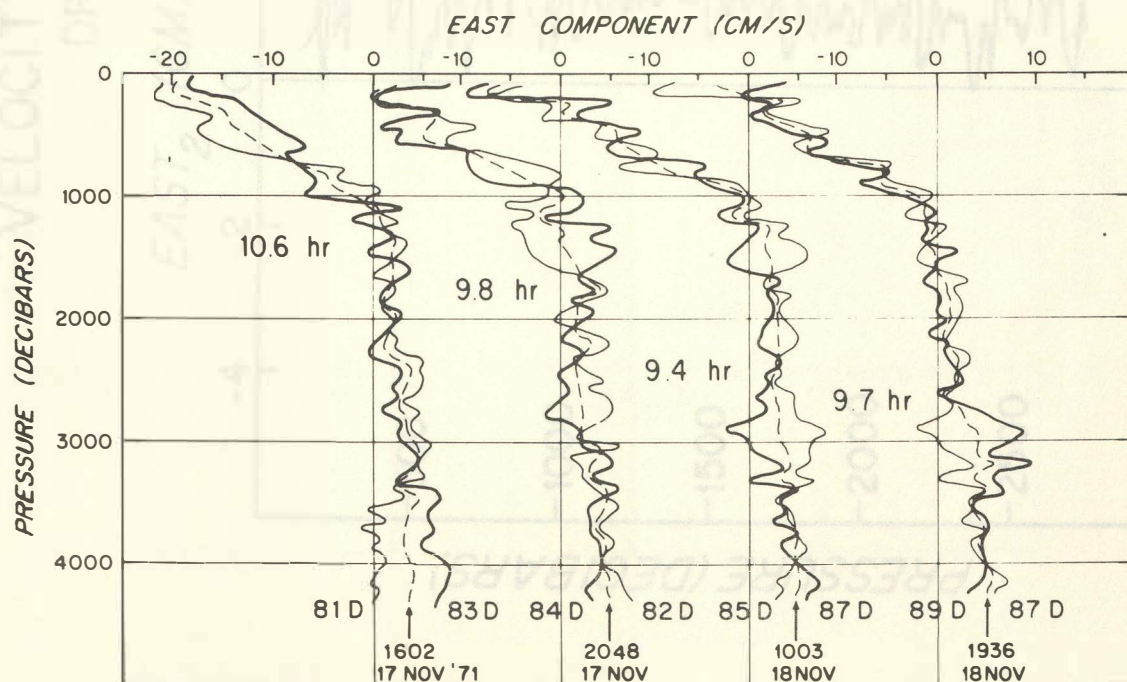


Figure I-6. Comparison of Velocity Profiles Taken $1/2$ Inertial Period Apart

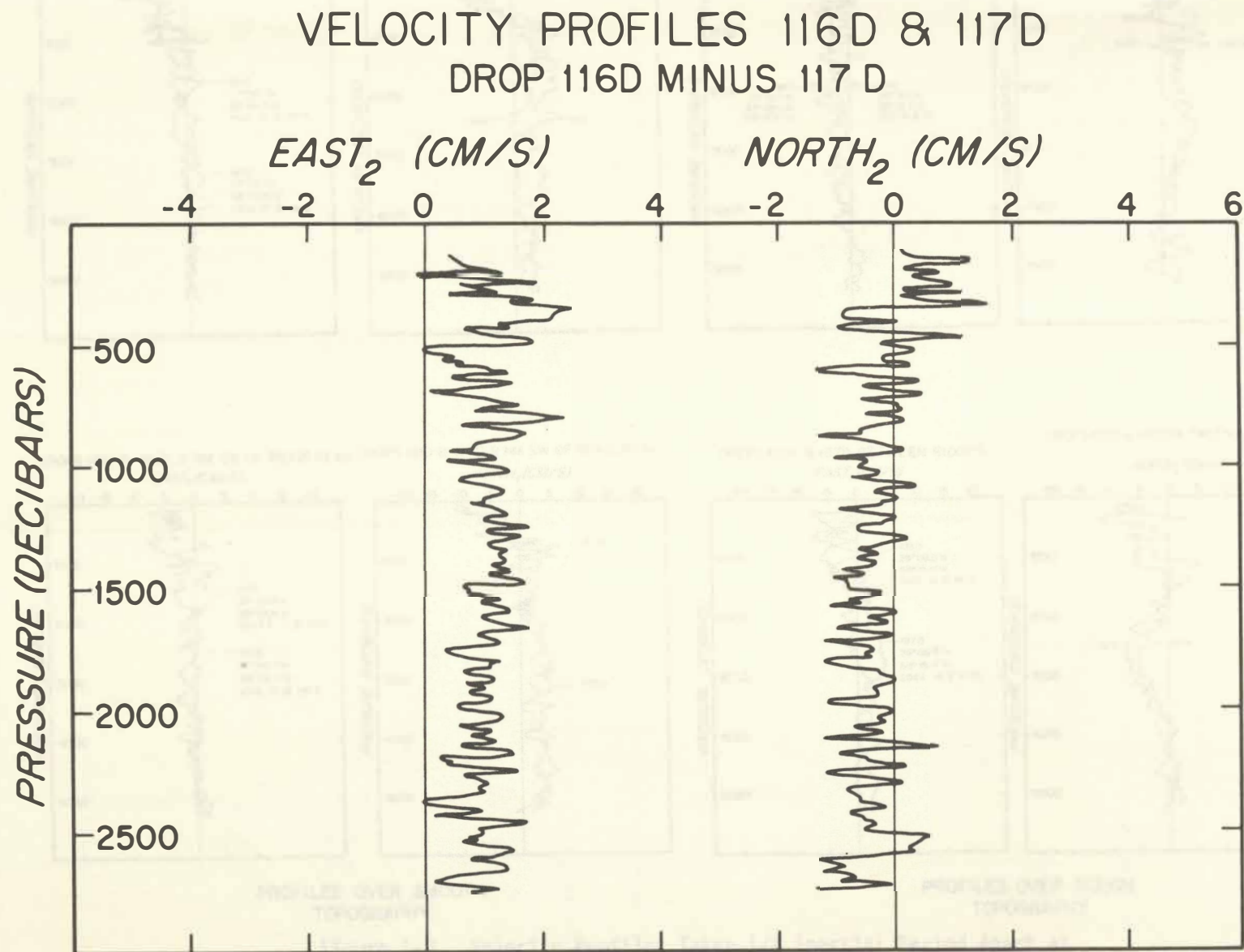
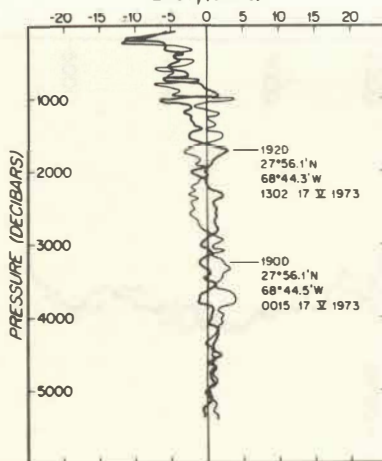
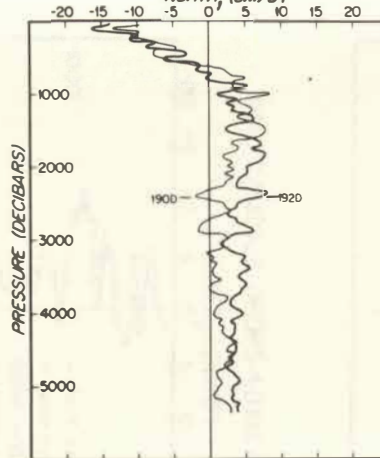


Figure I-7. Difference between Simultaneous Velocity Profiles
Taken by Two Instruments Separated by 100 m

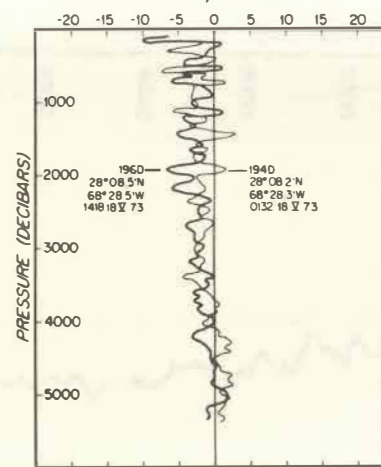
DROPS 190D & 192D, 13 NM SW OF RIDGE PEAK
EAST, (CM/S)



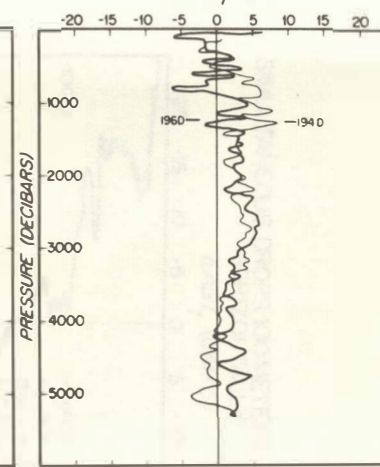
DROPS 190D & 192D, 13 NM SW OF RIDGE PEAK
NORTH, (CM/S)



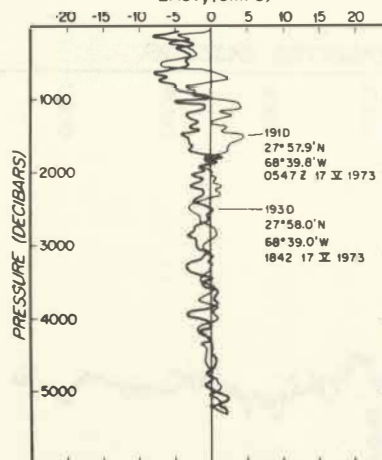
DROPS 194D & 196D, NORTH END OF RIDGE
EAST, (CM/S)



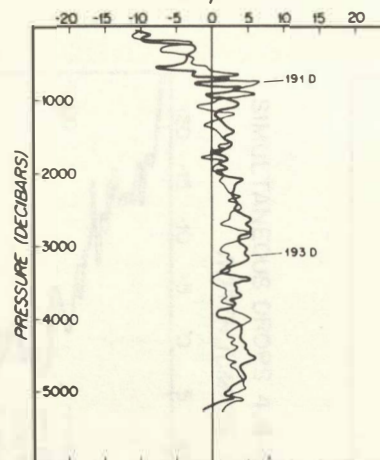
DROPS 194D & 196D, NORTH END OF RIDGE
NORTH, (CM/S)



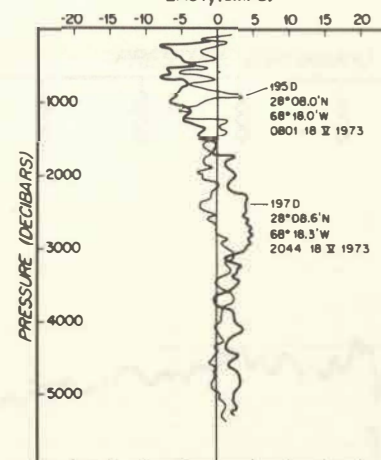
DROPS 191D & 193D, 9 NM SW OF RIDGE PEAK
EAST, (CM/S)



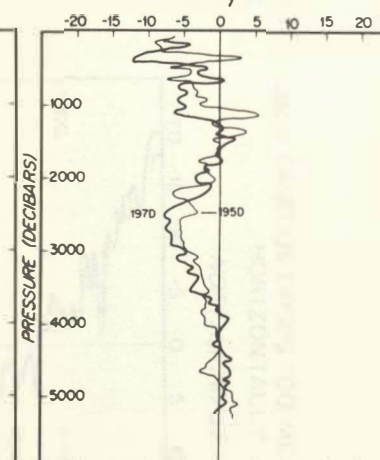
DROPS 191D & 193D, 9 NM SW OF RIDGE PEAK
NORTH, (CM/S)



DROPS 195D & 197D, BETWEEN RIDGES
EAST, (CM/S)



DROPS 195D & 197D, BETWEEN RIDGES
NORTH, (CM/S)



PROFILES OVER SMOOTH
TOPOGRAPHY

PROFILES OVER ROUGH
TOPOGRAPHY

Figure I-8. Velocity Profiles Taken 1/2 Inertial Period Apart at Four Locations along a Line Passing from Smooth to Rough Bottom Topography

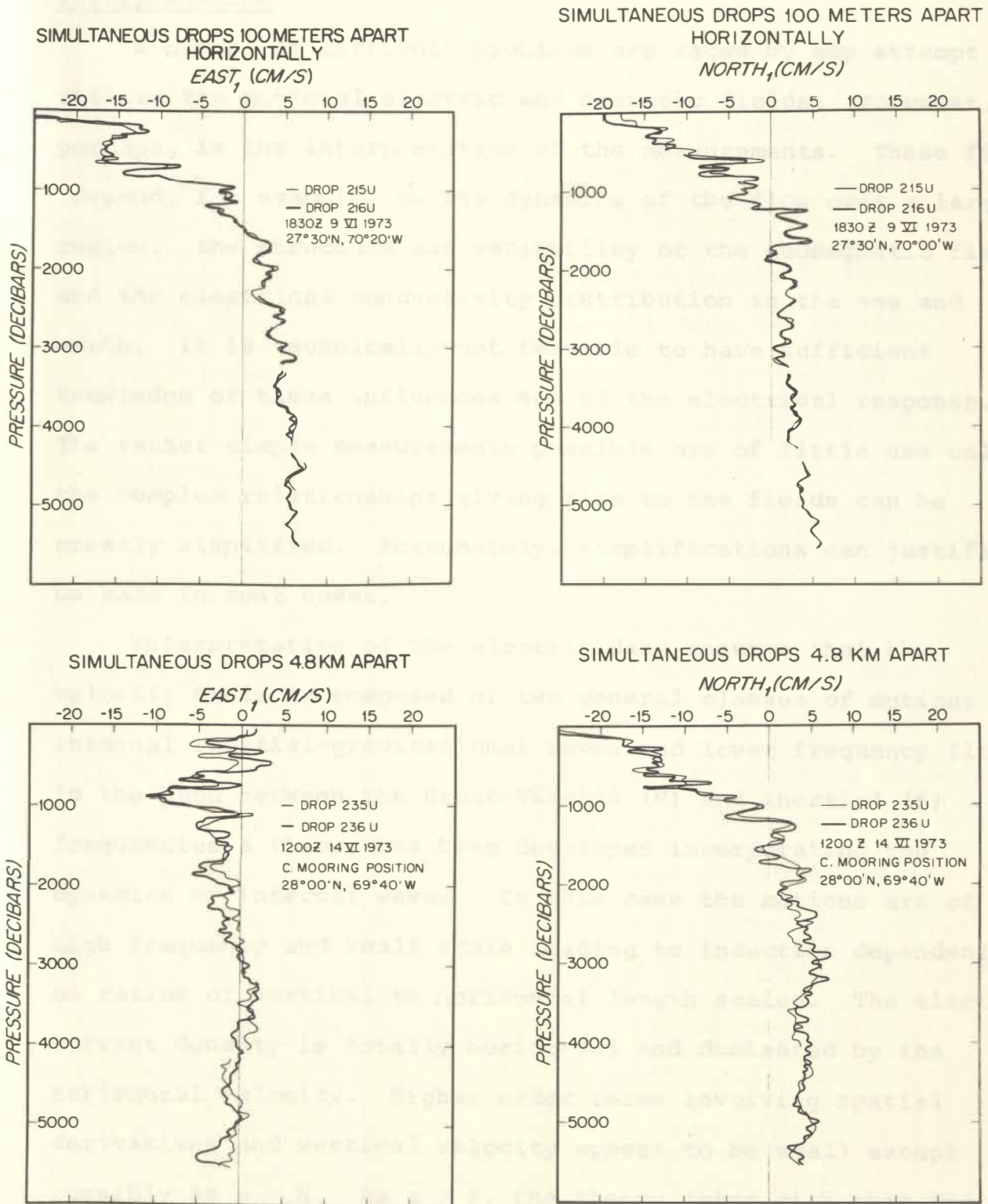


Figure I-9. Examples of Simultaneous Velocity Profiles Taken at Separate Locations

Interpretation

A number of difficult problems are faced by any attempt to utilize the motional electric and magnetic fields. Foremost, perhaps, is the interpretation of the measurements. These fields depend, for example, on the dynamics of the flow over a large region, the structure and variability of the geomagnetic field and the electrical conductivity distribution in the sea and earth. It is technically not feasible to have sufficient knowledge of these influences nor of the electrical response. The rather simple measurements possible are of little use unless the complex relationships giving rise to the fields can be greatly simplified. Fortunately, simplifications can justifiably be made in most cases.

Interpretation of the electric data assumes that the velocity field is composed of two general classes of motion; internal inertial-gravitational waves and lower frequency flows. In the band between the Brunt-Väisälä (N) and inertial (f) frequencies a theory has been developed incorporating the dynamics of internal waves. In this case the motions are of high frequency and small scale leading to induction dependent on ratios of vertical to horizontal length scales. The electric current density is totally horizontal and dominated by the horizontal velocity. Higher order terms involving spatial derivatives and vertical velocity appear to be small except possibly as $\omega \rightarrow N$. As $\omega \rightarrow f$, the theory joins with that for $\omega < f$.

A more exact evaluation of the higher order terms requires information not available about the structure and energy distribution of internal waves.

For $\omega < f$, the interpretation is based on a largely kinematic theory for low-frequency, large-scale flows. No dynamics are assumed for the ocean current because a priori knowledge is not usually available. The full suite of electrical response can be determined by such a kinematic theory. The dynamics will restrict the response to some set of the possible responses. Here again the electric current density is horizontal and dominated by the local horizontal velocity. Other important terms arise which are independent of depth, and some which are proportional to H/L , the ratio of the depth to the horizontal length scale.

A simple model of induction within ocean currents should help establish physical insight into the phenomenon of motional induction. Consider a two-dimensional ocean current as in Fig. I-10a, having variations in horizontal velocity in the cross-stream and vertical coordinates. Due to motion through the vertical component of the geomagnetic field, EMF's will arise everywhere within the current. The electric induction and resulting electric currents can be modelled by an electric network as shown in Figure I-10b, consisting of voltage sources, E_i , and resistances R_i . In this model we consider the ocean current to be composed of M layers insulated from each other except at the ends. The parameter, D/L , largely determines

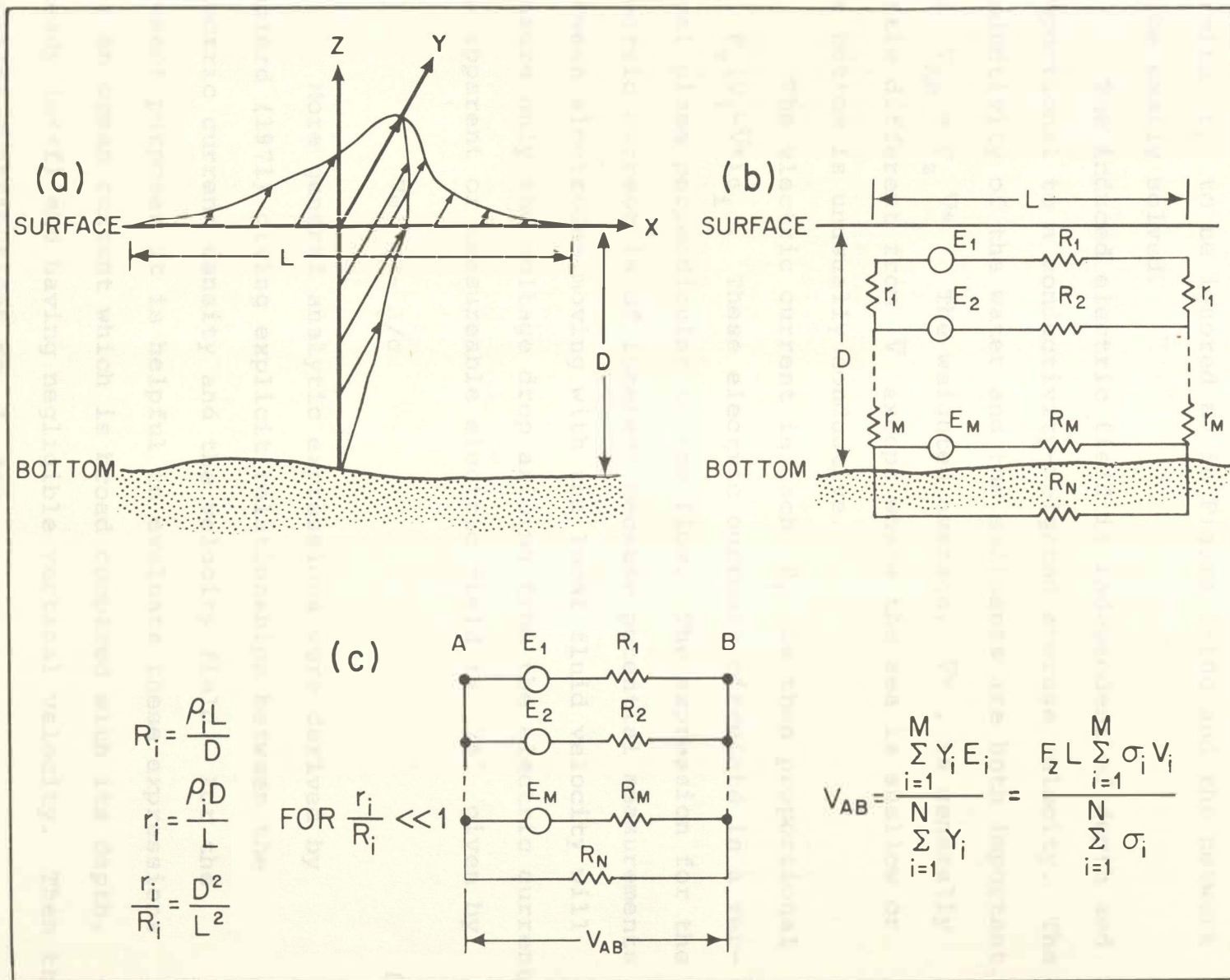


Figure I-10. Electric Network Analog of Motional Induction in the Deep Sea

the ratio of vertical to horizontal resistances. It is almost always true that $D/L \ll 1$ in oceanic flows, a condition which permits r_i to be ignored as in Figure I-10c and the network to be easily solved.

The induced electric field is independent of depth and proportional to a conductivity-weighted average velocity. The conductivity of the water and the sediments are both important. Let $V_{AB} = F_z \bar{V}^*$. The weighted average, \bar{V}^* , is generally little different from \bar{V} except where the sea is shallow or the bottom is unusually conductive.

The electric current in each R_i is then proportional to $F_z (V_i - \bar{V}^*) \sigma_i$. These electric currents circulate in a vertical plane perpendicular to the flow. The expression for the electric current is of interest because potential measurements between electrodes moving with the local fluid velocity will measure only the voltage drop arising from the electric currents. The apparent or measureable electric field is $\nabla \phi'$ given by

$$\nabla \phi' = - \underline{\underline{J}} / \sigma \quad (I-1)$$

More general analytic expressions were derived by Sanford (1971) giving explicit relationships between the electric current density and the velocity field. For the present purposes it is helpful to evaluate these expressions for an ocean current which is broad compared with its depth, steady ($\omega \ll f$) and having negligible vertical velocity. Then the dominant contributions to $\underline{\underline{J}}$ are

$$\underline{J} = \nabla x \left\{ \int_z^0 \sigma F_z (\underline{v} - \underline{\bar{v}}^*) dz + k \sigma Q \right\} \quad (I-2)$$

where $\underline{\bar{v}}^*$ is a conductivity weighted, vertically averaged velocity (vide Sanford, 1971),
and

$$Q = \frac{1}{2\pi} \int_{-\infty}^{\infty} \int_{-\infty}^{\infty} [\nabla \cdot F_z \underline{\bar{v}}^*] \ln [(x-x')^2 + (y-y')^2]^{\frac{1}{2}} dx' dy' \quad (I-3)$$

plus additional terms smaller by factor of H/L .

The term involving $\underline{v} - \underline{\bar{v}}^*$ arises from local induction as explained in the previous analog model and is the term which provides the basis of this free-fall measurement technique.

The second term involving Q represents large-scale electric currents generated by horizontal divergence of the flow.

Although this term can be large it is independent of depth.

Thus we have to order H/L

$$J_x = \sigma F_z (v_y - \bar{v}_y^*) + \frac{1}{2\pi} \frac{\partial}{\partial y} \sigma Q$$

but since $\frac{\partial}{\partial y} \sigma$ is negligible we have

$$J_x / \sigma = F_z v_y - \text{constant (independent of depth)}$$

Similarly

$$J_y / \sigma = - F_z v_x - \text{constant}$$

It follows that if a complete vertical profile of J/σ is measured then it is possible to compute

$$J_x/\sigma - (\overline{J_x/\sigma}) = F_z (v_y - \bar{v}_y)$$

which is the velocity profile relative to the local vertically averaged velocity assuming \bar{v}_y^* and Q do not change in time during the profile.

An alternative way of understanding how these signals are interpreted is to recall that the electric field is independent of depth and is given by

$$\frac{\partial \phi}{\partial x} = F_z \bar{v}_y^* - \frac{\partial Q}{\partial y}$$

A moving pair of electrodes would sense not only the electric field in the ocean but also a contribution due to its motion, v_y' . Thus the measured potential gradient $(\nabla \phi')$ obtained by integration along the line between the electrodes and returning through the surrounding sea water would yield

$$\frac{\partial \phi'}{\partial x} = - F_z (v_y - \bar{v}_y^*) - \frac{\partial Q}{\partial y}$$

If the electrode line is moving in equilibrium with the local horizontal velocity, then $v_y' = v_y$ and

$$\nabla \phi' = - J/\sigma$$

The Present Instrument

During 1971 a new, all-digital version of the EMVP (Figure I-4) was developed and tested. Two instruments of this type were made and have been used extensively (171 profiles).

Later in this report we describe the construction and operation of this instrument. Moreover information is presented regarding the performance of the device along with an extensive discussion of method errors and their influences.

The present version sought to extend the accuracy of the measurements, accommodate additional sensors, improve handling during launch and recovery and provide the results immediately after collection.

The accuracy of the first version was limited mostly by the resolution possible with the acoustical telemetry. However, this problem only masked others generated by electrode and amplifier noise. In order to increase resolution, improvements were made in the electrodes and salt-bridges and in the low-level input preamplifiers. To increase resolution the signals are digitized to 1 part in 4095 (12 bits). The digitized value of every variable measured is stored on an internal 7-track, 200 BPI incremental magnetic tape recorder (later replaced with a cassette tape recorder). The rate at which data are sampled and recorded can be varied to achieve the best reduction of noise for each variable. Depending on noise or expected variability some variables are recorded more frequently than others. Thus more data is available for a noisy variable such as an electrode pair.

Also to increase the sensitivity of the instrument to the ambient electric current density the measurements are made on the skin of an insulating cylinder. Because the electric currents must deviate to pass around the cylinder an increased potential gradient arises leading to a high measured signal.

In addition to pressure, temperature and electrical conductivity measurements were added. Pressure is measured with a strain gauge transducer; temperature is sensed with a platinum wire thermometer; conductivity is measured with an inductive sensor. These data are used to define the density profile.

Much attention was given to the mechanical construction of the probe in order to provide a vehicle which was rugged, easily handled at sea and protected the delicate temperature and conductivity sensors. The slender body is easily launched and recovered alongside of the ship. The guards at each end provide lifting points during handling. The interior pressure case is designed for a working depth of 6000 decibars.

Since there are two identical instruments a means is provided to preset the time an instrument leaves the surface. In this way both instruments can be set to start a profile at the same (or staggered) time even though located some distance apart.

An integral part of the development program has been the development of computer programs to read, process and display the profile data. These programs have been implemented on both the shipboard and shore-based computers. In addition to the basic display and analysis programs, extensive special programming has been done to examine various aspects of the data and to overcome unexpected problems.

SECTION II

The Design and Construction of Present EMVP

The purpose of the EMVP is to measure and record the electric current and density profiles as rapidly and accurately as practicable. The design sought to achieve these goals with an instrument and analysis system capable of revealing the velocity and density structure in near real time on a routine operational basis.

The Vehicle

The vehicle consists of a 7-inch diameter aluminum pressure cylinder, 5 feet in length ending with hemispherical end caps. The forward half of the cylinder is surrounded by 4 discs of buoyant syntactic foam. Covering the foam and cylinder is a 14-inch diameter cylindrical shell or skin of polyethylene. Attached to each end of the pressure cylinder are cages or guards made of aluminum tubing sealed so as to provide buoyancy. Near the center of the skin are four holes connected by hollow plastic tubes to two pairs of electrodes. The electrodes sense the potential along the line connecting diametrically opposed holes and surrounding sea water. Mounted on the forward end within a cage are pressure, temperature and electrical conductivity sensors. At the opposite end, a collar is mounted holding 8 pitched fins.

An extra 13 kg (30 lb) of expendable weights overcomes the positive buoyancy of the instrument (6.5 kg) and forces it to fall toward the bottom. The weights are released either on con-

tact with the bottom or at some mid-depth. The mechanisms shown in Figure II-1 are identical to those used by Richardson and Schmitz (1965).

The weight release is attached to the end of a 5 m line. When using bottom releases, two weights are used. The lighter one weighs 4.3 kg and is attached directly to the release mechanism. The other 8.7 kg, attached to the release device through a guide on the first weight, is at the end of a 6 m line. Only this element touches the bottom for once the tension is removed on its line, the mechanism releases both weights and begins its ascent. As a safety measure a small, inexpensive corrosion link is put in the lower weight line. In the event the weights did not release, the link would ultimately (~5 hrs) corrode releasing the lower weight. The instrument would then return even if the upper weight were still connected.

The release line can be attached to the instrument at either the sensor or projector end. When connected to the sensor end, the instrument falls with T & C sensors in front. When the weights are released, it turns over since the stable orientation in the water is with sensor end up. This is called an inverting drop. Its only advantage is that the T & C sensors are leading the body and not in its wake. The disadvantages include loss of radio and flasher signals and acoustic signal once launched, since radio and flasher are underwater while the acoustic projector is above or just below the surface. Also, this mode is not as stable, for the instrument has a strong righting moment due to its buoyancy.

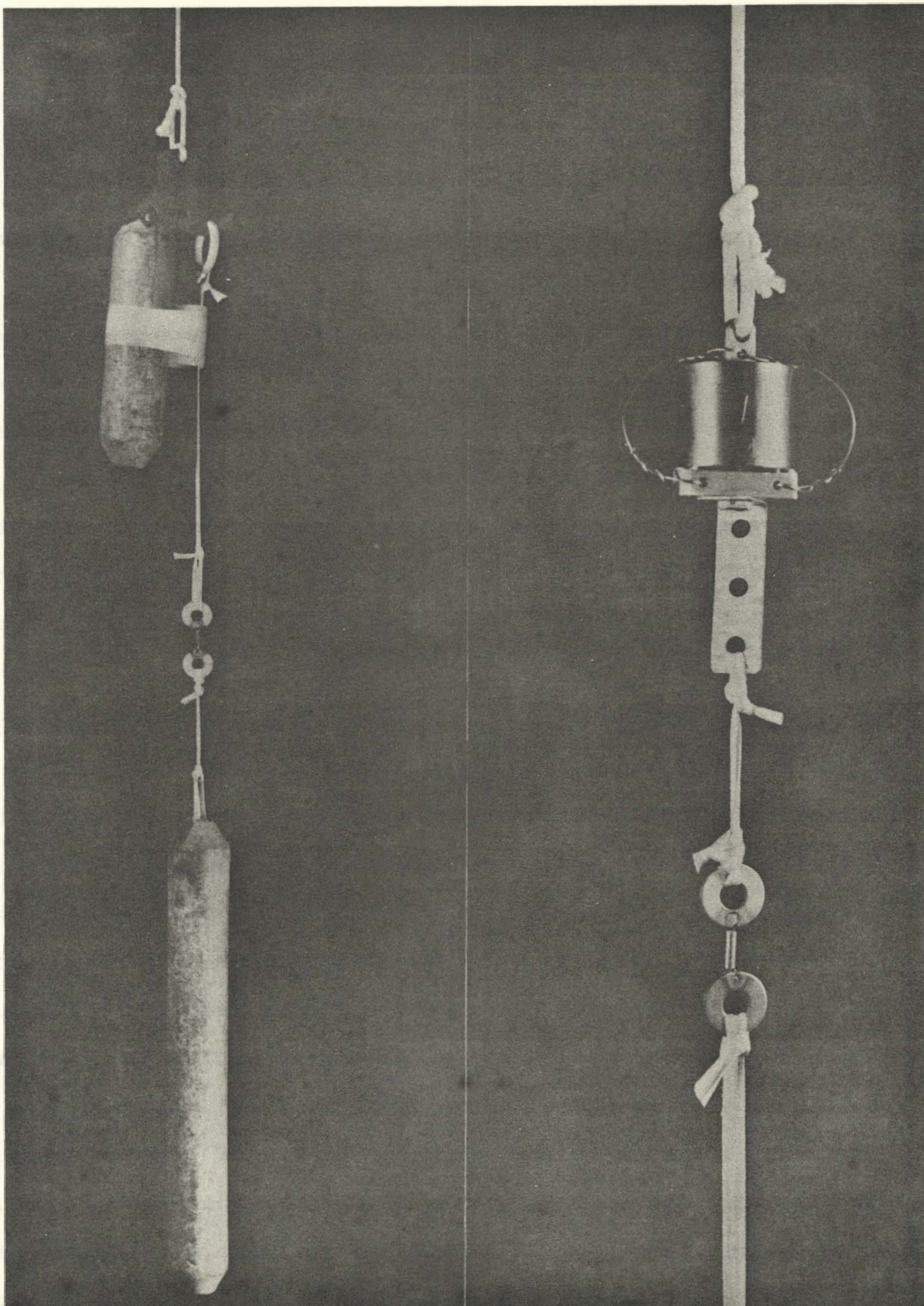


Figure II-1. Bottom Contact (Left) and Mid-Depth Pressure (Right) Releases and Safety Links of Corrodible Magnesium

A so-called non-inverting drop occurs when the release line is attached to the projector end. In this case, the instrument does not turn over when weights are released.

Attached to the sensor end guard is a package containing the recovery aids: a Citizens Band radio-transmitter and a Xenon flasher. These units, made by OAR Inc., are self-contained, having no electrical connection with the main instrument. Each unit has a pressure switch which turns the device off once below the surface.

The package, shown in Figure II-2, is mounted on a frame able to flex relative to the instrument. This facility has proved to be valuable in reducing damage to the flasher and radio during launch and recovery.

The Sensors

The sensors consist of two pairs of electrode assemblies (E1 & E2), bonded strain-gauge pressure transducer (P), pressure-protected platinum wire temperature sensor (T), inductively coupled electrical conductivity transducer (C), and a solenoid wound on a high magnetic permeability core (CC). The electrodes, solenoid (compass) and pressure transducer provide the information needed to calculate a velocity profile.

The "heart" of the instrument is the electrode and salt bridge system. The microvolt potential differences generated across a diameter of the instruments surface are sensed by the electrodes. In order for the method to be useful the measurement must be accurate to less than 1 μ V uncertainty. Such a performance exceeds by more than 100 the predictability and stability

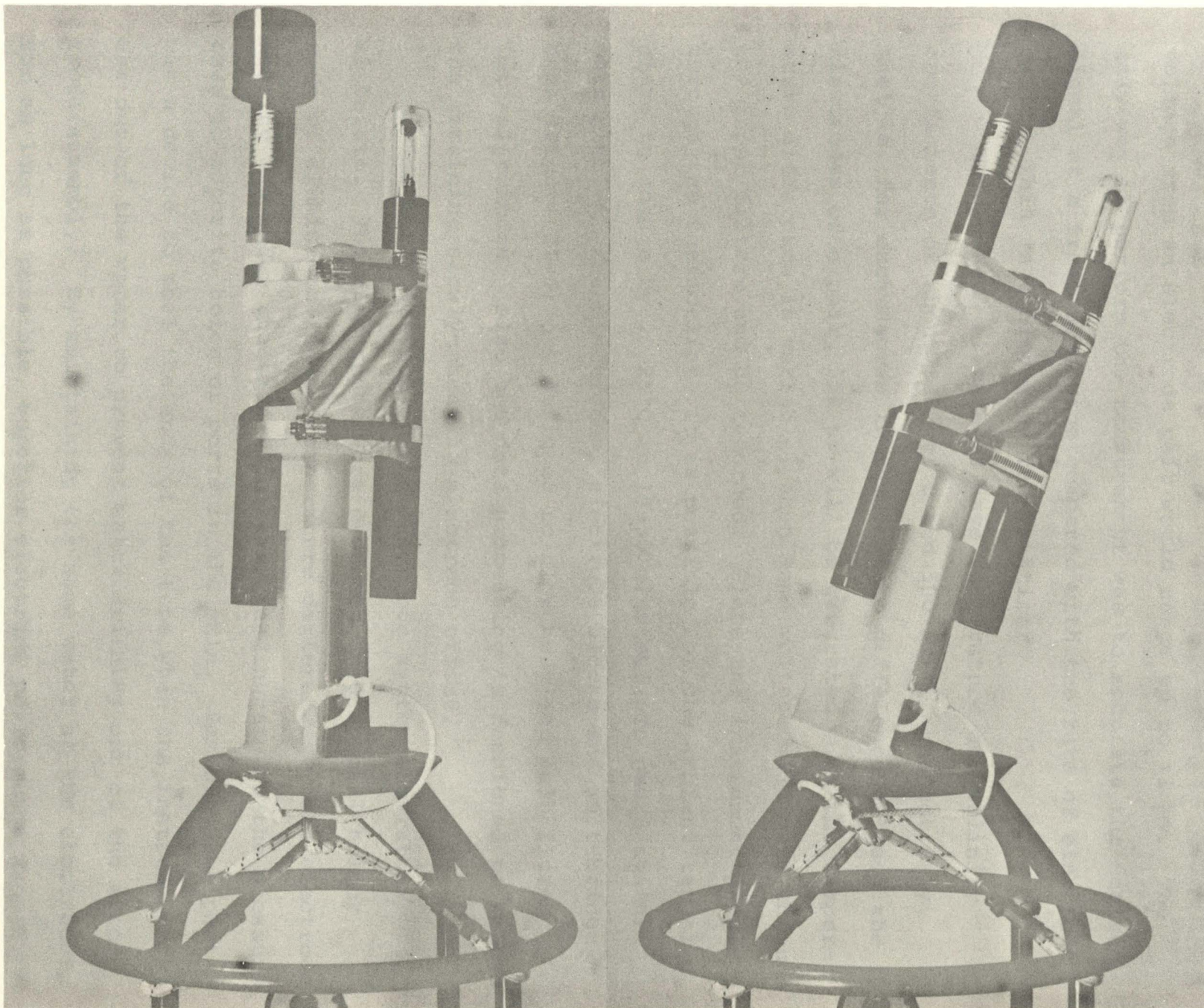


Figure II-2. Radio and Xenon Flasher Units Mounted on Flexible Frame on Sensor End Cage

of the best known electrodes. It was accepted that the basic voltage from an electrode pair would range up to ± 1 mv. The only way to perform the measurement was to modulate the desired signal at a frequency large compared with the rate of electrode drift. This is achieved by the rotation.

The Ag-AgCl electrodes have temperature and salinity coefficients of about $350 \mu\text{v}/^\circ\text{C}$ and $500 \mu\text{v}/\text{‰}$ respectively. That is, for each degree in temperature difference between the electrodes of a pair, $350 \mu\text{v}$ will be generated. If the temperature difference is variable, then some voltage will pass through the input filters and be recorded. Since the instrument passes through the thermocline, it is possible for the ambient temperature to change by $20\text{-}25^\circ\text{C}$ in 15-30 minutes. To guard against this problem, the electrodes, electrode blocks and salt-bridge arms (Figure II-3) are designed to slow heat and salt fluxes into electrodes. Also the data processing is fashioned to remove the remaining slowly-changing electrode offset.

The early version of the electrode system was rather elaborate. The electrodes were produced in a special holder made of alumina to reduce temperature differences. The electrode housing was under the skin with tubes leading around the pressure case to opposite holes or ports in the skin. Beneath each port was a device to seal the ends of the tube when the instrument was out of the water to prevent water draining out of the electrode assembly. By maintaining the same water at the electrodes for as long as possible, superior electrode performance was expected.

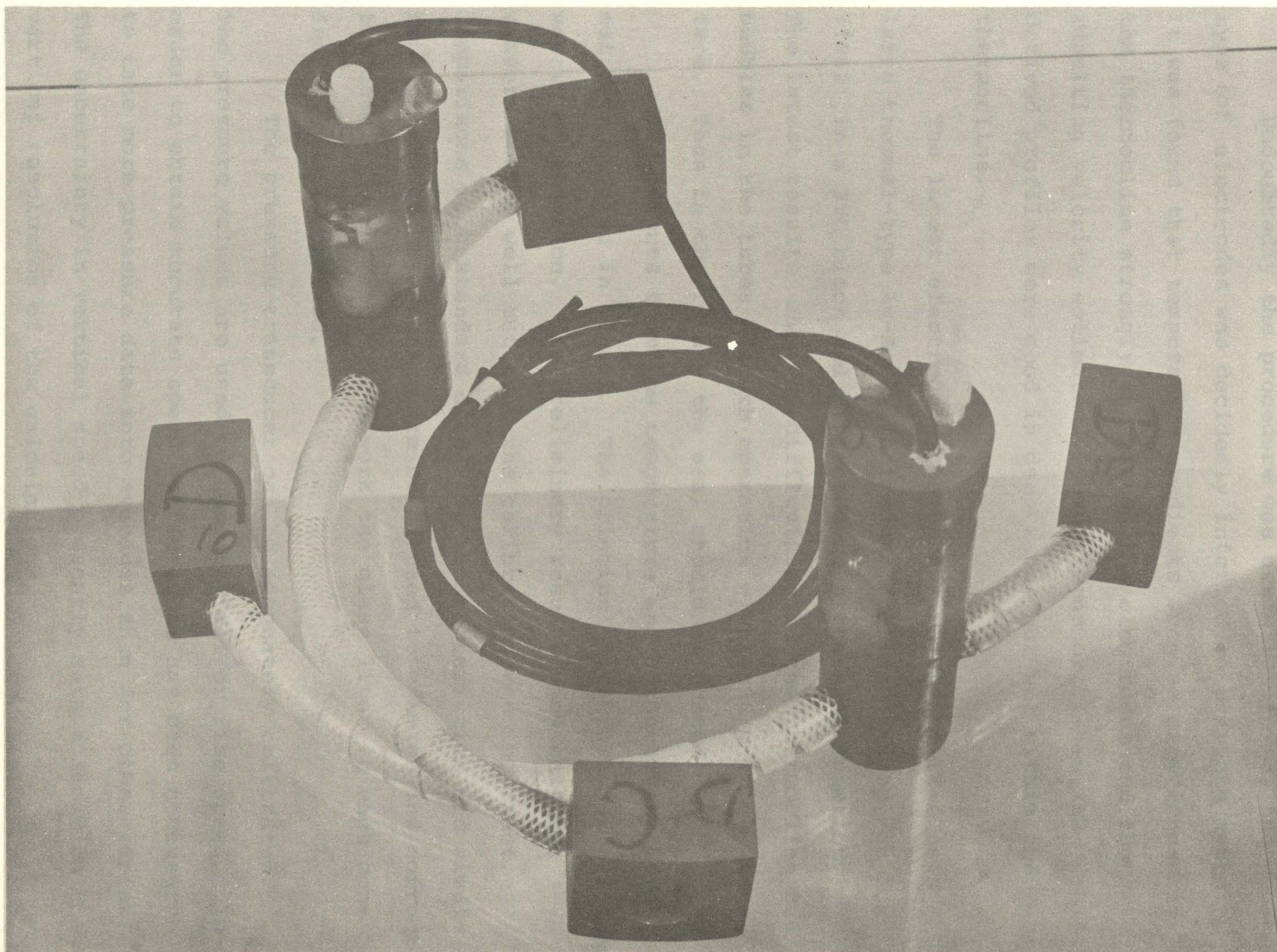


Figure II-3. Two Sets of Electrode Blocks, Salt-bridge Arms and Electrical Cables

Undoubtedly the procedure was useful, however, the new type of electrodes was decidedly inferior to previous types. It was found that temperature gradients such as experienced in the thermocline strongly influenced the electrodes and the resulting velocity estimates. Comparisons of E1- vs. E2-derived profiles were good in deep water but not within the thermocline.

The latest electrode system shown in Figure II-4 uses large thermal-type Ag-AgCl electrodes, much as used by von Arx (1962), in a PVC block and dispenses with the seal function. The latest results show no difficulties in the thermocline but bubbles in the tubes disturb operation within 30 m of the surface. Thus in the future the seal should be reused.

The outputs from the temperature and conductivity have not been studied in detail. The principal difficulty experienced was in calibration. The preliminary results show that the sensors worked well but that the calibration was incorrect. Comparisons with standard deep water characteristics and simultaneous STD and hydrocasts are being used to examine and correct the data. During the MODE-I work the glass liner in each conductivity cell cracked.

The pressure transducer can be adequately calibrated. The pressure values are used to compute fall or rise speed. In order to obtain accurate speed estimates it has been necessary to take more pressure data into averages than for other variables. The uncertainty in vertical speed presently sets a limit on the vertical resolution of the calculations.

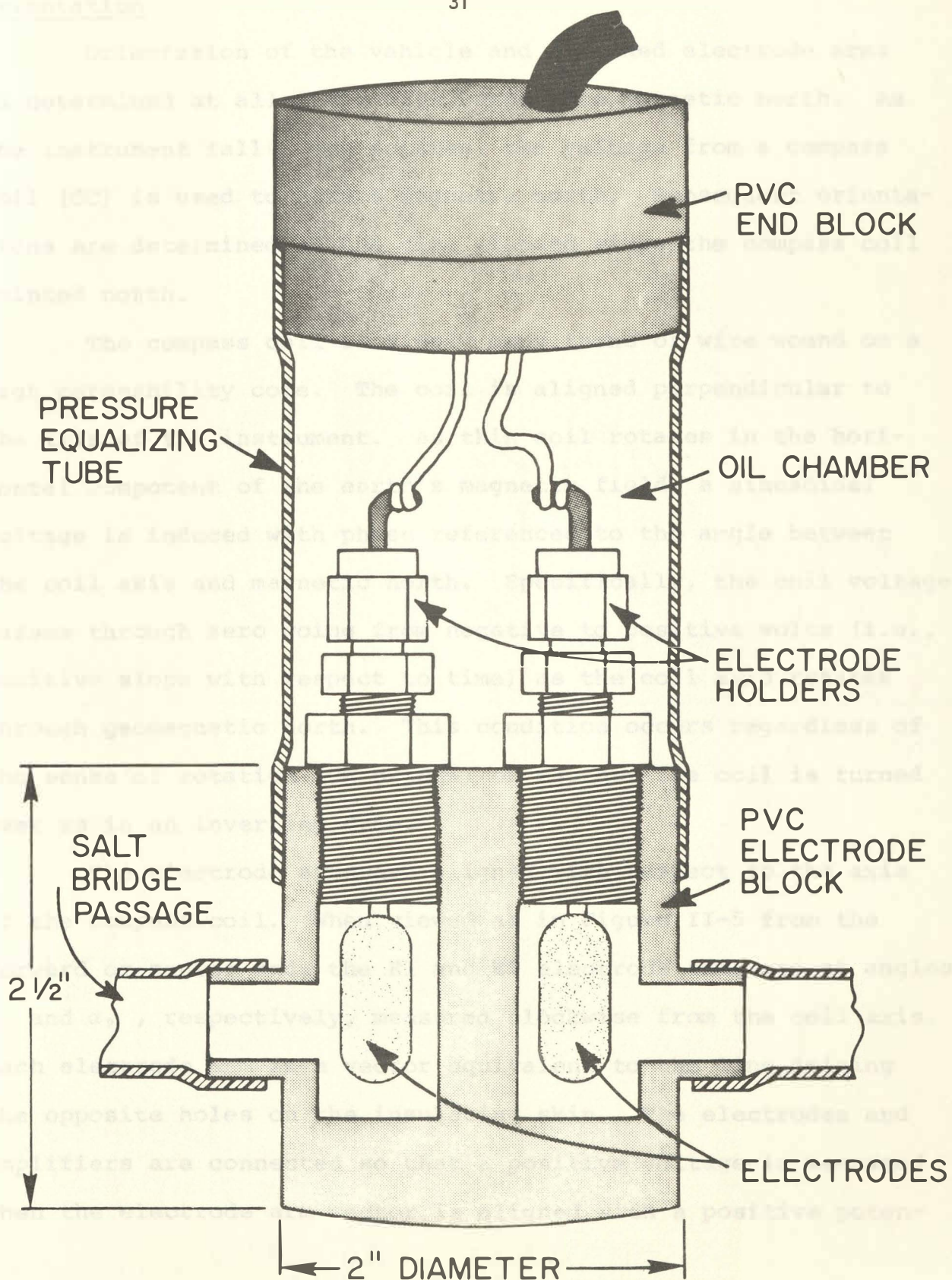


Figure II-4. Detail of Electrode Block Construction

Orientation

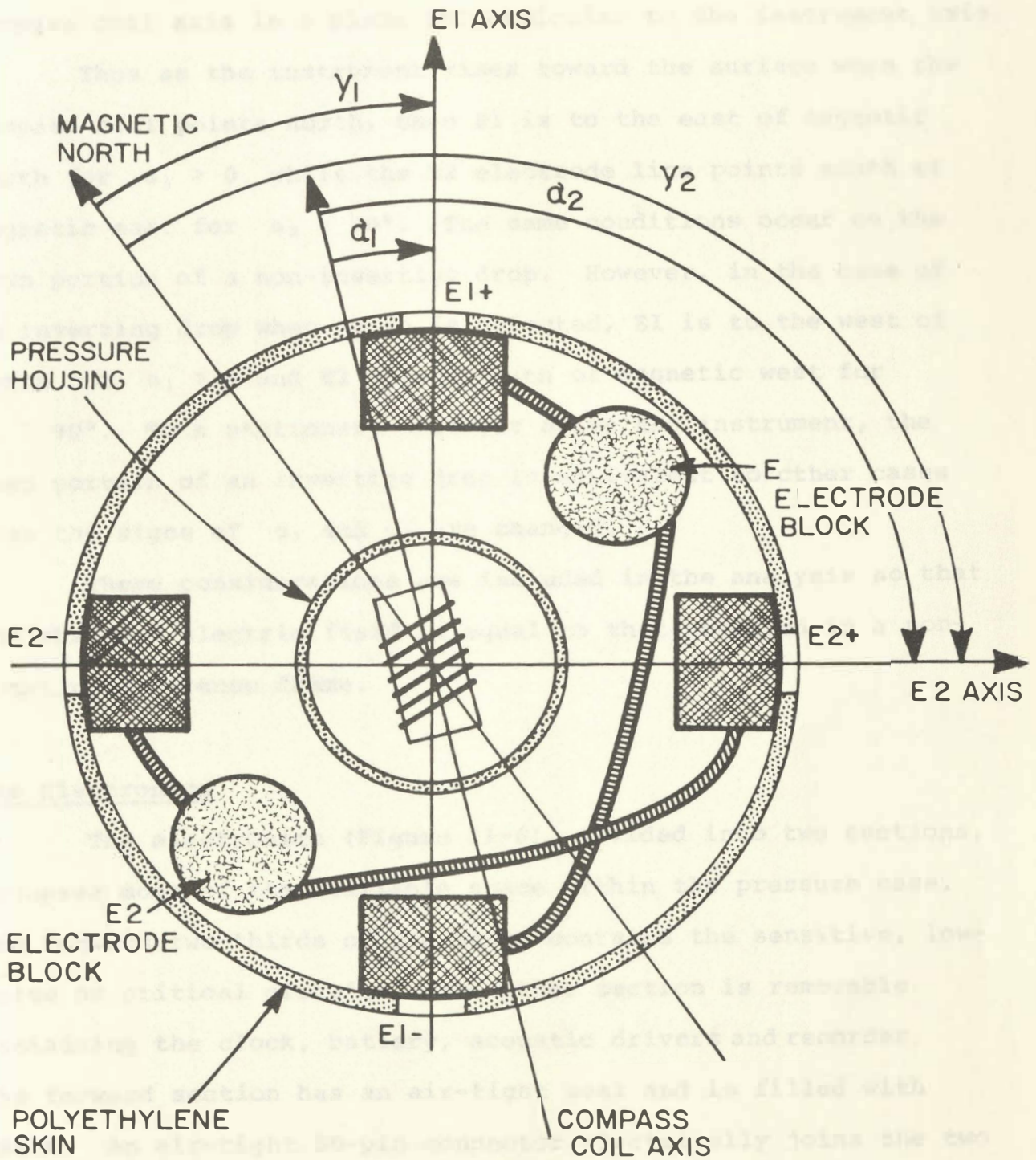
Orientation of the vehicle and attached electrode arms is determined at all times with respect to magnetic north. As the instrument falls, and rotates, the voltage from a compass coil (CC) is used to detect magnetic north. Subsequent orientations are determined as the time elapsed since the compass coil pointed north.

The compass coil is simply many turns of wire wound on a high permeability core. The coil is aligned perpendicular to the axis of the instrument. As this coil rotates in the horizontal component of the earth's magnetic field, a sinusoidal voltage is induced with phase referenced to the angle between the coil axis and magnetic north. Specifically, the coil voltage passes through zero going from negative to positive volts (i.e., positive slope with respect to time) as the coil axis rotates through geomagnetic north. This condition occurs regardless of the sense of rotation (CW or CCW) or whether the coil is turned over as in an inverting drop.

The electrode arms are aligned with respect to the axis of the compass coil. When viewed as in Figure II-5 from the forward or sensor end, the E1 and E2 electrode arms are at angles α_1 and α_2 , respectively, measured clockwise from the coil axis. Each electrode arm is a vector equivalent to the line joining the opposite holes on the insulating skin. The electrodes and amplifiers are connected so that a positive voltage is measured when the electrode arm vector is aligned with a positive poten-

VIEWED FROM SENSOR END

Figure II-5. Arrangement and Orientation of Electrode Arms and Compass Coil



VIEWED FROM SENSOR END

Figure II-5. Arrangement and Orientation of Electrode Arms and Compass Coil

tial gradient in the sea. The E1 line is aligned nearly parallel ($\alpha_1 \approx 0$) and the E2 line nearly perpendicular ($\alpha_2 \approx 90^\circ$) to the compass coil axis in a plane perpendicular to the instrument axis.

Thus as the instrument rises toward the surface when the compass coil points north, then E1 is to the east of magnetic north for $\alpha_1 > 0$ while the E2 electrode line points south of magnetic east for $\alpha_2 > 90^\circ$. The same conditions occur on the down portion of a non-inverting drop. However, in the case of an inverting drop when north is detected, E1 is to the west of north for $\alpha_1 > 0$ and E2 points south of magnetic west for $\alpha_2 > 90^\circ$. To a stationary observer above the instrument, the down portion of an inverting drop is equivalent to other cases when the signs of α_1 and α_2 are changed.

These considerations are included in the analysis so that the observed electric field is equal to that observed in a non-rotating reference frame.

The Electronics

The electronics (Figure II-6), divided into two sections, occupies most of the available space within the pressure case. The forward two-thirds of the space contains the sensitive, low-noise or critical circuits. The other section is removable containing the clock, battery, acoustic drivers and recorder. The forward section has an air-tight seal and is filled with FREON. An air-tight 50-pin connector electrically joins the two sections.

Figure II-6. Arrangement of Circuit Boards and Components within Electronics Pack

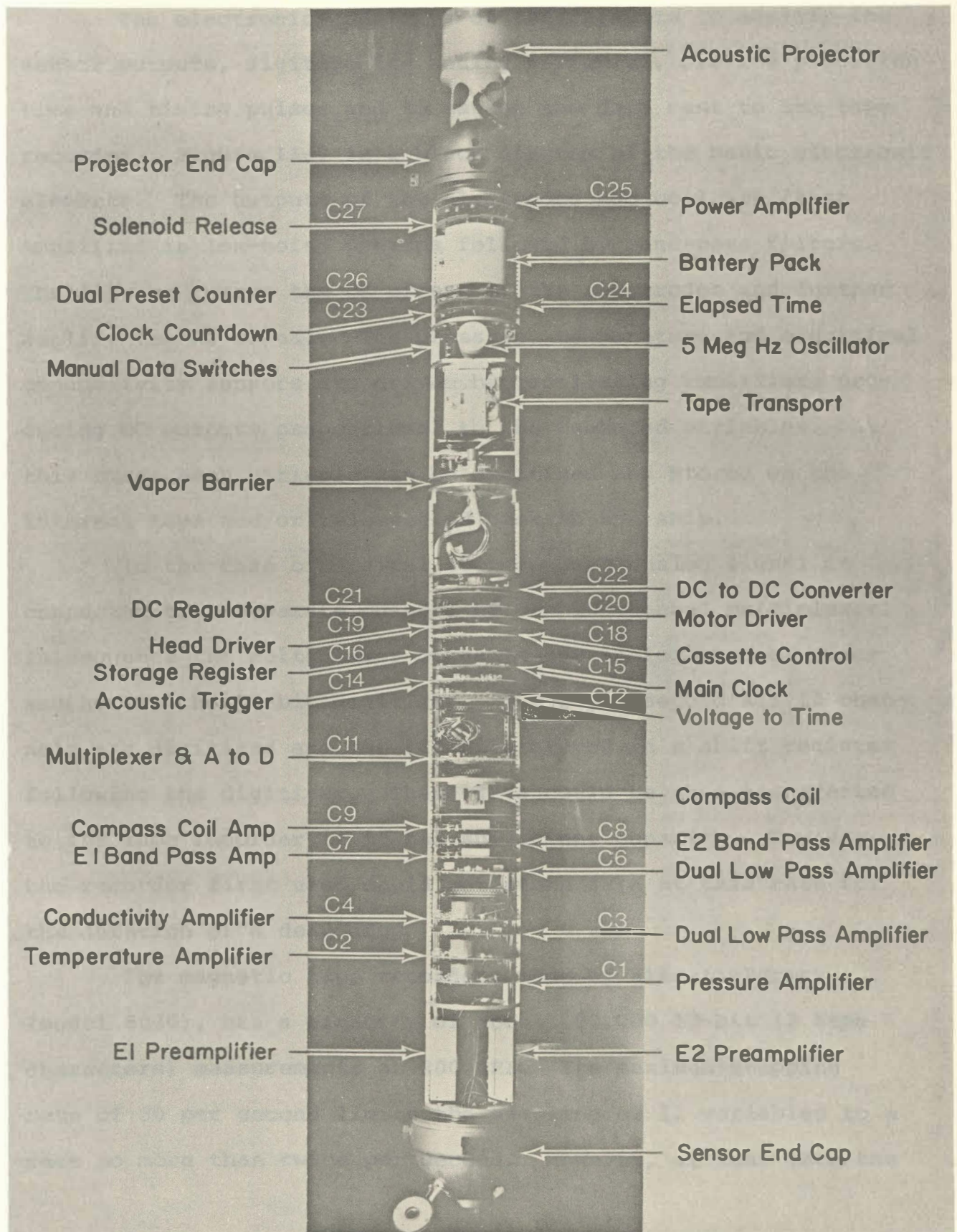


Figure II-6. Arrangement of Circuit Boards and Components within Electronics Rack

The electronics consists of the circuits to amplify the sensor outputs, digitize the analog variables, provide precision time and timing pulses and to manage the data sent to the tape recorder. Figure II-7 is a block diagram of the basic electronic elements. The outputs of the electrodes and coil are first amplified in low-noise preamps followed by band-pass filters. The filters remove the DC offset of the electrodes and further amplify the AC signal. The pressure, temperature and electrical conductivity sensors are driven by oscillating amplifiers producing DC outputs proportional to the measured variables. At this stage each variable can be digitized and stored on the internal tape and/or telemetered back to the ship.

In the case of digital storage each analog signal is connected to a separate channel of the 10-channel multiplexer. In sequence the multiplexer connects one analog channel after another to the 12-bit digitizer. Twice per second all 10 channels are digitized and the 120 bits stored in a shift register following the digitizer. These data could be then transferred to the tape recorder if it had sufficient capacity. However, the recorder first used could not store data at this rate for the duration of a deep drop.

The magnetic tape recorder, made by Bissett-Berman (model 8030), has a capacity of about 100,000 12-bit (2 tape characters) measurements at 200 BPI. Its maximum stepping rate of 50 per second limits the sampling of 12 variables to a rate no more than twice per second. However, at that rate the

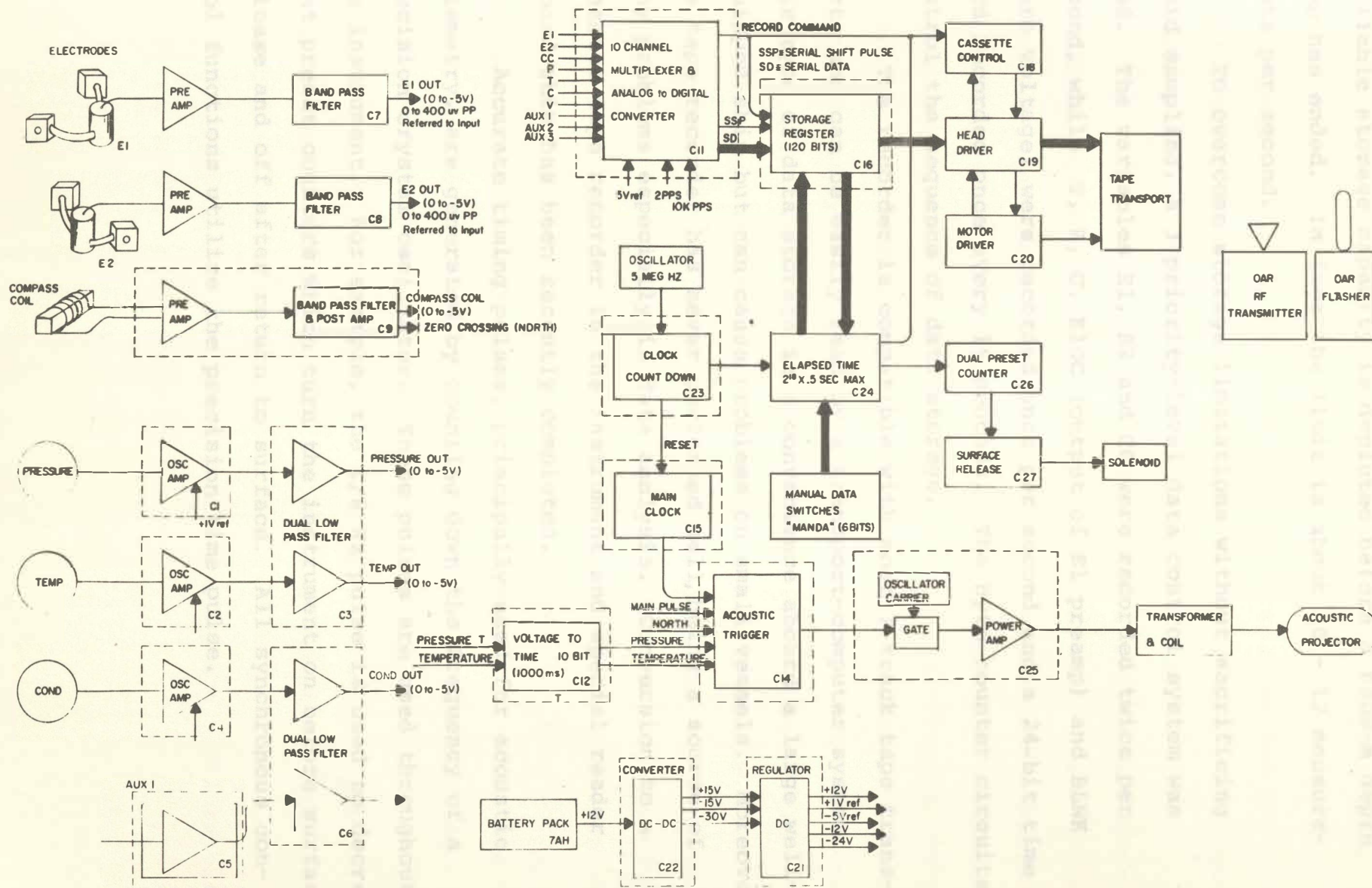


Figure II-7. Block Diagram of Electronics

available storage capacity is depleted before a 6000-m depth drop has ended. In fact the limit is about 10 - 12 measurements per second.

To overcome storage limitations without sacrificing rapid sampling, a 3 priority-level data control system was used. The variables E1, E2 and CC were recorded twice per second, while T, P, C, ElDC (output of E1 preamp) and BLNK (zero voltage) were recorded once per second and a 24-bit time word recorded once every 16 seconds. The Byte counter circuits control the sequence of data storage.

The recorder is compatible with most 7-track tape transports and can be easily read by a transport-computer system. This type of data storage is a convenience aboard a large well-equipped ship but can cause problems on small vessels. Moreover, the tape recorder has never performed well, being a source of many problems especially in data analysis. Conversion to a cassette tape recorder in the instrument and special reader aboard ship has been recently completed.

Accurate timing pulses, principally used for acoustic telemetry, are generated by counting down the frequency of a precision crystal oscillator. These pulses are used throughout the instrument. For example, the 1/8 Hz pulse is used to decrement preset counters which turn the instrument on before surface release and off after return to surface. All synchronous control functions utilize the precision time pulse.

The power supply provides power for all circuits except for the low-noise preamplifiers which use a small isolated battery pack. The main battery, made of nickel-cadmium cells, provides about 7 ampere-hours of capacity at 12 VDC. The other voltages used are produced in a DC-DC power converter.

The acoustic telemetry system provides real-time information about the velocity and temperature structure, slant range and depth. These data are coded in terms of time delays between a clock-controlled pulse generated precisely once per second and the pulses associated with the set of variables. The time delay is directly proportional to the variable being measured. The appropriate delays are generated by a voltage-to-time converter which compares the value of the analog variable with a voltage ramp. The ramp voltage starts at zero precisely at the one-second pulse from the clock and linearly increases to full scale in one second. Thus the time at which the ramp voltage is equal to that of the analog variable has the same ratio to 1 second as the variable has to full scale. So if an acoustic tone burst is emitted at the start of the ramp (the one-second or reference burst), followed by another at the instant of ramp-variable equality, the time delay recorded aboard the ship determines the scaled value of the variable. The true value in appropriate units can be calculated knowing the calibration or conversion factors.

The slant range is directly computed by the absolute time of arrival of the reference burst.

By this means temperature and pressure are transmitted once per second. However, there is no necessity that transmission be limited to the rate of once per second. In fact, E1 is coded at a 5 Hz rate using a 200 ms ramp. That is, 5 E1 values are sent each second. The orientation is sent asynchronously as a 200-ms-long tone burst at the instant E1 electrode arm points at magnetic north.

The system requires that the local oscillator be stable and synchronized with the lab oscillator. The lab oscillator in turn controls the sweep of the graphic recorder. Operation of the graphic recorder at a sweep rate of once per 200 ms results in direct display of E1 sinusoids. Also greater resolution of time delays corresponding to P and T and slant range are achieved.

The duration of the various tone bursts is used to identify the variable. Moreover, the duration of the reference pulse is modulated so as to have a distinctive appearance on the graphic recorder.

The preset counters control the start of telemetry after launch and the end after surfacing. The one-second or reference tone is not under counter control for it is needed for ranging during launch and recovery.

The full suite of acoustic telemetry data is illustrated in Fig. II-8. The upper panel of this figure is of the acoustic telemetry recorded on a 1 second per sweep scale. The instrument was about 420 meters from the ship when the preset timer released the surface float allowing the drop to start. At this time the

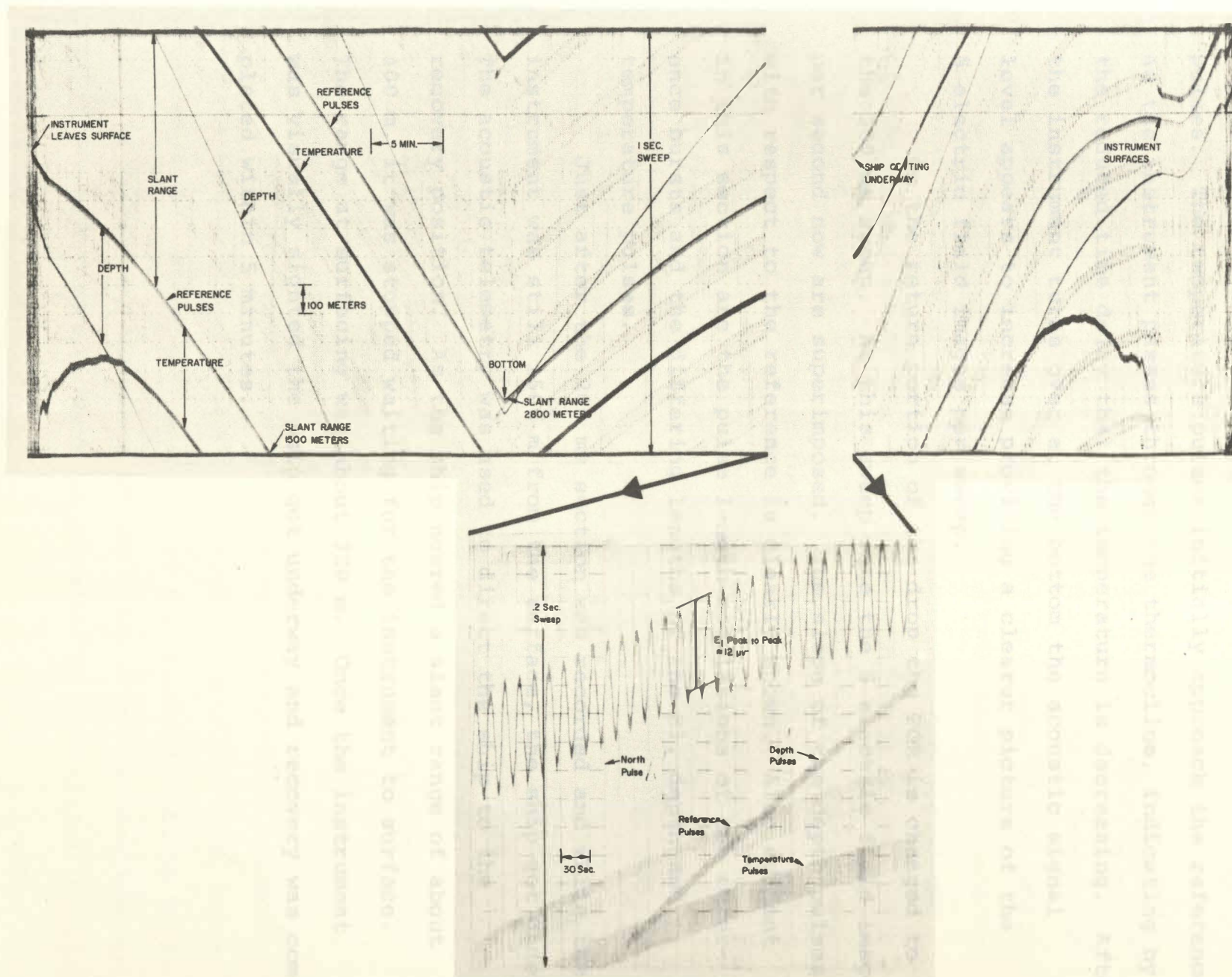


Figure II-8. Record of Acoustic Telemetry Pulses. Upper Panel was Recorded at One Sweep per Second. Lower Panel was Recorded at Five Sweeps per Second

depth (pressure) pulses begin to diverge from the reference pulses. The temperature pulses initially approach the reference as the instrument passes through the thermocline, indicating by the reduced time delay that the temperature is decreasing. After the instrument turns over at the bottom the acoustic signal level appears to increase providing a clearer picture of the 5 electric field images per sweep.

On the return portion of the drop the PGR is changed to the 200 ms sweep. At this sweep rate the 5 electric field images per second now are superimposed. The slope of the depth pulses with respect to the reference is clearly shown. Also evident in this section are the pulse length modulations of the reference bursts and the differing lengths of the E1, depth and temperature pulses.

Just after the 200 ms section was recorded and while the instrument was still 1500 m from the surface, the ship got underway. The acoustic telemetry was used to direct the ship to the recovery position. As the ship neared a slant range of about 400 m, it was stopped waiting for the instrument to surface. The range at surfacing was about 320 m. Once the instrument was visually sighted the ship got underway and recovery was completed within 5 minutes.

SECTION III

Response of Instrument to Electric Currents and Relative Velocity

The electric field sensed by the instrument depends on the applied electric currents and on the motion of the vehicle relative to the local water. The electric current pattern is modified in the vicinity of the instrument. Because of the insulating surface of the vehicle, the horizontal electric currents must diverge to pass by rather than to continue through the skin. The requirement that the normal component of electric current density vanish at the insulating skin is satisfied by the establishment of a surface charge distribution. It is necessary to account for the influence of this charge distribution on the measured potential differences.

The additional induction locally generated by relative motion must also be considered. Since it is reasonable that the vehicle is not always moving exactly with the local horizontal velocity, a question arises as to which velocity is measured; that of the local water or of the vehicle. This analysis seeks to answer this question.

The instrument resembles a truncated cylinder for most of its length ending with various elements such as fins, cages and sensors. Since the influence of these attachments is difficult to determine, the shape of the instrument was idealized as a prolate spheroid with axis of rotation in the vertical direction.

The solutions are found in terms of spheroidal harmonics about the body spheroid having foci at $x = y = 0$ and $z = \pm a/2$. It is convenient to align the x, y, z coordinate axes with the geomagnetic elements. Then the x axis points toward geomagnetic east; the y axis points toward geomagnetic north; the z axis points vertically up.

The coordinate transformations are

$$\begin{aligned} x &= \frac{a}{2} \sqrt{(\xi^2 - 1)(1 - \eta^2)} \cos \phi \\ y &= \frac{a}{2} \sqrt{(\xi^2 - 1)(1 - \eta^2)} \sin \phi \\ z &= \frac{a}{2} \xi \eta \end{aligned} \tag{III-1}$$

$$\xi = (r_1 + r_2)/a ; \quad \eta = (r_1 - r_2)/a ; \quad \phi = \tan^{-1} y/x$$

where

$$r_1^2 = x^2 + y^2 + (z + a/2)^2$$

$$r_2^2 = x^2 + y^2 + (z - a/2)^2$$

Figure III-1 shows the prolate spheroidal coordinates in the xz plane (i.e. $\phi = 0$). The surfaces $\xi = \text{constant}$ and $\eta = \text{constant}$ are surfaces of revolution about the z axis. The surface $\xi = 1.02$ is taken as the approximate shape of the EMVP.

First consider the electric perturbation field as a horizontal electric current, \vec{J}^0 , uniform at infinity flows

Figure III-1. Prolate Spheroidal Coordinates

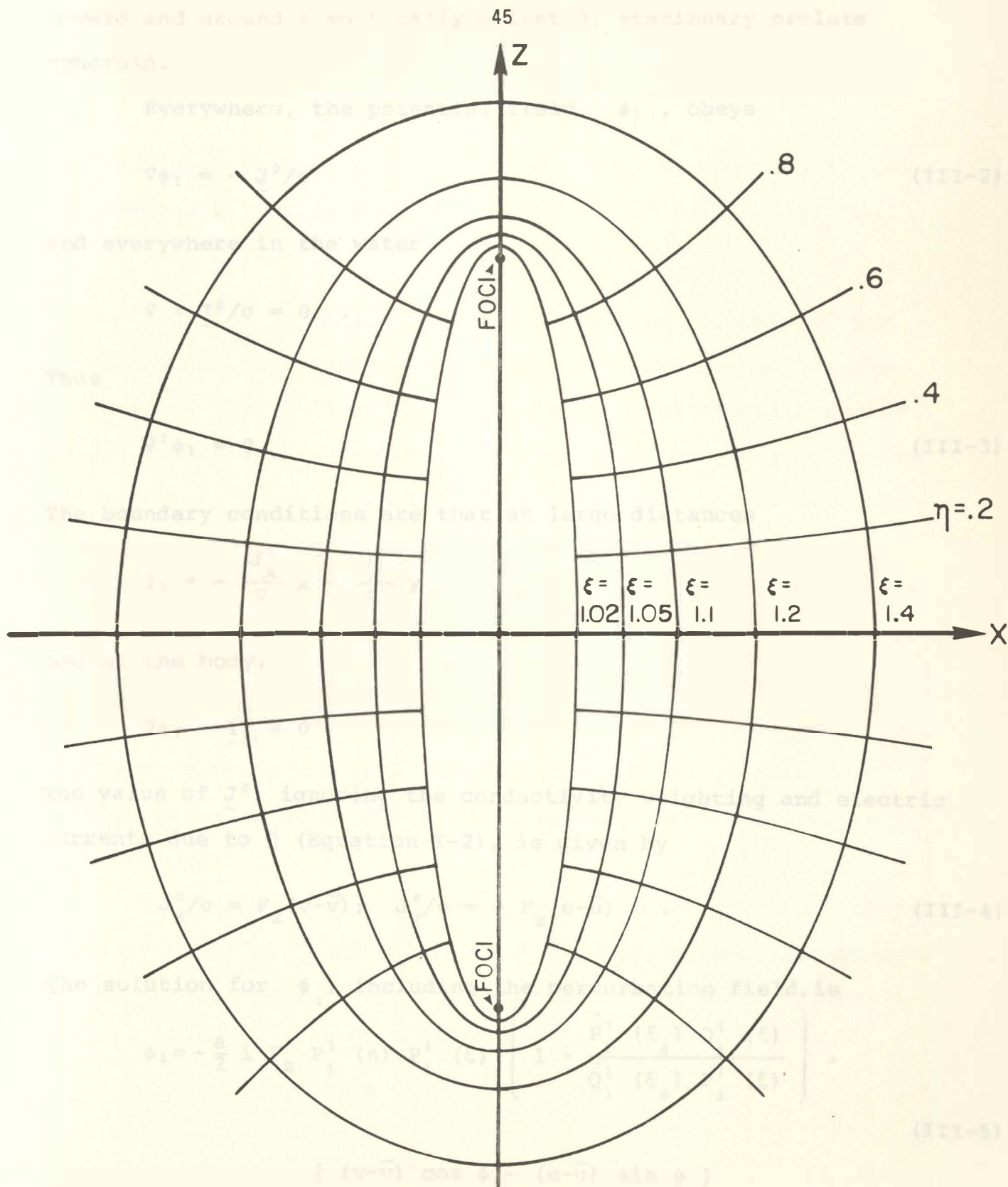


Figure III-1. Prolate Spheroidal Coordinates

toward and around a vertically oriented, stationary prolate spheroid.

Everywhere, the potential field, ϕ_1 , obeys

$$\nabla \phi_1 = - \tilde{J}^0 / \sigma \quad (\text{III-2})$$

and everywhere in the water

$$\nabla \cdot \tilde{J}^0 / \sigma = 0 .$$

Thus

$$\nabla^2 \phi_1 = 0 \quad (\text{III-3})$$

The boundary conditions are that at large distances

$$\phi_1 \rightarrow - \frac{\tilde{J}_x^0}{\sigma} x - \frac{\tilde{J}_y^0}{\sigma} y$$

and at the body,

$$\nabla \phi_1 \cdot \hat{n}_\xi = 0$$

The value of \tilde{J}^0 , ignoring the conductivity weighting and electric currents due to Q (Equation I-2), is given by

$$\tilde{J}_x^0 / \sigma = F_z (v - \bar{v}) ; \quad \tilde{J}_y^0 / \sigma = - F_z (u - \bar{u}) \quad (\text{III-4})$$

The solution for ϕ_1 , including the perturbation field, is

$$\phi_1 = - \frac{a}{2} i F_z P_1^1(\eta) P_1^1(\xi) \left(1 - \frac{\hat{P}_1^1(\xi_0) Q_1^1(\xi)}{\hat{Q}_1^1(\xi_0) P_1^1(\xi)} \right) . \quad (\text{III-5})$$

$$[(v - \bar{v}) \cos \phi - (u - \bar{u}) \sin \phi]$$

where

$$\hat{P}_1^1(\xi) = \frac{d}{d\xi} P_1^1(\xi) \text{ and } \hat{Q}_1^1(\xi) = \frac{d}{d\xi} Q_1^1(\xi)$$

The imaginary unit is needed because the usual convention (Morse and Feshbach, 1953) is that $P_1^1(x) = \sqrt{1-x^2}$ for $x < 1$; so for $\xi > 1$ we define $i P_1^1(\xi) = \sqrt{\xi^2 - 1}$.

Next the induction is computed for the velocity of the instrument allowing for relative velocity with respect to the local ocean flow. In order to compute the additional induction due to the relative velocity, it is assumed that this motion is irrotational, non-divergent (potential) flow. In practice the relative velocity has a large vertical component due to the buoyancy excess and a small horizontal component due to inertial drag and vertical shear. The boundary conditions are equivalent to those used for the electric current density perturbation.

The part of the instrument's velocity which is equal to the local water components does not produce any measurable voltage since both the instrument and water move together at that component.

Relative velocity, however, can produce additional contributions. Let U , V and W be the additional velocity components of the instrument (u', v', w') relative to the water (u, v) :

That is, let

$$U = u' - u$$

$$V = v' - v$$

$$W = w' \quad (w \equiv 0)$$

(III-6)

Using a velocity potential Φ such that $\nabla\Phi = -\tilde{\mathbf{v}}$, the governing equation is

$$\nabla^2\Phi = 0 \quad (\text{III-7})$$

Boundary conditions are

$$\Phi \rightarrow Ux + Vy + Wz$$

at distance and

$$\nabla\Phi \cdot \frac{1}{\xi} = 0$$

at $\xi = \xi_0$.

The solution for the velocity potential is

$$\begin{aligned} \Phi = & -\frac{a}{2} P_1^1(\eta) P_1^1(\xi) \left(1 - \frac{\dot{P}_1^1(\xi_0) Q_1^1(\xi)}{\dot{Q}_1^1(\xi_0) P_1^1(\xi)} \right) (U \cos \phi + V \sin \phi) \\ & - \frac{a}{2} P_1^0(\eta) P_1^0(\xi) \left(1 - \frac{\dot{P}_1^0(\xi_0) Q_1^0(\xi)}{\dot{Q}_1^0(\xi_0) P_1^0(\xi)} \right) W \end{aligned} \quad (\text{III-8})$$

The components of the relative velocity are easily computed in spheroidal coordinates by taking grad Φ .

Expressing $\tilde{\mathbf{F}}$, the geomagnetic field, having components F_Y and F_Z , in terms of ξ , η and ϕ :

$$F_\xi = \frac{F_Y \xi \sqrt{1 - \eta^2}}{\sqrt{\xi^2 - \eta^2}} \sin \phi + \frac{F_Z \eta \sqrt{\xi^2 - 1}}{\sqrt{\xi^2 - \eta^2}} \quad (\text{III-9})$$

$$F_{\eta} = - \frac{F_y \eta \sqrt{\xi^2 - 1}}{\sqrt{\xi^2 - \eta^2}} \sin \phi + \frac{F_z \xi \sqrt{1 - \eta^2}}{\sqrt{\xi^2 - \eta^2}} \quad (\text{III-9})$$

$$F_{\phi} = F_y \cos \phi$$

In a medium of uniform conductivity, the condition of charge conservation requires that

$$\nabla \cdot \tilde{J}/\sigma = 0$$

Hence, the electric potential, ϕ_2 , is related to the velocity by

$$\nabla^2 \phi_2 = \tilde{F} \cdot \nabla \times \tilde{v} = 0$$

since \tilde{v} is irrotational.

Thus we seek the solution to

$$\nabla^2 \phi_2 = 0 \quad (\text{III-10})$$

with the conditions that

$$\phi_2 \rightarrow -(F_z V - F_y W) x + F_z U_y - F_y U_z$$

as $\xi \rightarrow \infty$ and

$$\nabla \phi_2 \cdot \frac{1}{\xi} = \tilde{v} \times \tilde{F} \cdot \frac{1}{\xi} = F_{\phi} \tilde{v}_{\eta} - F_{\eta} \tilde{v}_{\phi}$$

for $\xi = \xi_0$.

The solution for ϕ_2 combined with that for ϕ_1 gives the total potential field, ϕ_m , as measured:

$$\begin{aligned}
\phi_m(\xi, \eta, \phi) = & -\frac{ai}{2} F_Z P_1^1(\eta) P_1^1(\xi) \{ \cos \phi [(v-\bar{v})(1+C_1) + v(1+C_3)] \\
& - \sin \phi [(u-\bar{u})(1+C_1) + u(1+C_3)] \} \\
& + \frac{ai}{2} F_H W(1+C_2) P_1^1(\eta) P_1^1(\xi) \cos \phi \\
& - \frac{a}{2} F_H U P_1^0(\eta) P_1^0(\xi) (1+C_4)
\end{aligned} \tag{III-11}$$

where

$$C_1(\xi) = -\frac{\dot{P}_1^1(\xi_0) Q_1^1(\xi)}{\dot{Q}_1^1(\xi_0) P_1^1(\xi)}$$

$$C_2(\xi) = \frac{Q_1^0(\xi_0) Q_1^1(\xi)}{i Q_1^1(\xi_0) \dot{Q}_1^1(\xi_0) P_1^1(\xi)}$$

$$C_3(\xi) = -\left(\frac{\dot{P}_1^1(\xi_0)}{\dot{Q}_1^1(\xi_0)} \right)^2 \frac{Q_1^1(\xi_0) Q_1^1(\xi)}{P_1^1(\xi_0) P_1^1(\xi)}$$

$$C_4(\xi) = -\frac{i \dot{P}_1^1(\xi_0) Q_1^0(\xi)}{\dot{Q}_1^1(\xi_0) P_1^0(\xi)}$$

$$\dot{P}_i^j = \frac{d}{d\xi} P_i^j$$

$$\dot{Q}_i^j = \frac{d}{d\xi} Q_i^j$$

Three special cases illustrate the basic principles governing electrical measurements from a free body. The first situation is as ξ becomes large (a held constant) which corresponds to measurements made distant from the body. The first free instrument used to measure motional fields was built some-

what this way. The second case is for $\xi = \xi_0$; that is, measurements made from the outer surface of the body. The present instrument is built in this way. The third case is when the body is a very long cylinder. This case is a limit of the solution as $a \rightarrow \infty$ and corresponds perhaps to a useful construction in the future.

Case I: $\xi \gg \xi_0$

$$\begin{aligned} \phi_m \sim & -\frac{ai}{2} P_1^1(\eta) P_1^1(\xi) [(v+V-\bar{v}) F_z \cos \phi \\ & - (u+U-\bar{u}) F_z \sin \phi \\ & - W F_H \cos \phi] \\ & - \frac{a}{2} F_H U P_1^0(\eta) P_1^0(\xi) \end{aligned} \quad (\text{III-12})$$

The result to notice is that in the F_z terms the quantities $u + U$ and $v + V$ appear. Thus electrodes widely spaced from the body respond to the horizontal velocity of the body.

Case II: $\xi = \xi_0$

The length-to-diameter ratio is about 5 for the present instrument. Then

$$a = 4\sqrt{6} R$$

$$\xi_0^2 = 25/24$$

$$R = 7'' = 18.75 \text{ cm}$$

Evaluation of the spheroidal functions for the given ξ_0 yields

$$\begin{aligned} \phi_m \sim & -\frac{ai}{2} P_1^1(\eta) P_1^1(\xi_0) \{ [1.9(v-\bar{v}) + 0.2 V] F_Z \cos \phi \\ & - [1.9(u-\bar{u}) + 0.2 U] F_Z \sin \phi \\ & - 0.9 W F_H \cos \phi \} \end{aligned} \quad (\text{III-13})$$

Summary

These results show that the influence of relative velocity is less significant than that of the induction due to relative velocity. The important results here are that the influences of U and V are reduced an order of magnitude relative to u and v , while that of W is down by a factor of about 2. Thus the measurement is less sensitive to relative velocity, even the large vertical component, when made on surface of body. For a fixed electrode separation the Case II method receives twice as large a signal as Case I.

Case III:

As $a \rightarrow \infty$ the spheroid surface becomes a circular cylinder on which ξ_0 corresponds to $R = R_0$, the diameter of the cylinder. Then

$$\begin{aligned} \phi_m \sim & -F_Z R(1+R_0^2/R^2) [\cos \phi (v-\bar{v}) - \sin \phi (u-\bar{u})] \\ & -F_Z R(1-R_0^2/R^2) [\cos \phi V - \sin \phi U] \\ & -F_H R W \cos \phi \end{aligned} \quad (\text{III-14})$$

As in Case I, when $R \gg R_0$ the relative velocity

contributes to the measured signal. For $R = R_0$, the relative horizontal velocity is unimportant, not just small as in Case II.

To the extent that the idealization is valid that the relative velocity is irrotational, these results suggest that measurements on the surfaces of very long cylinders are not sensitive to the induction due to relative velocity.

Summary

These results show, for a given electrode separation, that the measured signal is twice as large when an insulating cylinder is used and that in this case the relative velocity has no influence. The analysis is an idealization of the actual situation but it shows what is reasonable to expect in terms of calibration factors. A more realistic model involves the response of a prolate spheroid with a vertical axis of rotation. This analysis shows that the sensitivity factor is less than the two found for the infinite cylinder. This factor is reduced slightly to the range of 1.9 - 1.95 depending on the diameter-to-length ratio and placement of electrodes on the surface. Also the influence of relative velocity is not zero; yet it is not large compared with other terms.

This analysis is useful for estimating bounds for various factors. However, the actual instrument is not a spheroid and has various attachments such as fins. There remain small uncertainties, of the order of several percent, as to the exact calibration factors.

SECTION IV

Data Analysis

Values of the motional potential and other variables as a function of time are stored in analog form via the acoustic telemetry and in digital form on the tape recorder. Both forms of data are used.

Figure II-8 presents one example of the recording of the acoustic telemetry and Figure IV-1 shows an analog trace of some of the digitally recorded data. Figure IV-1 is of a section of data, E1, E2, CC and DP (the 1st difference of pressure is proportional to fall rate) as the instrument nears the surface on its return. Note loss of data near the surface due to the presence of bubbles of air in electrode arms.

The electric field vector can be determined in two ways. Firstly, simultaneous measurements of E1 and E2 can be used to determine the vector. Secondly, a series of E1 and/or E2 values taken at different times within a rotation can be used independently to determine the vector.

The first method has the advantage of providing maximum vertical resolution. With E1, E2 and CC measured twice per second, the electric vector can be determined at this rate, which corresponds to values every 0.5 - 1 m. However, the signals are not sufficiently noise-free to achieve this performance with accuracy. As a result, a number of individual determinations are averaged together.

Figure IV-1. Plot of Raw Data on E1, E2, and CC Channels and of First Difference of Pressure (DP) as the Instrument Nears the Sea Surface for Drop 226

RECORD
NUMBER

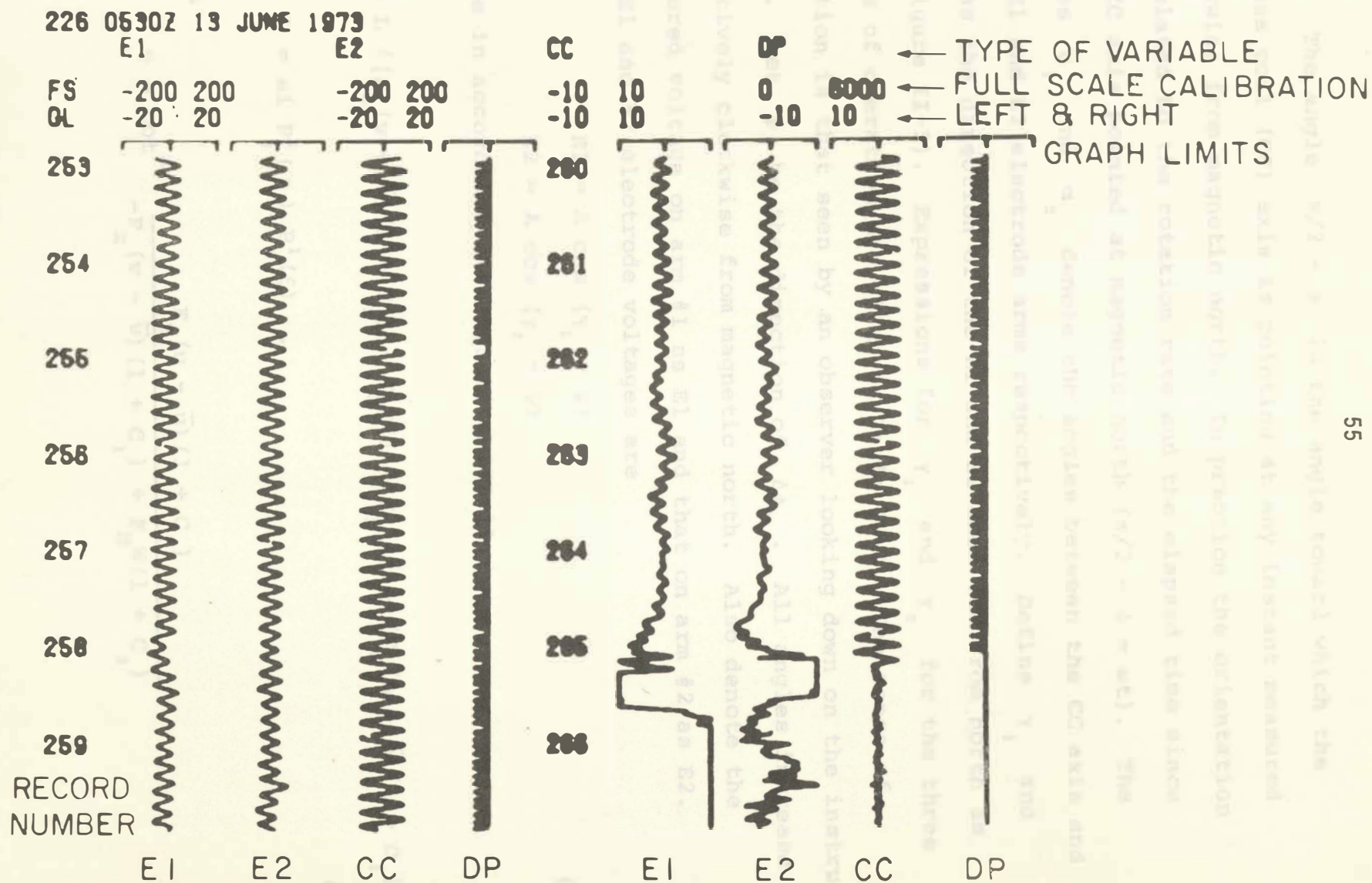


Figure IV-1. Plot of Raw Data on E1, E2, and CC Channels and of First Difference of Pressure (DP) as the Instrument Nears the Sea Surface for Drop 226

The angle $\pi/2 - \phi$ is the angle toward which the compass coil (CC) axis is pointing at any instant measured clockwise from magnetic north. In practice the orientation is related to the rotation rate and the elapsed time since the CC axis pointed at magnetic north ($\pi/2 - \phi = \omega t$). The angles α_1 and α_2 denote the angles between the CC axis and the E1 and E2 electrode arms respectively. Define γ_1 and γ_2 as the direction of the E1 and E2 axes (CW from north as in Figure II-5). Expressions for γ_1 and γ_2 for the three modes of operation are given in Table IV-1. The sense of rotation is that seen by an observer looking down on the instrument. Let ψ be the direction of $\Delta\phi_m$. All angles increase positively clockwise from magnetic north. Also denote the measured voltage on arm #1 as E1 and that on arm #2 as E2. The E1 and E2 electrode voltages are

$$\begin{aligned} E1 &= A \cos (\gamma_1 - \psi) \\ E2 &= A \cos (\gamma_2 - \psi) \end{aligned} \quad (IV-1)$$

where in accordance with Equation III-11:

$$A = L \{ [F_Z (v - \bar{v}) (1 + C_1) - F_H W (1 + C_2)]^2 + [F_Z (u - \bar{u}) (1 + C_1)]^2 \}^{1/2} \quad (IV-2)$$

$$\text{and } L = a_i P_1^1(\eta) P_1^1(\xi) .$$

Then

$$\psi = \cot^{-1} \frac{F_Z (u - \bar{u}) (1 + C_1)}{-F_Z (v - \bar{v}) (1 + C_1) + F_H W (1 + C_2)} \quad (IV-3)$$

TABLE IV-1

Mode of Operation	Sense of Rotation As Viewed From Above	For E1 γ_1	For E2 γ_2
Down: Inverting	CW	$\omega t - \alpha_1$	$\pi + \omega t - \alpha_2$
Down: Non-Inverting	CW	$\omega t + \alpha_1$	$\omega t + \alpha_2$
Up	CCW	$2\pi - \omega t + \alpha_1$	$2\pi - \omega t + \alpha_2$

ω = rotation rate

t = elapsed time since CC detected north

Solving for ψ in terms of the measured E1 and E2 yields

$$\psi = \tan^{-1} \left[\frac{E2 - E1}{E1 + E2} \cot \frac{1}{2} (\gamma_2 - \gamma_1) \right] + \frac{\gamma_1 + \gamma_2}{2} \quad (\text{IV-4})$$

and substituting this value into the expression for E1 or E2 determines A.

The second method determines the amplitudes of E1 and E2 and the phase differences between CC and E1 and E2. A time series of simultaneous values of CC, E1 and E2 corresponding to about 1-2 rotations (~40 values or 20 seconds) is used. The CC values are first processed to determine the exact frequency of rotation. Then each signal is fit in a least-square procedure to the equation

$$CC = a \sin \omega t + b \cos \omega t + c + dt \quad (\text{IV-5})$$

The c and d coefficients eliminate DC offsets and linear trends from the input series. These effects occasionally arise from drift, DC offsets and recovery from overload within the bandpass filters.

Let

$$A_c = \sqrt{a^2 + b^2}$$

$$\beta_c = \tan^{-1} a/b$$

The first least-square fit on CC is made using an assumed frequency, ω_0 . The fit is calculated on n cycles of CC and then on the next n cycles, yielding β'_c and β''_c respectively.

If $|\beta''_C - \beta'_C| > n\epsilon$, where ϵ is usually chosen to be 1 or 2 degrees, then the fit is repeated using a corrected frequency given by

$$\omega_1 = \omega_0 \left(1 - \frac{\beta''_C - \beta'_C}{2n\pi} \right) . \quad (\text{IV-6})$$

Again the new value of $\beta''_C - \beta'_C$ is examined and if greater in magnitude than $n\epsilon$, the procedure is repeated. The true frequency is obtained usually after 2 or 3 iterations. The same procedure is applied to E1 and E2 to obtain (A_1, β_1) and (A_2, β_2) . The phases are all relative to the arbitrary choice of the first values used. This is of no consequence since what is desired is $\beta_1 - \beta_C$ and $\beta_2 - \beta_C$. Note that $\beta_1 - \beta_C + 90^\circ =$ angle between E1 and north measured in the sense of rotation. Likewise for $\beta_2 - \beta_C + 90^\circ$. The 90° is required because CC always has its positive peak 90° after passing through magnetic north. Table IV-2 presents relations used to determine ψ .

After the amplitude and direction of the electric vector are determined, it is necessary to eliminate the contribution due to $F_H W$. The corrected east and north electric components are

$$\begin{aligned} e1 &= A_1 \sin \psi_1 - LF_H W(1 + C_2) \\ &= -F_Z L(v - \bar{v})(1 + C_1) \end{aligned} \quad (\text{IV-7})$$

$$\begin{aligned} n1 &= A_1 \cos \psi_1 \\ &= F_Z L(u - \bar{u})(1 + C_1) \end{aligned} \quad (\text{IV-8})$$

TABLE IV-2

Mode of Operation	Sense of Rotation As Viewed From Above	For E1	For E2
		ψ_1	ψ_2
Down: Inverting	CW	$\beta_1 - \beta_C + 90^\circ - \alpha_1$	$\beta_2 - \beta_C + 90^\circ - \alpha_2$
Down: Non-Inverting	CW	$\beta_1 - \beta_C + 90^\circ + \alpha_1$	$\beta_2 - \beta_C + 90^\circ + \alpha_2$
Up	CCW	$360^\circ - \beta_1 + \beta_C - 90^\circ + \alpha_1$	$360^\circ - \beta_2 + \beta_C - 90^\circ + \alpha_2$

Hence

$$u - \bar{u} = \frac{nl}{F_z(1 + C_1)L} \quad (\text{IV-9})$$

$$v - \bar{v} = - \frac{el}{F_z(1 + C_1)L} \quad (\text{IV-10})$$

Determination of α_1 and α_2

The orientations of the E1 and E2 electrode arms with respect to CC are defined as α_1 and α_2 . These angles can be mechanically determined to an uncertainty of a degree or two. However, the resulting uncertainties produce systematic errors of the order of 1 cm/s. These errors are particularly evident when velocity profiles from E1 and E2 are compared and when E1 and E2 down are compared with up. It is possible to estimate α_1 and α_2 using non-inverting profiles.

Suppose α_1 and α_2 are the true angles and ϵ_1 and ϵ_2 are the unknown errors. The apparent electric field directions are ψ'_1 and ψ'_2 . Recall that Equations IV-7 & 8 state that

$$A_1 \sin \psi'_1 = - F_z L(v - \bar{v})(1 + C_1) + F_H L W(1 + C_2) \quad (\text{IV-11})$$

and

$$A_1 \cos \psi'_1 = F_z L(u - \bar{u})(1 + C_1) .$$

A useful relation is that

$$\begin{aligned} A_1 \sin (\psi_1 + \varepsilon_1) &= A_1 \sin \psi_1 \cos \varepsilon_1 \\ &+ A_1 \cos \psi_1 \sin \varepsilon_1 . \end{aligned}$$

Let F'_H , W' , L' and C'_2 be the values assumed in processing.

On a down inverting drop $\psi'_1 = \psi_1 - \varepsilon_1$ and the electric field measured has components e_1 and n_1 given by

$$\begin{aligned} e_1 &= -F_Z L(v-\bar{v})(1+C_1) \cos \varepsilon_1 + F_H L W^D (1+C_2) \cos \varepsilon_1 \\ &- F_Z L(u-\bar{u})(1+C_1) \sin \varepsilon_1 - F'_H L' W'^D (1+C'_2) \end{aligned} \quad (IV-12)$$

$$\begin{aligned} n_1 &= +F_Z L(u-\bar{u})(1+C_1) \cos \varepsilon_1 + F_H L W^D (1+C_2) \sin \varepsilon_1 \\ &- F_Z L(v-\bar{v})(1+C_1) \sin \varepsilon_1 \end{aligned}$$

On down non-inverting and up profiles (for up-change W^D to W^U),

$\psi'_1 = \psi_1 + \varepsilon_1$ and the equations for e_1 and n_1 are

$$\begin{aligned} e_1 &= -F_Z L(v-\bar{v})(1+C_1) \cos \varepsilon_1 + F_H L W^D (1+C_2) \cos \varepsilon_1 \\ &+ F_Z L(u-\bar{u})(1+C_1) \sin \varepsilon_1 - F'_H L' W'^D (1+C'_2) \end{aligned} \quad (IV-13)$$

$$\begin{aligned} n_1 &= +F_Z L(u-\bar{u})(1+C_1) \cos \varepsilon_1 - F_H L W^D (1+C_2) \sin \varepsilon_1 \\ &+ F_Z L(v-\bar{v})(1+C_1) \sin \varepsilon_1 \end{aligned}$$

Thus the difference between e_l measured on corresponding portions of down non-inverting and up profiles (assuming $u^D, v^D = u^U, v^U$ a condition valid only for small time differences) is

$$\begin{aligned} \Delta e_l = & -F_H L (|W^D| + |W^U|) (1+C_2) \cos \varepsilon_1 \\ & + F_H' L' (|W^D| + |W^U|) (1+C_2') \end{aligned} \quad (\text{IV-14})$$

Similarly,

$$\Delta n_l = F_H L (|W^D| + |W^U|) (1+C_2) \sin \varepsilon_1 .$$

These relations not only allow ε_1 to be determined but also the assumed product $F_H' L' (1+C_2') (|W^D| + |W^U|)$ to be compared with the measured product given by $\partial \Delta n_l / \partial \varepsilon_1$. If these two values are different, then there is an error in one or more of the factors.

In the case of an inverting drop:

$$\begin{aligned} \Delta e_l = & -F_H L (|W^D| + |W^U|) (1+C_2) \cos \varepsilon_1 \\ & + F_H' L' (|W^D| + |W^U|) (1+C_2') \\ & - 2F_Z L (u - \bar{u}) (1+C_1) \sin \varepsilon_1 \end{aligned} \quad (\text{IV-15})$$

$$\begin{aligned} \Delta n_l = & -L \{ 2F_Z (v - \bar{v}) (1+C_1) + F_H (|W^D| - |W^U|) \cdot \\ & (1+C_2) \} \sin \varepsilon_1 . \end{aligned}$$

It is possible but unlikely that the quantity in braces is zero, so the ε_1 null can be determined using Δn_l .

Quality Control and Graphical Analysis

The quality of the data is checked during the computer fitting procedure and data points are eliminated which fail certain statistical tests.

To prevent the calculation of velocity components from poor data, several tests are applied to the data. After a fit has been made, the fit is subtracted from the original data. The standard deviation, σ , of the residue series is computed. Then each point in the residue series is examined and flagged if greater in value than $m\sigma$ where m is usually 2.0-2.4. The values in the original series corresponding to the flagged residues are removed from the series. The least-square fit is then applied again on the reduced series. The residues are examined and additional points eliminated. This procedure continues until all remaining values (1) satisfy the $m\sigma$ criteria or (2) four iterations have been performed or (3) more than 1/3 of the original data has been eliminated.

For a variable's fit to be accepted and used, the standard deviation of the residue, σ , must be less than a maximum acceptable value, and more than two thirds of the data must have been used.

In the case of CC, E1 and E2 the fit is to the sinusoid, mean and trend. However, if CC does not satisfy all tests, then no fit is made on E1 and E2 and no velocity estimates are produced.

The temperature, pressure and electrical conductivity values are fitted to a mean and trend. The residues are tested in the same fashion as for CC, E1 and E2; bad values are eliminated and the resulting series tested for overall quality.

Standard Printed and Graphed Analysis

After recovery of the EMVP, the raw data is usually plotted as shown in Figure IV-1. Such plots reveal the quality of the data and may indicate that special processing is necessary.

Next the data is processed under the analysis and quality control procedures already outlined. A listing such as Figure IV-2 of the computed velocity values for E1 (VE & VN), E2 (VE2&VN2), vertical fall speed (W) and rotation period (PER) versus pressure is made. Since the calculations are time consuming on the rather slow shipboard computer, velocity is computed over 50-60 dbar intervals. A punched tape is also produced containing the same information as being listed.

The punched paper tape is then used to produce a computer generated plot such as shown in Figure IV-3. Either or both velocity profiles (E1 and/or E2) can be plotted as either cartesian (east and north) or polar (speed and direction) variables. The plots can be of the individual data points with or without connecting lines between points.

After the cruise the raw data tapes (7 track or cassette) are reread and transferred to a new format (Maltais, 1969) onto a 9 track magnetic tape. The 9 track tape is processed by a program called QDEM. Although velocity, temperature, etc. profiles are computed and listed by QDEM, the main purpose of this program is to fit the data to the analysis functions (e.g. sinusoids and linear trends) by the least-square editing scheme described earlier. The coefficients of the fit are stored on a new

202 E118 1025 24 MAY 1973 MODE F6 CENTER													
	PRES	VE	VN	SPD	DIR	W	PER	VE2	VN2	SPD2	DIR2		
S 90	-14.4	-24.9	28.8	210	1.26	4.41R	7	-12.8	-25.5	28.5	207		3
S 154	-2.7	-17.8	18.0	189	1.26	4.39R	8	-2.3	-17.3	17.4	188		4
S 218	-2.7	-17.5	17.7	189	1.25	4.41R	9	-2.4	-16.9	17.0	188		5
S 282	-4.4	-11.0	11.0	182	1.24	4.41R	10	3	-10.0	10.0	178		6
S 346	-2.5	-10.0	10.3	194	1.25	4.41R	11	-1.8	-9.2	9.4	191		7
S 410	-5.0	-5.6	7.5	222	1.25	4.42R	12	-4.7	-4.9	6.8	224		8
S 474	-5.4	-1.6	5.6	254	1.26	4.40R	13	-5.0	-1.1	5.1	257		9
S 538	-4.6	2.0	5.0	293	1.26	4.42R	14	-4.2	2.5	4.8	301		10
S 603	-.4	-1.6	1.6	194	1.26	4.44R	15	.0	-.9	.9	178		11
S 667	-3.8	-.1	3.8	268	1.26	4.44R	16	-3.2	.5	3.2	280		12
S 731	-2.7	.2	2.7	275	1.26	4.45R	17	-2.5	.8	2.6	287		
S 795	-2.8	-4.7	5.4	211	1.26	4.46R	18	-2.5	-4.0	4.8	212		
S 859	-1.2	-5.7	5.8	191	1.25	4.47R	19	-.8	-5.1	5.2	188		
S 923	-.8	-.2	.8	258	1.25	4.48R	20	-.4	.3	.5	306		
S 987	3.5	1.4	3.8	68	1.26	4.49R	21	3.8	1.9	4.3	63		
S1051	4.1	-.4	4.1	96	1.25	4.49R	22	4.2	.2	4.2	88		
S1114	-1.6	-2.1	2.7	218	1.25	4.48R	23	-1.3	-1.3	1.9	225		
S1178	-4.0	1.8	4.4	295	1.25	4.49R	24	-3.4	2.1	4.0	303		
S1242	-2.7	1.4	3.1	298	1.26	4.48R	25	-2.4	1.8	3.0	307		
S1306	-.7	6.7	6.7	354	1.26	4.49R	26	-.5	7.1	7.1	356		
S1370	2.2	5.0	5.5	24	1.25	4.50R	27	2.4	5.6	6.1	23		
S1434	4.2	.0	4.2	89	1.25	4.49R	28	4.5	.5	4.5	84		
S1498	4.6	1.3	4.8	74	1.25	4.52R	29	5.0	1.8	5.3	70		
S1561	4.4	1.7	4.7	69	1.25	4.51R	30	4.5	2.5	5.2	61		
S1625	2.2	-.4	2.2	101	1.24	4.53R	31	2.3	.0	2.3	90		
S1689	-.3	1.1	1.1	347	1.25	4.51R	32	-.1	1.8	1.8	357		
S1753	-.8	4.0	4.1	349	1.24	4.52R	33	-.5	4.5	4.5	353		
S1816	-.6	5.4	5.4	354	1.25	4.51R	34	-.3	6.2	6.2	357		
S1880	1.7	6.0	6.2	16	1.26	4.53R	35	1.8	6.6	6.9	16		
S1944	4.1	4.5	6.2	42	1.26	4.54R	36	4.2	5.3	6.8	38		
S2008	3.1	2.4	3.9	53	1.26	4.53R	37	3.4	2.9	4.4	50		
S2072	1.7	.8	1.8	65	1.24	4.55R	38	2.0	1.3	2.4	56		
S2136	.9	.0	.9	90	1.26	4.54R	39	1.2	.6	1.3	62		
S2199	.3	1.0	1.0	18	1.25	4.54R	40	.4	1.6	1.6	16		
S2263	.6	.1	.6	78	1.25	4.52R	41	.9	1.0	1.3	41		
S2327	1.8	.8	2.0	66	1.25	4.56R	42	2.0	1.6	2.6	52		
S2390	.6	1.0	1.2	29	1.25	4.56R	43	.8	1.7	1.9	26		
S2454	.5	.8	.9	30	1.26	4.56R	44	.9	1.7	1.9	27		
S2518	1.1	1.9	2.2	29	1.25	4.55R	45	1.2	2.4	2.7	27		
S2582	2.4	2.9	3.7	40	1.25	4.56R	46	2.5	3.5	4.3	35		
S2645	1.9	3.1	3.7	31	1.25	4.55R	47	2.0	3.7	4.2	29		
S2709	2.0	3.6	4.1	28	1.25	4.57R	48	2.2	4.4	4.9	27		
S2773	.6	3.5	3.6	10	1.25	4.60R	49	1.0	4.5	4.6	13		
S2836	.2	1.8	1.8	6	1.23	4.58R	50	.5	2.7	2.7	11		
S2899	.8	1.7	1.9	26	1.25	4.56R	51	1.1	2.3	2.5	25		
S2963	.4	1.4	1.4	14	1.24	4.60R	52	.5	2.3	2.3	13		
S3026	.8	2.8	2.9	16	1.24	4.60R	53	1.0	3.5	3.7	16		
S3089	1.0	3.7	3.8	16	1.24	4.60R	54	1.2	4.3	4.4	15		
S3152	1.2	3.6	3.8	18	1.24	4.60R	55	1.4	4.5	4.7	17		
S3216	2.2	3.2	3.9	34	1.24	4.60R	56	2.4	3.9	4.6	31		
S3279	1.9	2.7	3.3	35	1.23	4.63R	57	2.2	3.4	4.0	33		
S3341	2.9	1.5	3.3	62	1.23	4.61R	58	2.9	2.3	3.7	51		
S3404	2.7	2.2	3.5	51	1.23	4.62R	59	3.0	3.0	4.2	45		
S3467	2.6	3.5	4.4	37	1.23	4.62R	60	2.7	4.1	4.9	34		
S3530	3.5	4.0	5.3	42	1.23	4.62R	61	4.0	4.8	6.2	40		
S3592	2.9	3.1	4.2	43	1.23	4.62R	62	2.9	3.8	4.8	38		
S3655	1.7	1.9	2.5	43	1.23	4.64R	63	1.7	2.4	2.9	36		

PRINTED IN U.S.A.

Figure IV-2. List of Velocity Profile Values for Drop 202 as Computed by Shipboard Computer System

202 E118 DOWN SIN FT

NORTH

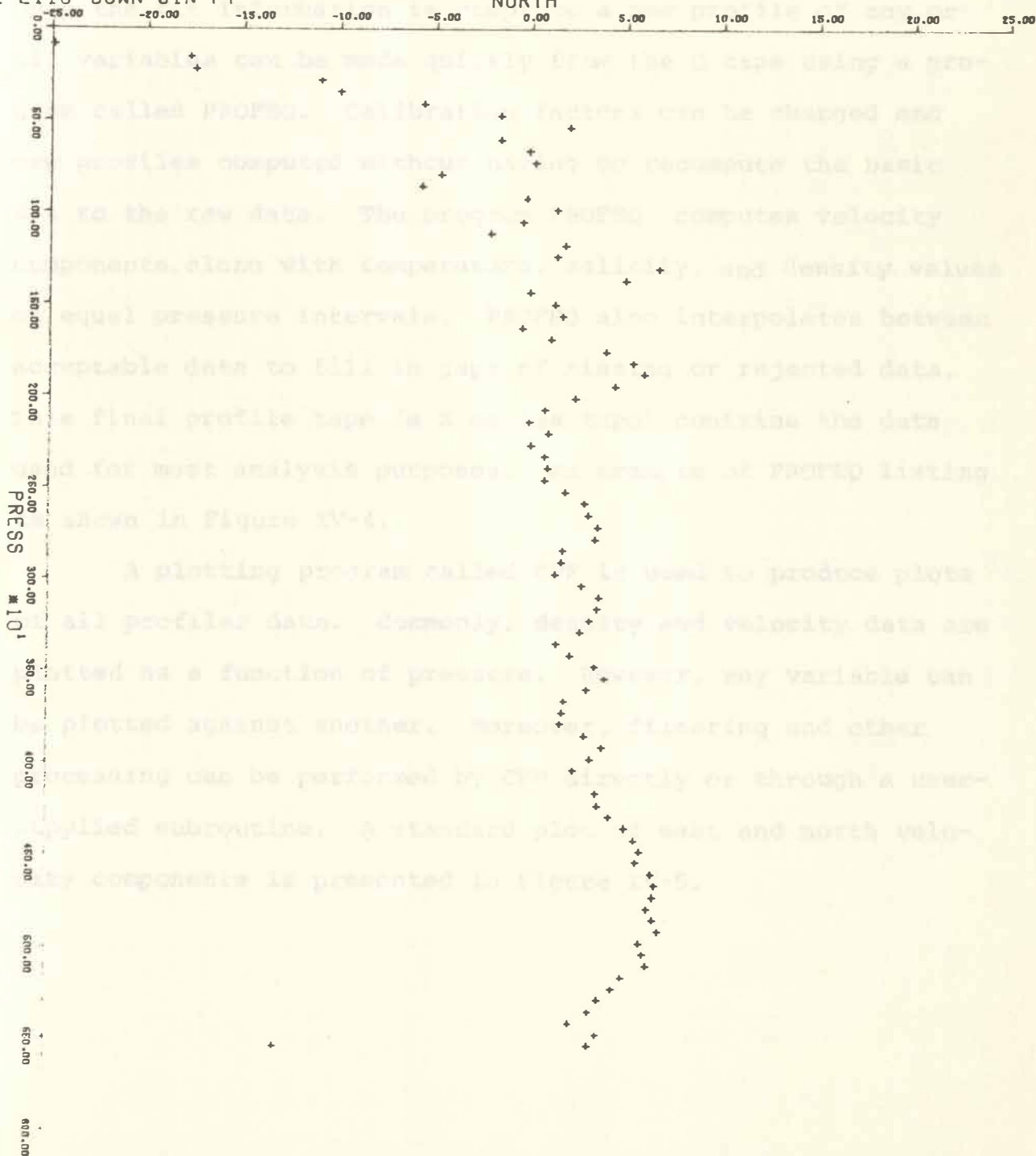


Figure IV-3. Plot of North Component of the Velocity Profile for Drop 202 as Produced by Shipboard Computer System

data tape (a Q series tape). The fit does not require any calibration information but does require much computer time. Once the fit information is complete a new profile of any or all variables can be made quickly from the Q tape using a program called PROFEQ. Calibration factors can be changed and new profiles computed without having to recompute the basic fit to the raw data. The program PROFEQ computes velocity components, along with temperature, salinity, and density values on equal pressure intervals. PROFEQ also interpolates between acceptable data to fill in gaps of missing or rejected data. This final profile tape (a Z series tape) contains the data used for most analysis purposes. An example of PROFEQ listing is shown in Figure IV-4.

A plotting program called CPP is used to produce plots of all profiler data. Commonly, density and velocity data are plotted as a function of pressure. However, any variable can be plotted against another. Moreover, filtering and other processing can be performed by CPP directly or through a user-supplied subroutine. A standard plot of east and north velocity components is presented in Figure IV-5.

REL	PRES	FALL	EAST1	NORT1	SPD1	DIR1	EAST2	NORT2	SPD2	DIR2	TEMP	COND	SALT	SIG=T	SIG=N	BRUNT	TIME
	DBAR	CM/S	CM/S	CM/S	CM/S	DEG	CM/S	CM/S	CM/S	DEG	DEG C	MMH0	PPT	MG/CC	MG/CC1	MINS	SECONDS
1	0	-124	-8.9	-34.2	35.3	194.5	-12.1	-33.2	35.4	200.0	21.957	41.039	28.103	22.576	19.034	149.0	.000
2	10	-124	-8.9	-34.21	35.3	194.5	-12.1	-33.2	35.4	200.0	21.957	41.039	28.103	22.576	19.034	149.0	.0001
3	20	-124	-8.9	-34.21	35.3	194.5	-12.1	-33.2	35.4	200.0	21.957	41.039	28.103	22.576	19.034	149.0	.000
4	30	-124	-8.9	-34.21	35.3	194.5	-12.1	-33.2	35.4	200.0	21.957	41.039	28.103	22.576	19.034	149.01	.0001
5	40	-124	-8.9	-34.21	35.3	194.5	-12.1	-33.2	35.4	200.0	21.957	41.039	28.103	22.576	19.034	149.0	.0001
6	50	-124	-8.9	-34.21	35.3	194.5	-12.1	-33.2	35.4	200.0	21.957	41.039	28.103	22.576	19.034	149.0	.0001
7	60	-124	-8.0	-34.11	35.0	193.3	-11.3	-33.3	35.2	198.7	21.957	40.981	28.059	22.541	19.000	138.7	1.513
8	70	-123	-3.6	-33.4	33.6	186.2	-7.12	-33.9	34.6	191.9	21.957	40.678	27.825	22.353	18.824	84.2	9.487
9	80	-123	-4.0	-30.31	30.5	187.5	-6.6	-29.0	29.8	192.9	21.699	40.402	27.777	22.314	18.857	29.7	17.468
10	90	-124	-2.9	-28.81	29.0	185.7	-4.8	-27.7	28.1	189.9	21.473	40.187	27.754	22.296	18.900	13.5	25.465
11	100	-124	-1.5	-27.51	27.5	183.2	-3.2	-26.8	27.0	186.9	21.286	40.013	27.738	22.283	18.937	15.0	33.461
12	110	-124	-.8	-24.71	24.8	181.8	-2.9	-23.8	24.0	187.0	21.116	39.856	27.723	22.271	18.970	15.9	41.447
13	120	-1231	.8	-20.2	20.2	177.71	-2.5	-19.7	19.9	187.2	20.935	39.691	27.710	22.260	19.007	15.5	49.436
14	130	-124	2.6	-18.41	18.6	171.9	.3	-17.61	17.6	179.1	20.741	39.511	27.692	22.246	19.044	15.1	57.421
15	140	-124	5.0	-18.2	18.9	164.6	2.7	-17.9	18.1	171.4	20.543	39.323	27.671	22.229	19.080	14.9	65.418
16	150	-124	6.1	-18.7	19.6	161.9	3.7	-18.8	19.2	169.0	20.360	39.152	27.653	22.214	19.113	15.4	73.423
17	160	-124	6.1	-19.4	20.3	162.6	3.6	-19.5	19.9	169.1	20.209	39.018	27.643	22.206	19.1431	17.1	81.4231
18	170	-123	10.4	-21.4	23.8	154.0	7.5	-21.6	22.8	160.8	20.099	38.936	27.648	22.210	19.175	19.8	89.381
19	180	-124	10.4	-22.3	24.6	154.8	8.1	-22.3	23.7	160.1	19.977	38.840	27.648	22.211	19.206	19.3	97.333
20	190	-124	8.8	-21.2	23.0	157.4	6.9	-21.2	22.3	162.0	19.817	38.702	27.641	22.204	19.241	17.3	105.325
21	200	-123	6.7	-19.5	20.6	161.1	5.0	-19.5	20.1	165.6	19.621	38.524	27.625	22.192	19.278	15.3	113.331
22	210	-122	5.2	-18.5	19.2	164.2	3.5	-18.1	18.4	169.0	19.406	38.324	27.603	22.174	19.3141	14.5	121.335
23	220	-122	6.0	-18.7	19.6	162.2	4.0	-18.11	18.5	167.6	19.216	38.142	27.579	22.155	19.343	15.4	129.376
24	230	-123	4.3	-18.8	19.3	167.2	2.4	-18.3	18.5	172.5	19.071	38.011	27.567	22.145	19.369	17.3	137.431
25	240	-124	6.5	-16.3	17.5	158.1	4.7	-15.7	16.3	163.4	18.932	37.892	27.560	22.140	19.398	18.1	145.456
26	250	-123	9.0	-13.5	16.2	146.2	7.0	-13.0	14.8	151.5	18.789	37.768	27.551	22.133	19.4261	18.0	153.495
27	260	-122	8.9	-12.1	15.0	143.7	6.8	-11.9	13.7	150.2	18.642	37.637	27.539	22.123	19.452	17.01	161.565
28	270	-122	7.1	-10.5	12.7	145.9	5.6	-10.5	11.9	151.9	18.511	37.520	27.528	22.114	19.474	18.8	169.601
29	280	-122	6.2	-10.5	12.12	149.6	4.8	-9.9	11.0	154.2	18.394	37.413	27.516	22.104	19.493	19.7	177.693
30	290	-123	4.5	-12.12	13.0	159.9	3.5	-10.9	11.4	162.2	18.282	37.310	27.503	22.094	19.510	20.3	185.780
31	300	-123	3.4	-13.4	13.8	165.8	2.6	-12.13	12.5	168.1	18.182	37.217	27.490	22.084	19.524	21.6	193.801
32	310	-123	3.4	-13.2	13.6	165.5	2.5	-13.1	13.3	169.2	18.101	37.142	27.480	22.076	19.536	23.9	201.772
33	320	-124	3.7	-12.5	13.1	163.4	2.9	-11.9	12.2	166.5	18.035	37.084	27.473	22.070	19.546	26.6	209.806
34	330	-124	5.1	-12.5	13.5	158.0	3.6	-11.9	12.4	163.1	17.968	37.020	27.462	22.061	19.553	26.4	217.772
35	340	-123	4.5	-11.8	12.7	159.0	3.0	-11.3	11.7	165.0	17.905	36.961	27.452	22.053	19.560	27.2	225.763
36	350	-123	4.3	-11.2	12.0	159.0	2.8	-10.7	11.1	165.4	17.846	36.906	27.444	22.046	19.5681	28.0	233.779
37	360	-123	4.8	-10.9	12.0	156.3	3.2	-10.2	10.6	162.7	17.786	36.853	27.437	22.040	19.576	28.2	241.807
38	370	-123	4.3	-10.18	11.7	158.3	2.2	-9.3	9.5	166.5	17.728	36.798	27.427	22.033	19.582	28.3	249.814
39	380	-123	2.0	-8.71	9.0	167.0	.2	-8.21	8.2	178.5	17.668	36.741	27.417	22.025	19.588	28.2	257.893
40	390	-122	.6	-8.31	8.3	175.6	-1.1	-7.91	8.0	187.7	17.613	36.687	27.406	22.016	19.593	29.0	265.930
41	400	-123	-.1	-8.0	8.0	180.4	-1.6	-7.61	7.8	191.9	17.556	36.631	27.395	22.007	19.597	29.0	273.945
42	410	-123	-1.3	-7.41	7.4	182.2	-1.7	-7.11	7.3	193.2	17.496	36.575	27.386	22.000	19.604	28.1	281.955
43	420	-124	-.2	-7.13	7.3	181.61	-1.9	-6.71	7.0	195.7	17.434	36.518	27.377	21.993	19.612	27.5	289.969
44	430	-124	.3	-7.61	7.6	177.61	-.8	-6.91	7.0	186.8	17.378	36.467	27.368	21.986	19.618	28.9	297.954
45	440	-123	.7	-7.61	7.6	174.7	-.9	-7.21	7.3	187.3	17.325	36.415	27.357	21.977	19.621	29.9	305.937
46	450	-123	.5	-6.8	6.8	175.4	-1.3	-6.71	6.8	190.7	17.269	36.357	27.344	21.966	19.624	29.4	313.923
47	460	-124	-.5	-5.41	5.4	185.1	-1.9	-5.4	5.7	199.4	17.206	36.291	27.329	21.954	19.626	27.6	321.903
48	470	-124	-2.6	-4.71	5.4	209.1	-3.9	-4.31	5.8	222.2	17.132	36.212	27.309	21.938	19.628	25.7	329.849
49	480	-124	-1.6	-1.71	2.4	223.5	-2.9	-1.51	3.3	242.3	17.061	36.136	27.290	21.923	19.630	25.8	337.820
50	490	-124	-.4	-.61	.7	217.81	-1.9	-.1	1.9	267.3	16.998	36.073	27.276	21.912	19.633	27.5	345.769

Figure IV-4. Listing of Velocity and Density Profile for Drop 202 as Computed by PROFEQ (Salinity and Density Values in Error Due to Broken Liner in Conductivity Sensor)

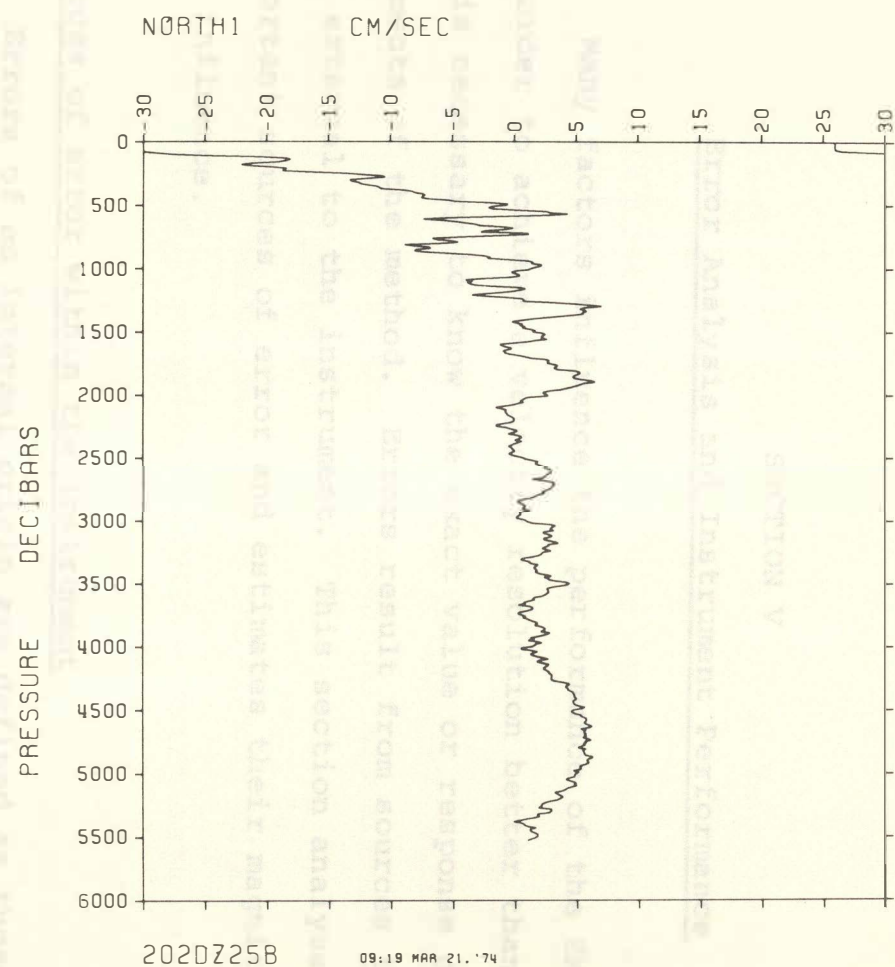
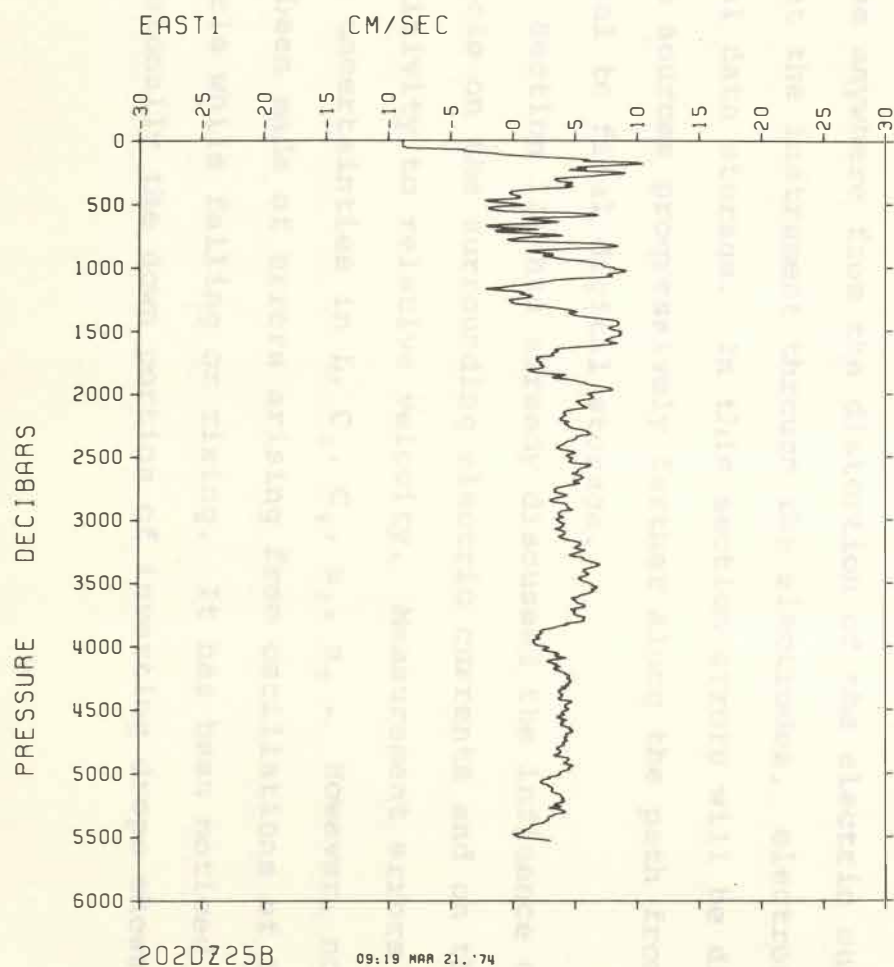


Figure IV-5. Plot of East and North Velocity Components for Drop 202 as Produced by PROFEQ

SECTION V

Error Analysis and Instrument Performance

Many factors influence the performance of the EMVP.

In order to achieve a velocity resolution better than 1 cm/s it is necessary to know the exact value or response of most elements of the method. Errors result from sources internal and external to the instrument. This section analyses the important sources of error and estimates their magnitudes and influence.

Sources of error within the instrument

Errors of an internal origin are defined as those which arise anywhere from the distortion of the electric currents about the instrument through the electrodes, electronics and final data storage. In this section errors will be discussed from sources progressively farther along the path from induced signal to final digital storage.

Section III has already discussed the influence of the vehicle on the surrounding electric currents and on the sensitivity to relative velocity. Measurement errors result from uncertainties in L , C_1 , C_2 , α_1 , α_2 . However, no analysis has been made of errors arising from oscillations of the vehicle while falling or rising. It has been noticed that occasionally the down portion of inverting drops shows more

variability than the corresponding up portion. It seems likely that pendulum-like oscillations occur.

The principal problem with the electrodes arises in their use in the changing temperature and salinity environment during a drop. The salt bridges are effective in eliminating significant salinity errors. The bridges and electrode block reduce the heat flux into the electrodes and the resulting rapid offset variations.

Even under normal conditions the offset of an electrode pair will change. A typical electrode drift rate is about $.1 \mu\text{v/s}$. When the temperature changes, signals will arise due to the difference in temperature between the electrodes and due to the temperature dependence of the offset.

Figure V-1 shows the output of a pair of electrodes within the electrode block and arm when the ambient temperature changed abruptly by 15°C . The test was performed by connecting the two electrode chambers with an external salt bridge. A column of water was temperature-stratified with warm over cold water. After the electrodes came to equilibrium within the warm region, the block was quickly lowered into the cold region.

The result of this test shows that the temperature effect is dominated by the offset. The temperature difference effect should reach a peak and then vanish, while the offset effect should grow as the temperature changes at both electrodes and then levels out at large elapsed time.

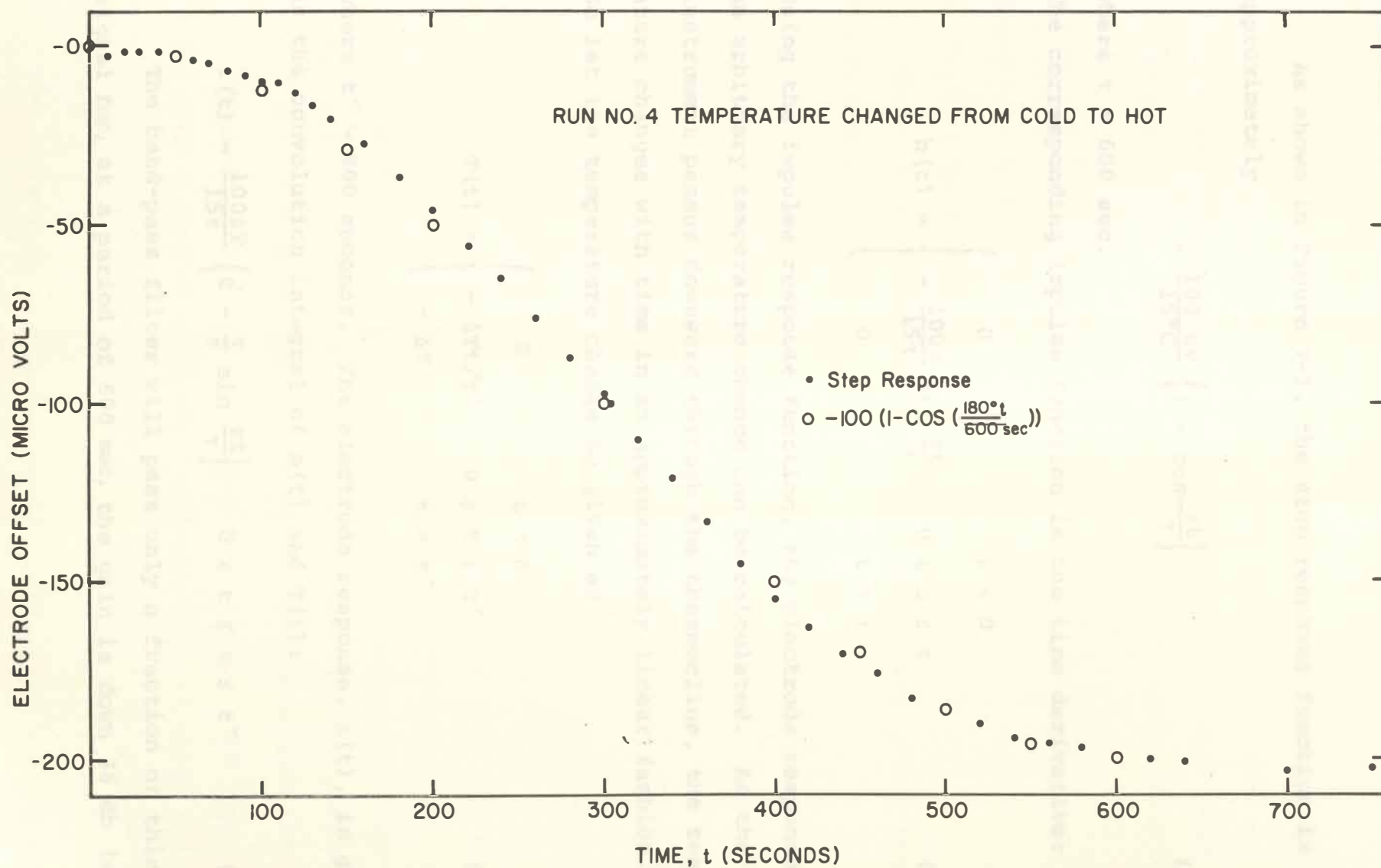


Figure V-1. Electrode Offset Due to Step Change in Ambient Temperature

Fig. As shown in Figure V-1, the step response function is approximately

$$- \frac{100 \mu\text{V}}{15^\circ\text{C}} \left(1 - \cos \frac{\pi t}{\tau} \right) \quad (\text{V-1})$$

where $\tau = 600$ sec.

The corresponding impulse function is the time derivative:

$$h(t) = \begin{cases} 0 & t < 0 \\ - \frac{100\pi}{15\tau} \sin \frac{\pi t}{\tau} & 0 \leq t \leq \tau \\ 0 & t > \tau \end{cases} \quad (\text{V-2})$$

Using the impulse response function, the electrode response to an arbitrary temperature change can be calculated. As the instrument passes downward through the thermocline, the temperature changes with time in an approximately linear fashion.

So let the temperature change be given as

$$T(t) = \begin{cases} 0 & t < 0 \\ - \Delta T t / t' & 0 \leq t \leq t' \\ - \Delta T & t > t' \end{cases} \quad (\text{V-3})$$

where $t' \sim 800$ seconds. The electrode response, $\epsilon(t)$, is given as the convolution integral of $h(t)$ and $T(t)$:

$$\epsilon(t) = \frac{100\Delta T}{15\tau} \left(t - \frac{\tau}{\pi} \sin \frac{\pi t}{\tau} \right) \quad 0 \leq t \leq \tau \leq t' \quad (\text{V-4})$$

The band-pass filter will pass only a fraction of this signal for, at a period of 600 sec, the gain is down 36 db (see

Fig. V-3). The least square fit in processing will further reduce the resulting variance. Even if the filter had no effect, the error due to temperature changes is negligible. To demonstrate this fact, consider a fit over a 20-sec period. Let

$$\varepsilon(t) = \varepsilon_0 + \varepsilon' t + \varepsilon'' t^2 + \dots \quad 0 \leq t \leq 20s \quad (V-5)$$

where $\varepsilon' < \frac{1}{3} \mu V/s$

$$\varepsilon'' < \frac{1}{1200} \mu V/s^2.$$

The variance after the least-square fit (Eq. IV-5) over 20 seconds is

$$\begin{aligned} \sigma^2 &= \frac{1}{20} \int_0^{20} \{\varepsilon(t) - c - dt\}^2 dt \\ &= \frac{\varepsilon'^2 20^2}{30} \\ \sigma &= 1/15 \mu V \end{aligned} \quad (V-6)$$

This level of interference is negligible even without accounting for the extra reduction achieved in the filter.

One problem remains with the present electrode system; the water drains out of electrode block and bridges when brought aboard the ship. When redeployed, trapped air prevents adequate filling of the system at the surface. As a result data are often lost until the ambient pressure reduces the bubbles in size. It is thought that filling the ends of the bridge with a plug of agar would prevent loss of water yet maintain electrical contact between the electrodes and the surrounding sea water.

The resistance of the sea water in the salt bridges changes

from about 500Ω near the surface to about 1000Ω in the cold, deep water. This change causes negligible error in signal into the high impedance pre-amp ($Z_{in} > 50 M\Omega$).

The amplifier system is designed to provide stable gain and phase characteristics with low noise. The principal source of noise is the low-level pre-amp. Figure V-2 presents typical noise tests on currently used pre-amps. The rms noise in the frequency band .01 - 10 Hz is less than $0.1 \mu v$.

The gain and phase response of the amplifiers and filter are shown in Figure V-3. As nearly as possible the CC, E1 and E2 channels have the same phase response. In order to detect accurately the direction of the motional electric field, each signal must have the same phase shift. In this way $\beta_1 - \beta_c$ will be the true relative phase even though E1 and CC are shifted individually. This phase tracking is achieved to $1 - 2^\circ$ at the rotation frequency ($\sim .2$ Hz). However, the difference is still large enough to cause ~ 1 cm/s velocity errors. To avoid this error $\beta_1 - \beta_c$ and $\beta_2 - \beta_c$ are corrected for the actual tracking errors. Figure V-4 presents the relative phase errors.

Another phase error arises due to the fact that E1, E2 and CC are digitized in sequence over a span of 24 ms. Thus E1 is digitized 24 ms before CC. For a rotation rate of 4.8 sec this time difference corresponds to a phase error of 1 part in 200 or about 2° . During analysis the rotation period is used to remove this error.

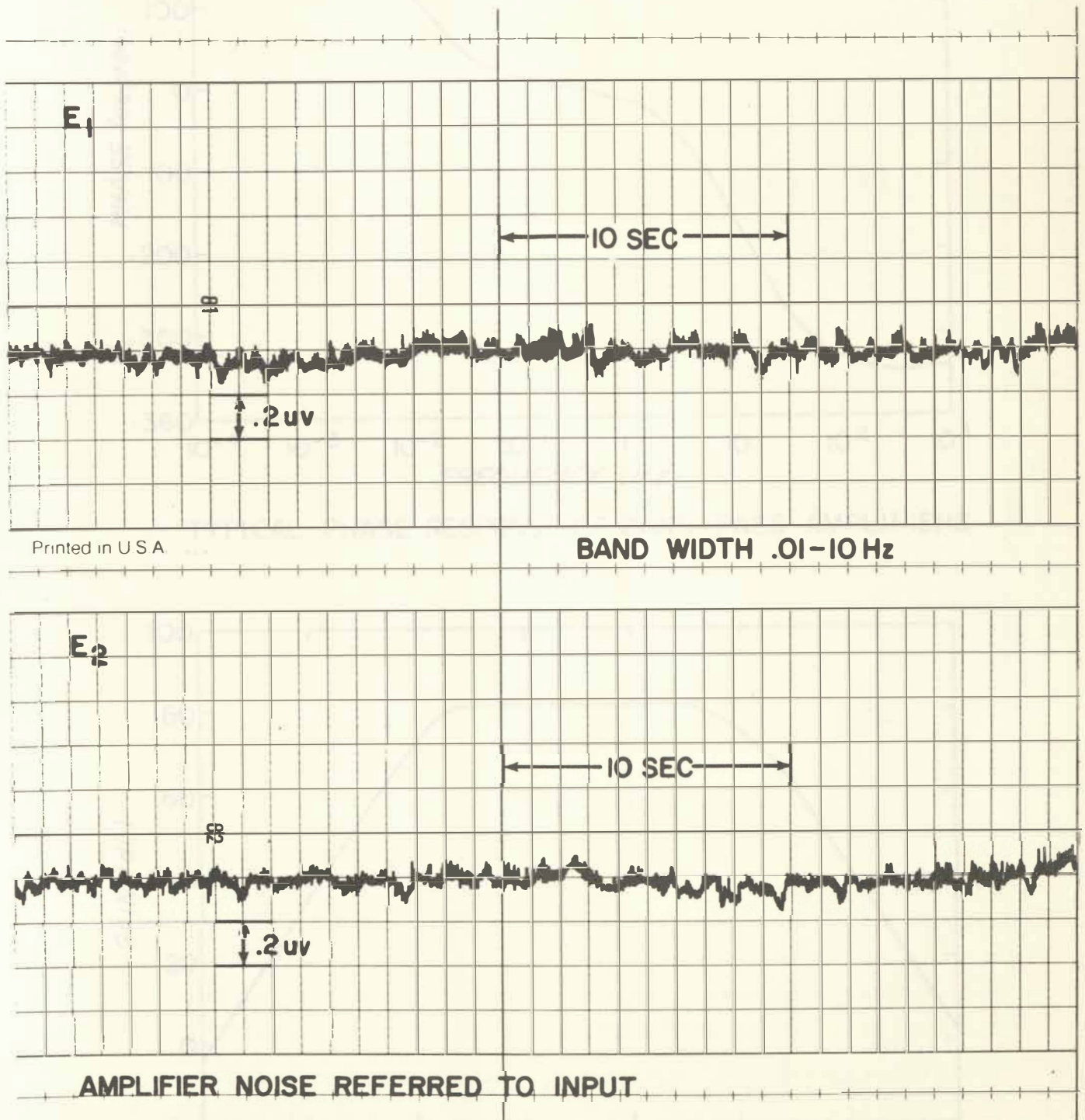
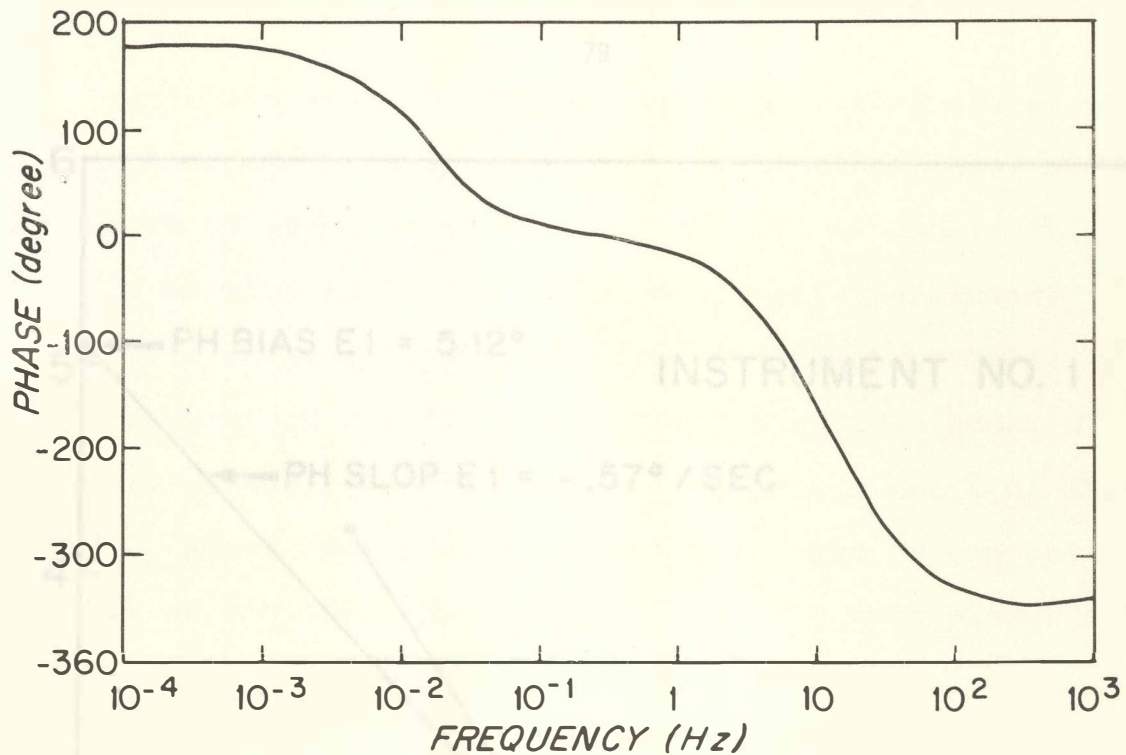
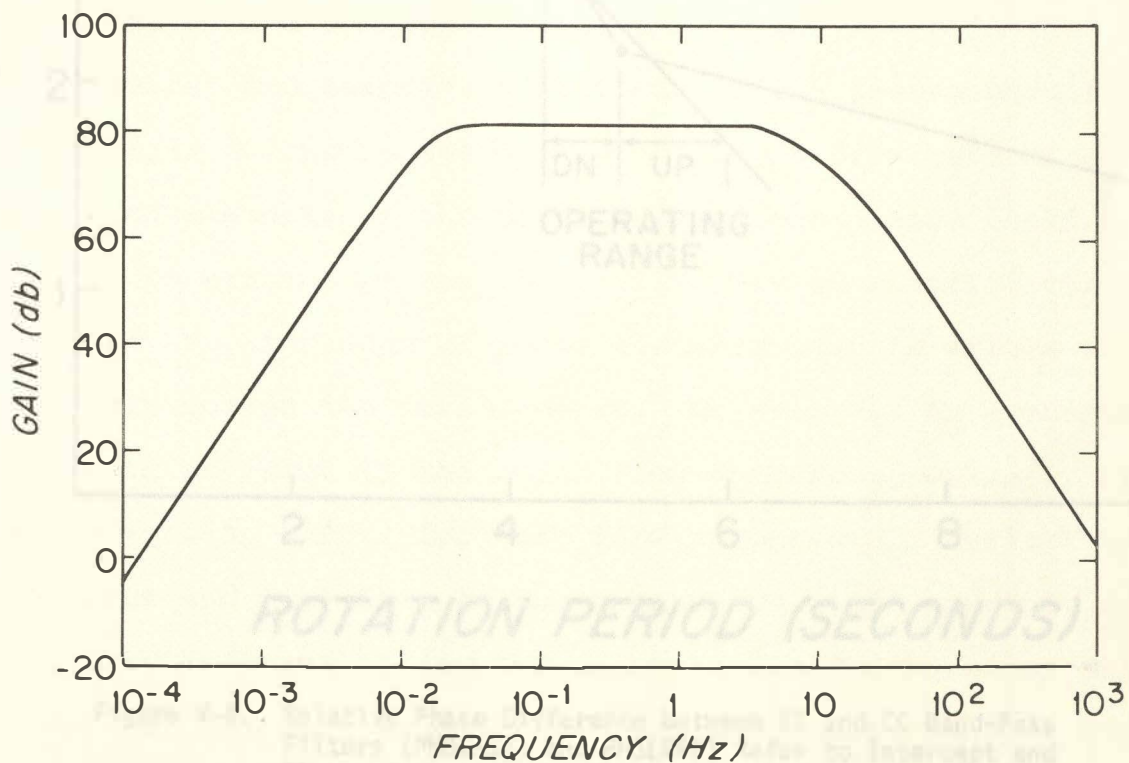


Figure V-2. Noise on E1 and E2 Preamplifier Channels



TYPICAL PHASE RESPONSE OF BAND-PASS AMPLIFIERS



TYPICAL GAIN RESPONSE OF BAND-PASS AMPLIFIERS

Figure V-3. Gain and Phase Response of Band-Pass Amplifiers

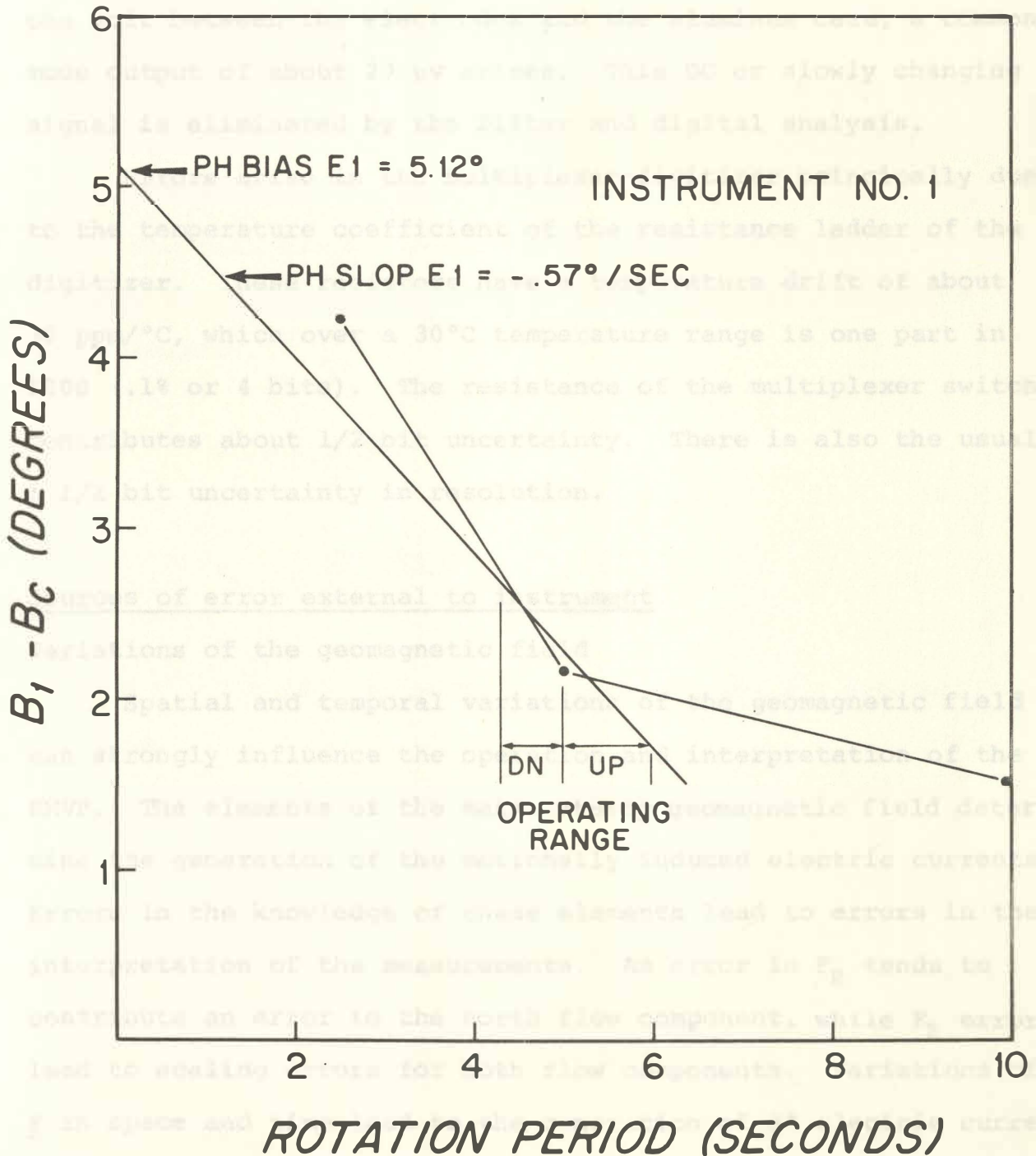


Figure V-4. Relative Phase Difference between E1 and CC Band-Pass Filters (PHBIASE1 and PHSLOPE1 Refer to Intercept and Slope of $B_1 - B_c$ versus Period in the Operating Range)

Due to the electrochemical potential difference of about one volt between the electrodes and the aluminum case, a common mode output of about 20 μv arises. This DC or slowly changing signal is eliminated by the filter and digital analysis.

Errors arise in the multiplexer-digitizer principally due to the temperature coefficient of the resistance ladder of the digitizer. These resistors have a temperature drift of about 30 ppm/ $^{\circ}\text{C}$, which over a 30 $^{\circ}\text{C}$ temperature range is one part in 1000 (.1% or 4 bits). The resistance of the multiplexer switches contributes about 1/2 bit uncertainty. There is also the usual $\pm 1/2$ bit uncertainty in resolution.

Sources of error external to instrument

Variations of the geomagnetic field

Spatial and temporal variations of the geomagnetic field can strongly influence the operation and interpretation of the EMVP. The elements of the main, steady geomagnetic field determine the generation of the motionally induced electric currents. Errors in the knowledge of these elements lead to errors in the interpretation of the measurements. An error in F_H tends to contribute an error to the north flow component, while F_Z errors lead to scaling errors for both flow components. Variations of \underline{F} in space and time lead to the generation of \underline{J}^* electric currents.

Errors in estimating the magnetic field components arise mainly from magnetic anomalies of spatial scales smaller than

detailed on the world charts (H.O. 1700 et seq.) The magnitude of temporal variations is generally less than 1% of the steady field. However, these time variations generate induced electric currents which can be quite large compared with the motionally induced signals.

The main field, approximately that of a magnetic dipole aligned along the axis of rotation, has components or elements:

$$F_H = \frac{M \cos \theta}{r^3} \quad (V-7)$$

$$F_Z = - \frac{2M \sin \theta}{r^3}$$

where $M \doteq 8 \times 10^{15}$ weber-m, θ = latitude and r = geocentric radius.

The variations with depth are small: ($1\gamma = 10^{-5}$ oe = 10^{-9} weber/m²)

$$\frac{\partial F_H}{\partial z} \doteq - 1.4 \times 10^{-6} \cos \theta \text{ weber/m}^2/\text{m}$$

$$\doteq - 1.4 \cos \theta \gamma/100 \text{ m} \quad (V-8)$$

$$\frac{\partial F_Z}{\partial z} \doteq 2.8 \sin \theta \gamma/100 \text{ m}$$

Within a 5 km deep ocean

$$\frac{\Delta F_H}{F_H} \approx \frac{\Delta F_Z}{F_Z} \approx - .25\% \quad (V-9)$$

The horizontal variations are

$$\frac{1}{r} \frac{\partial F_H}{\partial \theta} = \frac{1}{2} F_Z / r \sim - 4\gamma / \text{km} \quad (V-10)$$

$$\frac{1}{r} \frac{\partial F_Z}{\partial \theta} = 2 F_H / r \sim - 8\gamma / \text{km} .$$

An uncertainty in latitude, $\Delta\theta$, leads to

$$\frac{\Delta F_H}{F_H} = - \Delta\theta \tan \theta \quad (V-11)$$

$$\frac{\Delta F_Z}{F_Z} = \Delta\theta \cot \theta .$$

At mid-latitudes ($\theta \approx 40^\circ$) the errors are $\sim 1-2\%$ per degree of latitude. The world charts are contoured every .02 oe and can be scaled to at least .002 oe. If the charts were accurate to .002 oe then $\Delta F_H / F_H \sim 1\%$ and $\Delta F_Z / F_Z \sim .5\%$. However, it is known that the World Chart is not accurate to this extent everywhere.

Small-scale magnetic anomalies exist over many topographic features such as seamounts, islands and submarine ridges. For instance, a fine scale aeromagnetic survey of Plantagenet Bank, 25 nm SW of Bermuda (Young and Kontis, 1964), reveals that the undisturbed field is 4-6% different from the World Chart. Over the Bank itself the errors reach 10-15%. Vertical and horizontal field gradients are 100 times larger than over an undisturbed area.

The magnetic field generated by the motionally induced electric currents has components no larger than .25% of the main geomagnetic field.

Variations in time of the geomagnetic field generate electric fields and currents in the ocean. These magnetotelluric fields depend on the frequency and structure of the source magnetic field and on the depth and electrical conductivity of the ocean crust and mantle.

Magneto-telluric currents represent one of the largest sources of error in the E-M profiling method. These effects are generally not independently measured or easily inferred from land based magnetic measurements.

Cox et al. (1971) and Fonarev (1968) have provided estimates of the electric fields generated by geomagnetic variations. The magnetic variations are described by Chapman and Bartels (1940). Variations having periods

longer than one day generate only weak electric fields ($\ll 1 \text{ mV/km}$). Shorter period variations are responsible for significant electric induction. The major categories for the high frequency variations are the solar-diurnal variations, bay-like disturbances, magnetic storms and short-period variations.

Solar-diurnal variations are always present even on magnetically quiet days. These variations result in electric fields of the order of $3 \times 10^{-2} \text{ mV/km-}\gamma$ in the open ocean. According to Fonarev (1968) the maximum influence of these variations is given in Table V-1.

Bay-like disturbances derive their name from their appearance as bays or gulfs on magnetograms. These events provide mainly horizontal magnetic fields which decrease away from the auroral zone (70°). Frequencies from tens of minutes to a few hours are present. Bay disturbances occur 10 to 40 times per year with an amplitude of 40-100 γ . An estimate of the resulting induction is

$$E = \frac{B}{\mu\sigma H} \quad (V-12)$$

where $\mu = 4\pi \times 10^{-7} \text{ henry/m}$, $\sigma = 2.7 \text{ mho/m}$ and $H = 5 \times 10^3 \text{ m}$. For $B = 40\gamma = 4 \times 10^{-8} \text{ weber/m}^2$, the electric field is

*From Eq. V-12 for water depth of 5km and $\sigma = 2.7 \text{ mho/m}$.

Table V-1

Solar-Diurnal Variations

<u>Latitude</u>	<u>Activity</u>	<u>B, γ</u>	<u>E, mv/km</u>	<u>V, cm/s</u>
<30°	Quiet	30-80	.9-2.4	4.5-12
	Disturbed	60-100	1.8-3.0	9.0-15
30-60	Quiet	15-60	.45-1.8	1.1-4.2
	Disturbed	25-110	.75-3.3	1.9-8.2
>60°	Quiet	90-400	2.7-12	4.6-20
	Disturbed	50-460	1.5-14	2.5-22

Table V-2 (after Fonarev, 1968)

Magnetic Storm Variations*

<u>Latitude</u>	<u>Activity</u>	<u>B, γ</u>	<u>E, mv/km</u>	<u>V, cm/s</u>
<30°	Weak	0-30	0-2	0-9
	Moderate	15-60	1-4	4-18
	Strong	30-90	2-5	9-26
30-60	Weak	40-120	2-7	6-17
	Moderate	70-300	4-16	10-44
	Strong	150-700	9-41	22-103
>60°	Weak	70-600	4-32	7-60
	Moderate	150-900	9-52	15-88
	Strong	900-1500	52-88	88-150

*From Eq. V-12 for water depth of 5km and $\sigma = 2.7$ mho/m.

$$E = 2.4 \text{ mv/km}$$

leading to a velocity error of about 5 cm/s. Since the bay-like disturbances are of very large scale it is possible to estimate the errors, perhaps even to correct the measurements, using landbased magnetic records.

Magnetic storms are more irregular than bay disturbances, often having rapid changes at the commencement over a few hours followed by a gradual recovery over tens of hours. The E/B ratios are as for the bay but the amplitude of B can be much larger, particularly in the auroral zone. According to Fonarev (1968) magnetic storms are as frequent as 20-50 times per year during years of maximum solar activity while 3-5 times fewer in years of minimum activity. The peak-to-peak variations and the expected electric induction and velocity errors are listed in Table V-2.

Short period variations (1-10 min) contribute little induced electric field except in polar regions.

According to Figure 16 of Cox et al. (1971) the electric field has a variance of about 0.1 (mv/km)^2 in the frequency band from 0.1 to 12 CPH. Thus we might expect deviations between down and up profiles of the order of .6 cm/s due to changes in ambient electric field. Over a shorter period, say, 1 to 12 CPH, the variance is about $10^{-2} \text{ (mv/km)}^2$ yielding

a standard deviation of .2 cm/s. It is interesting to note that this estimate of geomagnetically induced noise is comparable to that observed by comparing portions of down and up profiles near the bottom.

Another source of error, but one not due to geomagnetic variations, is that due to the local distortion of the geomagnetic field and the corrosion produced electric field near a large steel vessel. Such influences are difficult to estimate. In general, the instrument is deployed so that it releases buoyancy and starts falling at least 1 ship length away from the support vessel.

Other terms in conversion formula

The velocity profile is computed from the measured electric field using a general conversion equation as derived by Sanford (1971) for broad, low-frequency motions. This expression involves a series of integral and differential operators applied to the velocity field. The relative importance of various terms depends on the kinematics of the flow. Fortunately, the most significant terms in the conversion formula for broad, low-frequency flows involve \vec{v} directly and certain depth-independent terms. This is indeed fortunate because the much smaller, unused terms depend on characteristics of the flow which are not generally measurable or known in sufficient detail.

Another class of important motions is that of internal waves. The electrical response here is very sensitive to the dynamics of the flow. In this case, the conversion formula is again dominated by a term directly involving \underline{y} .

The free-fall probe measures the electric current density within the local surrounding water. The expression for \underline{J}/σ which we will use is

$$\underline{J} = \nabla \times \int_z^0 \sigma \underline{k} \times [(\underline{v} - \bar{\underline{v}}) \times \underline{F}] d\xi - \nabla_H \int_{-H}^z \sigma \underline{k} \cdot \underline{v} \times \underline{F} d\xi + \bar{\underline{J}} \quad (\text{V-13})$$

Then for $\underline{F} = (0, F_Y, F_Z)$ and $\underline{v} = (u, v, w)$ and σ uniform:

$$J_X/\sigma = F_Z(v - \bar{v}) - F_Y w - \frac{\partial}{\partial x} \int_{-H}^z F_Y u d\xi + \bar{J}_X/\sigma \quad (\text{V-14})$$

$$J_Y/\sigma = -F_Z(u - \bar{u}) - \frac{\partial}{\partial y} \int_{-H}^z F_Y u d\xi + \bar{J}_Y/\sigma \quad (\text{V-15})$$

where $\bar{\underline{J}}/\sigma = \text{constant vector independent of depth}$. Since $\nabla \cdot \underline{v} = 0$ everywhere and $w(-H) = 0$ on the seafloor, Equations V-14 and 15 can be rewritten as

$$J_X/\sigma = F_Z v + F_Y \int_{-H}^z \frac{\partial v}{\partial y} d\xi + \text{constant} \quad (\text{V-16})$$

$$J_Y/\sigma = -F_Z u - F_Y \int_{-H}^z \frac{\partial u}{\partial y} d\xi + \text{constant.}$$

As has been previously discussed the measurement of J/σ is interpreted as being due to the first term on the right of V-16. Hence the integral terms represent error contributions which are depth dependent. Estimates of the magnitudes of the integral terms can be made.

Consider a broad, low-frequency flow ($w = 0$) of typical velocity U , width L and depth H . Then

$$J_Y/\sigma \approx -F_Z U \left(1 + \frac{F_Y H}{F_Z L} \right). \quad (V-17)$$

The parameter, $F_Y H/F_Z L$, is a measure of relative error. For example, in the Gulf Stream $F_Y/F_Z = .5$ and $H/L = .1$, leading to an error of 5% or about 1 cm/s for a vertically averaged U of 20 cm/s.

At the opposite end of the frequency spectrum are the internal waves. According to Equation V-16, a plane internal wave propagating in the x direction will result in no measurement error since $\partial/\partial y \equiv 0$. On the other hand, a plane wave propagating in the y direction would produce

$$J_X/\sigma = F_Z v - F_Y w \quad (V-18)$$

$$J_Y/\sigma = 0.$$

Thus in the latter case, an additional electric current arises from the vertical velocity. The magnitude of this term relative to the first term becomes large as $\omega \rightarrow N$ but decreases rapidly at lower frequencies. From internal wave theory the ratio of w and u behaves as

$$w/u = \sqrt{\frac{\omega^2 - f^2}{n^2 - \omega^2}}. \quad (V-19)$$

The absolute error depends on the magnitude of w near N . In an absolute sense the contribution of this error term is very small compared with that due to v (and u) at all other frequencies.

The contribution due to \bar{J} currents can be large only for large-scale organized flows such as the tides in the open ocean or meanders of the Gulf Stream or in shallow water over highly conducting sediments. These electric currents produce electric fields which are independent of depth. As in the case of geomagnetic variations the character of these fields depends on the velocity field structure and period, and on the depth and electrical conductivity of the ocean crust and mantle.

In general, the magnitude should be less than 1 mv/km except in regions where the flow is moving over variable bottom topography. Sanford (1971) discusses this term in more detail.

Sensitivity Analysis

The purpose of this subsection is to determine the sensitivity of the method toward errors in the knowledge or measurement of each parameter and variable required to calculate a velocity profile. Given the conversion formulas which specify the influence of each term and the range of uncertainty, it is now possible to estimate expected method errors.

According to equations IV-7 through 10:

$$u - \bar{u} = R(A_1, \psi_1, L, F_H, F_Z, W, C_1, C_2)$$

$$v - \bar{v} = S(A_1, \psi_1, L, F_H, F_Z, W, C_1, C_2)$$

where

$$R = \frac{A_1 \cos \psi_1}{F_Z L (1 + C_1)}$$

$$S = - \frac{A_1 \sin \psi_1 - F_H L W (1 + C_2)}{F_Z L (1 + C_1)}$$

Uncertainties in the values of $A_1 \dots C_2$ result in errors in the computed velocity profile. Taking the variation of R and S gives

$$\Delta(u-\bar{u}) = \frac{\delta R}{\delta A_1} A_1 \frac{\Delta A_1}{A_1} + \frac{\delta R}{\delta \psi} \Delta \psi_1 + \frac{\delta R}{\delta L} L \frac{\Delta L}{L} + \dots$$

and a similar expression for $\Delta(v-\bar{v})$. In order to evaluate the above terms we assign mean or expected values for some of the variables:

$$u-\bar{u} = v-\bar{v} = 0.1 \text{ m/s}$$

$$W = 1.4 \text{ m/s}$$

$$F_H = \frac{1}{2} F_Z = 0.25 \text{ weber/m}^2$$

$$L = .4 \text{ m}$$

$$C_1 = 1$$

$$C_2 = 0$$

The error estimates are given in Table V-3. Several considerations should be kept in mind with regard to these estimates:

1. These errors are expected RMS errors for the bulk of the ocean depth at mid-latitudes. Some of the errors will increase in zones of high current, strong magnetic anomalies or near the geomagnetic equator.
2. The error in relative velocity profiles ($v-\bar{v}$) should be less than indicated. This is because most of the errors are systematic, producing profile errors which are independent of depth and indistinguishable from \bar{v} .

Table V-3

Error Summary

Type of variable or parameter	Estimated error or uncertainty in value	Errors in inferred velocity components	
		<u>u</u> (cm/s)	<u>v</u>
A_1	2%	.2	1.0
$\psi_1 (\alpha_1, \beta_1, \beta_c)$	1°	.6	.2
L	1%	.1	.5
F_H	3%	0	1.0
F_Z	3%	.3	.3
W	2%	0	.7
C_1	5%	.5	.5
C_2	30%	0	1.0
U	1 cm/s	.1	.1
V	1 cm/s	.1	.1
Amplifier Noise	.2 μV	.4	.4
Ambient Electric field fluctuations (.1-12 CPH)	.3 $\mu V/m$.6	.6
Higher order terms in conversion formula due to horizontal shear:			
Gulf Stream (H/L)	.1	1.0	1.0
Internal Waves (ω)	1 cm/s	.5	.5

Experimental Evidence of Accuracy and Precision

Up to this point the various known sources of error have been discussed and their influence estimated as if each error acted individually. This approach provides the information required to design the instrumentation and data analysis. The consequences of uncertainties in the knowledge of a variable or analysis parameter can be readily evaluated. However, the overall system error results from some unknown weighting over the error sources. To estimate an error value appropriate to the method in actual operation, we studied two questions:

- 1) How well does an EM profile compare with a velocity profile from another technique?
- 2) How well does one EM profile compare with itself (E1 versus E2, up versus down) or with another EMVP nearby?

The first question might be rephrased as: How well can the electric currents in the sea be related to ocean currents? The experimental evidence available is quite meager. We have taken the position that the most suitable intercomparison experiment would involve the long-period ($\omega \ll f$) shear profile measured at a few levels by Swallow floats or moored current meters or the instantaneous shear profile obtained by another velocity profiler.

Results of the intercomparison between the EMVP (first version) and velocity profiles calculated from acoustical tracking of a freely-falling probe were shown in Figure I-3. The two profiles follow each other with an RMS difference of 1.5 cm/s. The north component contains larger errors due to uncertainties in the fall speed of the EMVP. In general, the profiles from the first EMVP are less accurate than those obtained later from the all digital version.

A similar comparison was obtained in MODE-I between the present digital version and an acoustical profiler developed and used by T. E. Pochapsky. Figure V-5 shows a comparison of a profile obtained by Pochapsky simultaneously with an EMVP drop. Since the float fell much more slowly than the EMVP, a considerable time difference exists between velocity values at a given depth except near the bottom. The relative EMVP profile has been superimposed on the float profile to match in the deep water. For time differences less than 30 minutes the agreement in shear is within less than 1 cm/s. In the upper regions many of the shear features are similar, being different to the extent expected for time differences greater than an hour.

Quite a different intercomparison was achieved using Swallow floats and the EMVP during MODE-I. John Swallow tracked a number of Swallow floats placed at several depth

VELOCITY PROFILE INTERCOMPARISON

EMVP DROP 247D AND ACOUSTIC FLOAT DROP 10 DOWN

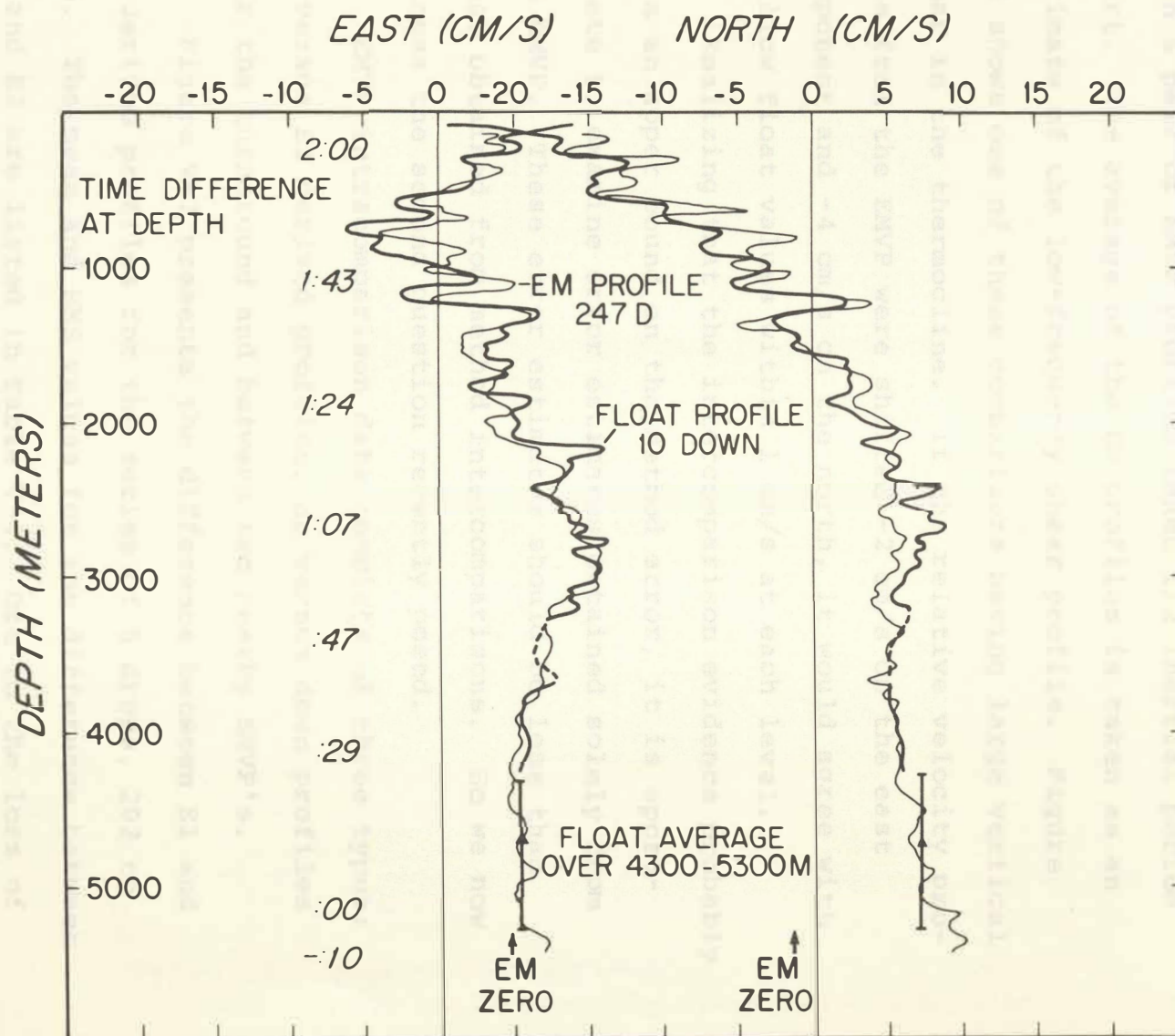


Figure V-5. Comparison of EMVP and Acoustic Float Velocity Profiles

levels. From floats within 5 km of an EMVP drop the 2- to 3-day mean velocities were computed and compared with a pair of EMVP profiles taken 1/2 inertial period apart. The average of the EM profiles is taken as an estimate of the low-frequency shear profile. Figure V-6 shows one of these comparisons having large vertical shear in the thermocline. If the relative velocity profile from the EMVP were shifted -2 cm/s on the east component and -4 cm/s on the north, it would agree with Swallow float values within 1 cm/s at each level.

Realizing that the intercomparison evidence probably sets an upper bound on the method error, it is appropriate to examine error estimates obtained solely from the EMVP. These error estimates should be less than those obtained from method intercomparisons. So we now address the second question recently posed.

EMVP intracomparison data consists of three types: E1 versus E2 derived profiles, up versus down profiles near the turnaround and between two nearby EMVP's.

Figure V-7 presents the difference between E1 and E2 derived profiles for the series of 5 drops, 202 to 206. The mean and RMS values for the difference between E1 and E2 are listed in Table V-4. Due to the loss of near-surface data, the first 500 dbar interval is not reliable and is not listed. The mean difference over

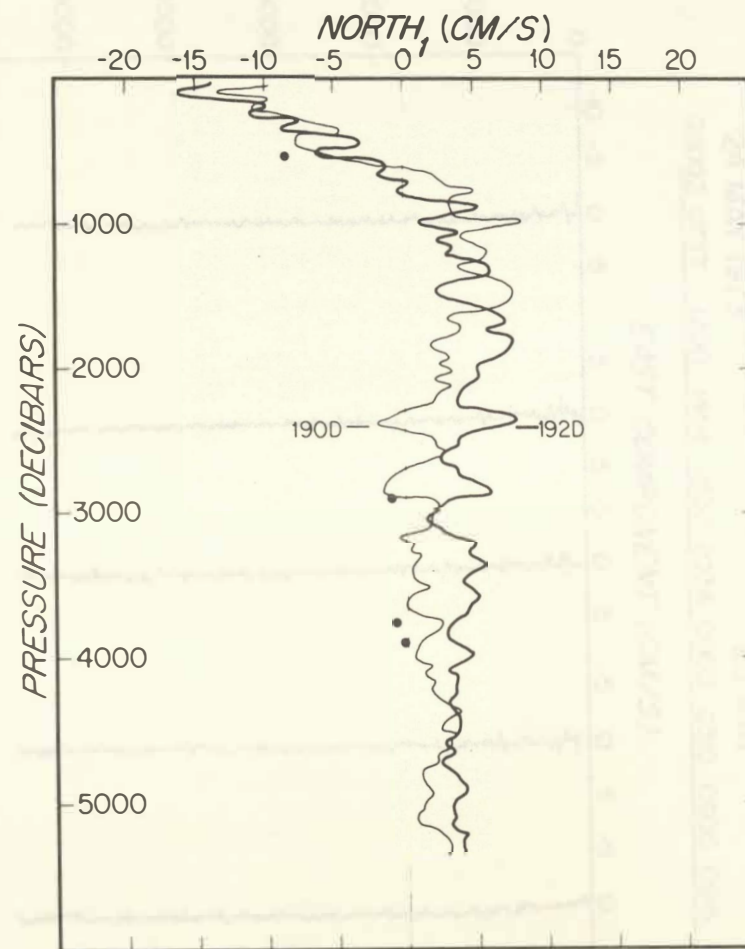
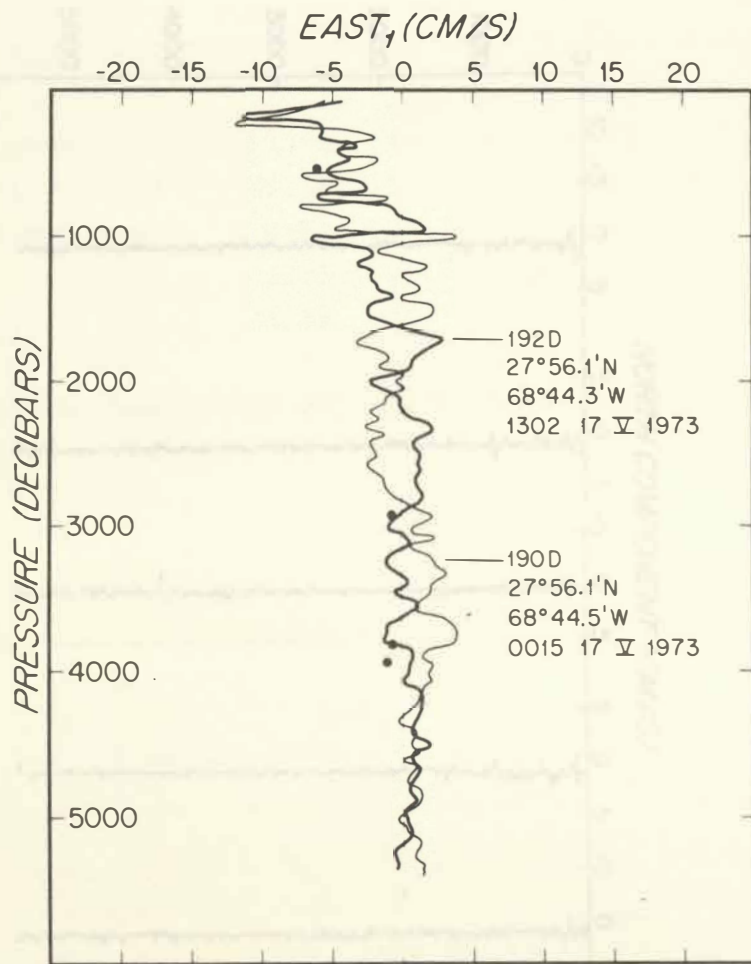


Figure V-6. Comparison of EMVP Profiles (solid) and Velocity Values at Several Depths Determined from Tracking Swallow Floats (dots)

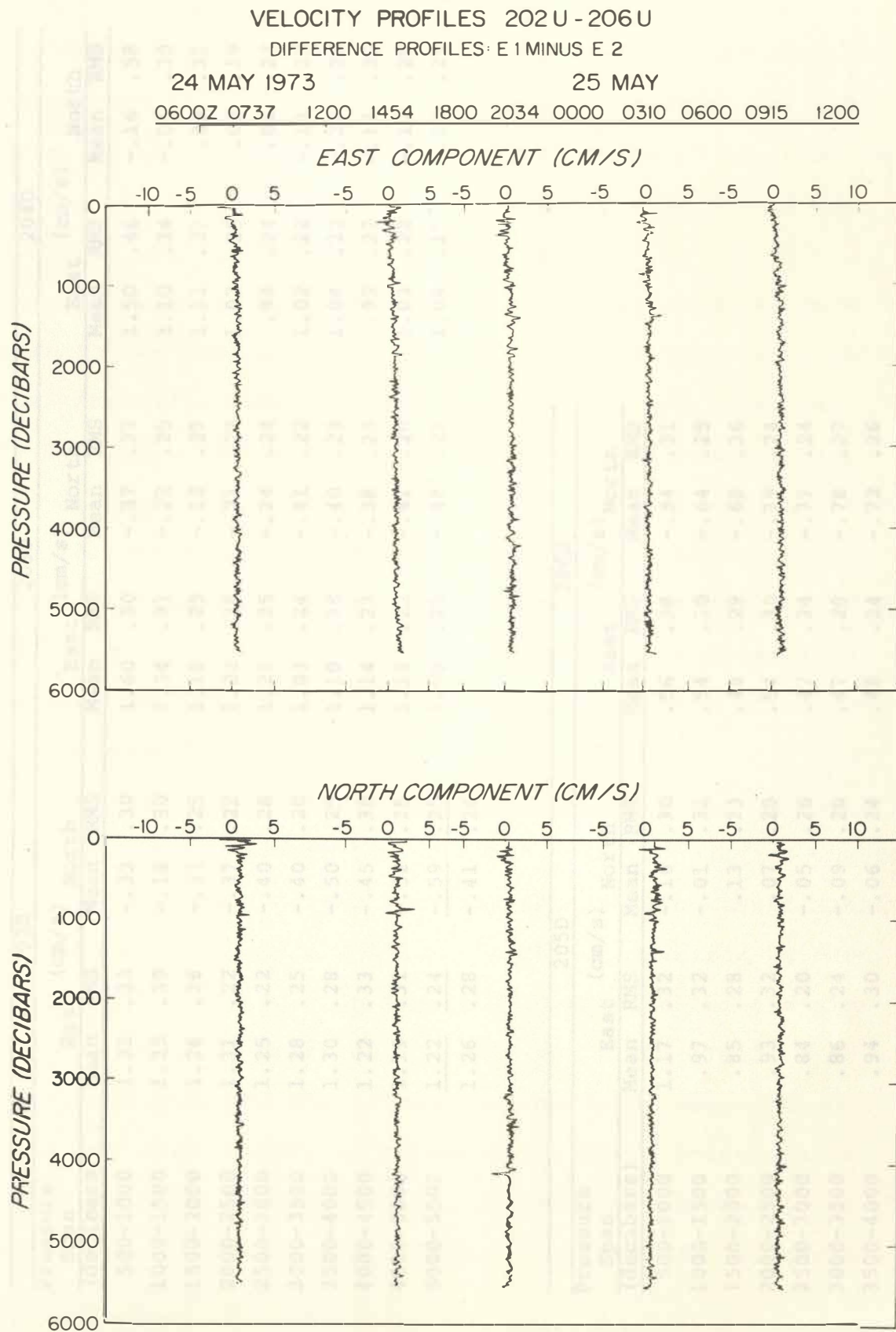


Figure V-7. Profiles of Velocity Differences between E1 and E2 Profiles

Table V-4

E1 MINUS E2 STATISTICS

Pressure Span (decibars)	202D				203D				204D			
	East (cm/s)		North		East (cm/s)		North		East (cm/s)		North	
	Mean	RMS	Mean	RMS	Mean	RMS	Mean	RMS	Mean	RMS	Mean	RMS
500-1000	1.32	.33	-.33	.30	1.60	.30	-.37	.37	1.50	.46	-.16	.58
1000-1500	1.25	.39	-.18	.30	1.34	.31	-.22	.25	1.10	.34	-.01	.30
1500-2000	1.26	.26	-.31	.25	1.18	.29	-.12	.27	1.11	.27	.08	.31
2000-2500	1.31	.22	-.37	.22	1.22	.26	-.21	.27	1.03	.25	.02	.19
2500-3000	1.25	.22	-.40	.28	1.21	.25	-.24	.24	.94	.24	.01	.23
3000-3500	1.28	.25	-.40	.20	1.03	.24	-.41	.22	1.02	.22	-.13	.23
3500-4000	1.30	.28	-.50	.25	1.19	.38	-.40	.23	1.04	.32	-.22	.26
4000-4500	1.22	.33	-.45	.30	1.14	.23	-.38	.23	.92	.27	-.13	.20
4500-5000	1.19	.31	-.52	.25	1.13	.22	-.41	.20	1.03	.22	-.17	.28
5000-5500	<u>1.22</u>	<u>.24</u>	<u>-.59</u>	<u>.25</u>	1.00	.25	-.48	.27	1.04	.15	-.22	.23
	1.26	.28	-.41	.26								

Pressure Span (decibars)	205D				206D			
	East (cm/s)		North		East (cm/s)		North	
	Mean	RMS	Mean	RMS	Mean	RMS	Mean	RMS
500-1000	1.17	.32	-.16	.30	.56	.38	-.54	.31
1000-1500	.97	.32	-.01	.32	.54	.30	-.64	.25
1500-2000	.85	.28	.13	.23	.48	.29	-.68	.36
2000-2500	.93	.32	.07	.25	.54	.30	-.79	.24
2500-3000	.84	.20	-.05	.26	.47	.24	-.77	.24
3000-3500	.86	.24	-.09	.20	.47	.29	-.78	.27
3500-4000	.94	.30	-.06	.24	.48	.24	-.72	.26
4000-4500	.84	.28	-.06	.22	.34	.32	-.75	.28
4500-5000	.81	.32	-.15	.22	.28	.21	-.76	.21
5000-5500	.88	.33	-.15	.34	.32	.24	-.71	.28

500 dbars results from errors in the knowledge of analysis parameters and is largely independent of depth. The RMS error of .2-.3 cm/s is due largely to noise in the measurement of E1 and E2 electrode voltages and errors or uncertainties arising during data analysis.

The next level of intracomparison examines the differences between up and down profiles near the bottom where the time differences between measurements are less than 30 minutes. Figure V-8 shows such a comparison for Drops 202 through 206. Table V-5 presents the mean and RMS values for the difference velocities. As would be expected, the RMS differences of .4-.5 cm/s are larger than for E1 minus E2. Also as expected, the RMS differences increase with larger time differences and become particularly large in the thermocline.

Perhaps the most severe test of the ability of the instruments to measure the inferred velocity profile occurs with a comparison of two simultaneous profiles taken nearly side-by-side. Figure V-9 shows such a comparison between Drops 213U and 214U. In Figure V-10 are plotted the difference velocity profiles for 213D and 214D. Table V-6 lists the mean and RMS values for the differences between 213D and 214D. Again as expected the RMS differences of .4-.6 cm/s are larger than the difference between E1 and E2 or between up and down profiles. The tendency for the RMS

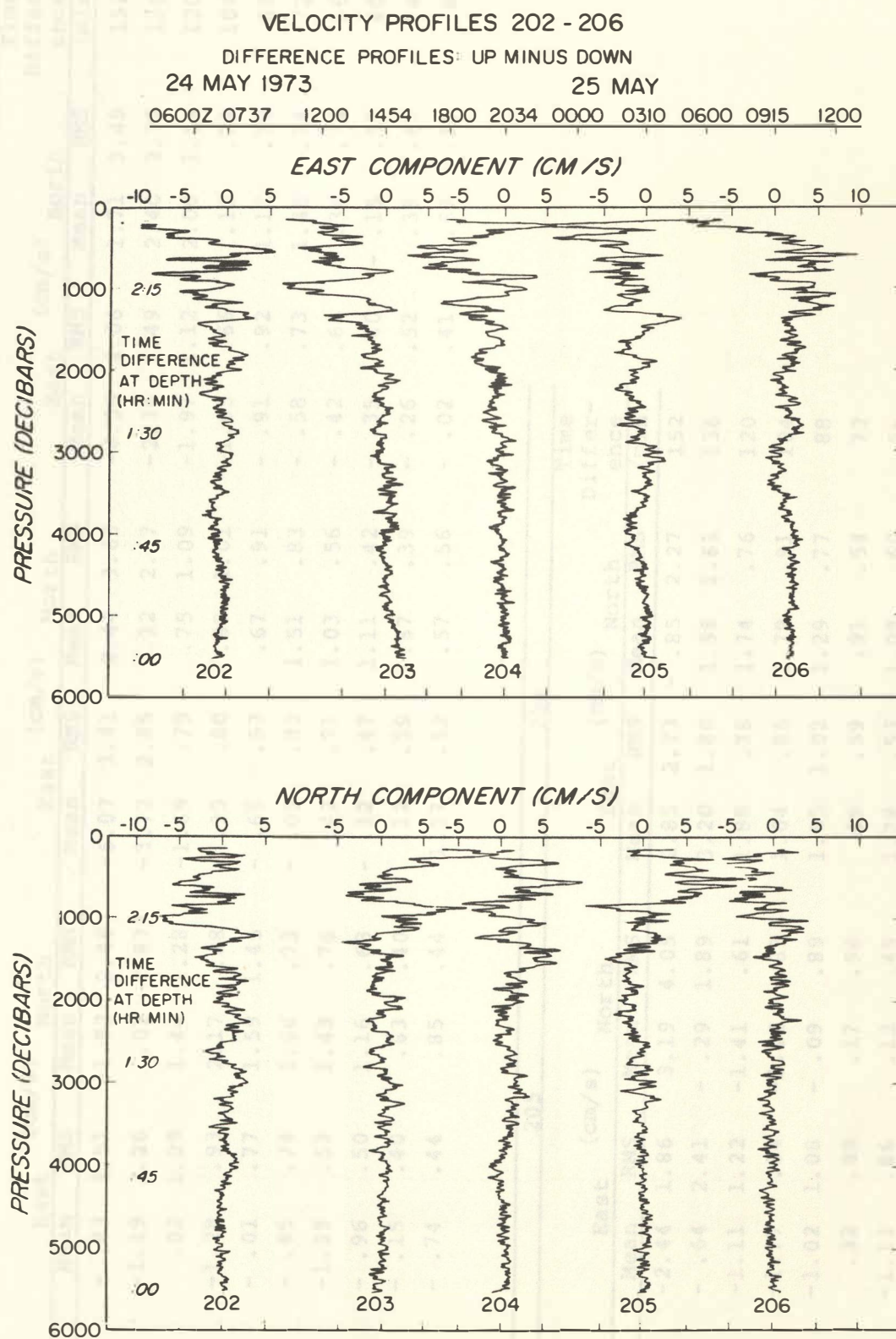


Figure V-8. Profiles of the Velocity Differences between Up and Down Profiles

Table V-5

UP MINUS DOWN STATISTICS

Pressure Span (decibars)	202				203				204				Time Differ- ence (min)
	East (cm/s)		North		East (cm/s)		North		East (cm/s)		North		
	Mean	RMS	Mean	RMS	Mean	RMS	Mean	RMS	Mean	RMS	Mean	RMS	
500-1000	- .83	3.51	-1.82	2.48	-6.07	3.41	2.44	3.63	-4.36	4.06	1.71	3.49	152
1000-1500	-1.19	2.26	.02	2.87	-3.72	2.85	1.12	2.17	-2.36	2.49	2.40	2.37	136
1500-2000	.02	1.29	1.44	1.28	-1.69	.79	.75	1.09	-1.97	1.12	2.00	1.59	120
2000-2500	-1.28	.93	2.17	.88	- .35	.80	.88	1.01	-1.05	.66	.12	.74	104
2500-3000	- .01	.77	1.59	1.45	- .65	.57	.67	.91	- .91	.92	1.17	.78	88
3000-3500	- .45	.74	1.68	.73	- .09	.82	1.51	.83	- .58	.73	1.48	.74	72
3500-4000	-1.39	.53	1.43	.76	.42	.71	1.03	.56	- .42	.64	.34	.74	56
4000-4500	- .96	.50	1.16	.63	- .12	.47	1.11	.42	- .35	.40	- .15	.52	40
4500-5000	- .15	.40	.63	.40	.12	.39	.87	.39	- .26	.52	.38	.47	24
5000-5500	- .74	.44	.85	.44	1.17	.52	.57	.56	- .02	.41	.69	.35	8

103

103

Pressure Span (decibars)	205				206				Time Differ- ence (min)
	East (cm/s)		North		East (cm/s)		North		
	Mean	RMS	Mean	RMS	Mean	RMS	Mean	RMS	
500-1000	-2.44	1.86	3.19	4.05	2.85	2.73	- .85	2.27	152
1000-1500	- .64	2.41	- .29	1.89	3.20	1.80	1.98	1.61	136
1500-2000	-1.11	1.22	-1.41	.61	1.88	.78	1.74	.76	120
2000-2500	-1.77	.84	-1.22	.83	1.04	.85	1.79	.91	104
2500-3000	-1.02	1.08	- .09	.89	1.55	1.02	1.29	.77	88
3000-3500	.32	.89	.17	.96	.09	.59	.91	.54	72
3500-4000	-1.13	.86	.12	.48	1.38	.53	1.09	.60	56
4000-4500	-1.01	.68	.26	.34	1.91	.45	.92	.54	40
4500-5000	- .20	.46	.67	.42	1.83	.37	1.06	.42	24
5000-5500	- .07	.40	.41	.49	1.61	.37	1.29	.40	8

VELOCITY PROFILES 213U & 214U

SIMULTANEOUS DROPS 100 M APART

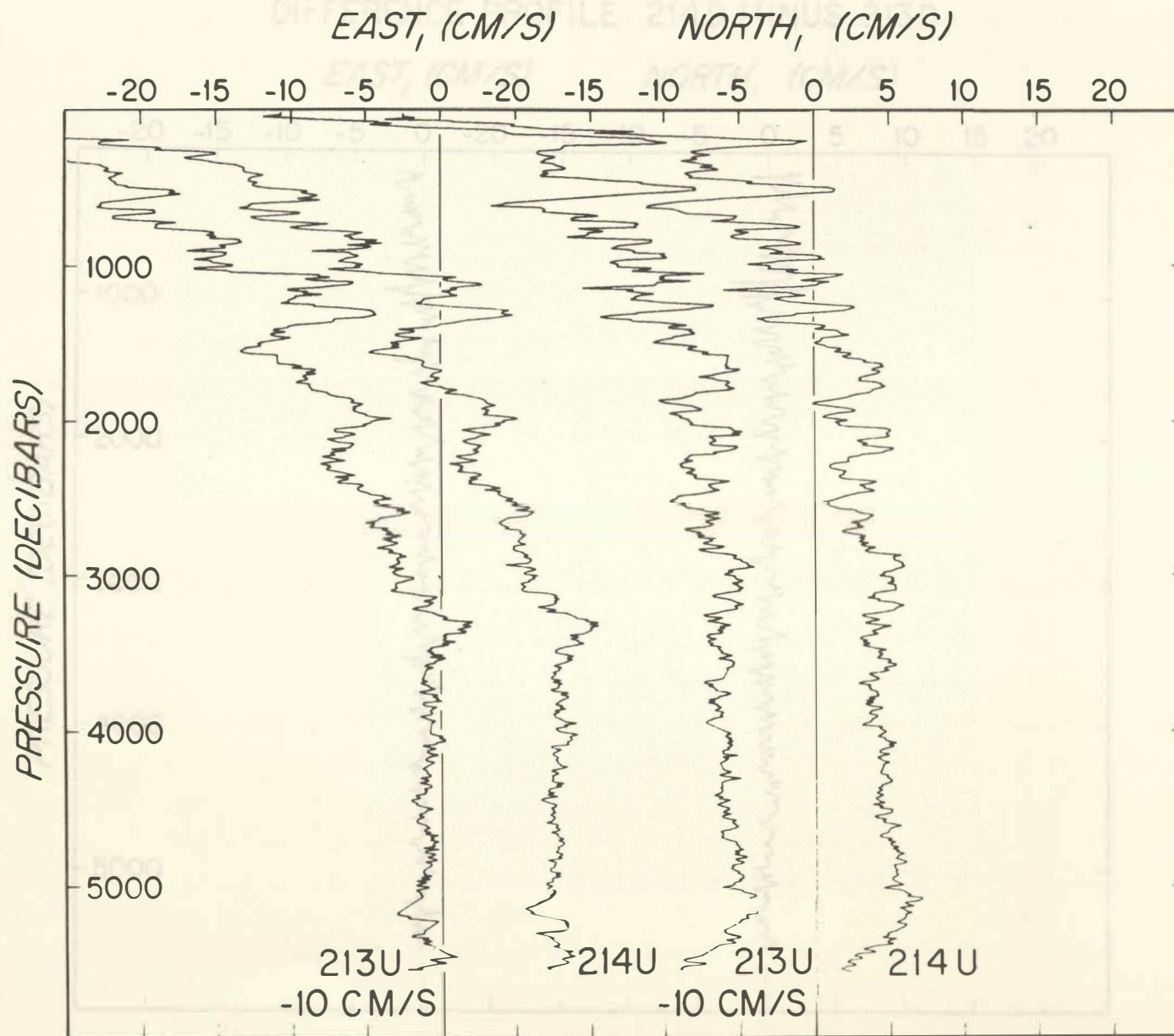


Figure V-9. Two Velocity Profiles Taken Simultaneously in Time at 100 Horizontal Separation

VELOCITY PROFILES 213D & 214D

DIFFERENCE PROFILE: 214D MINUS 213D

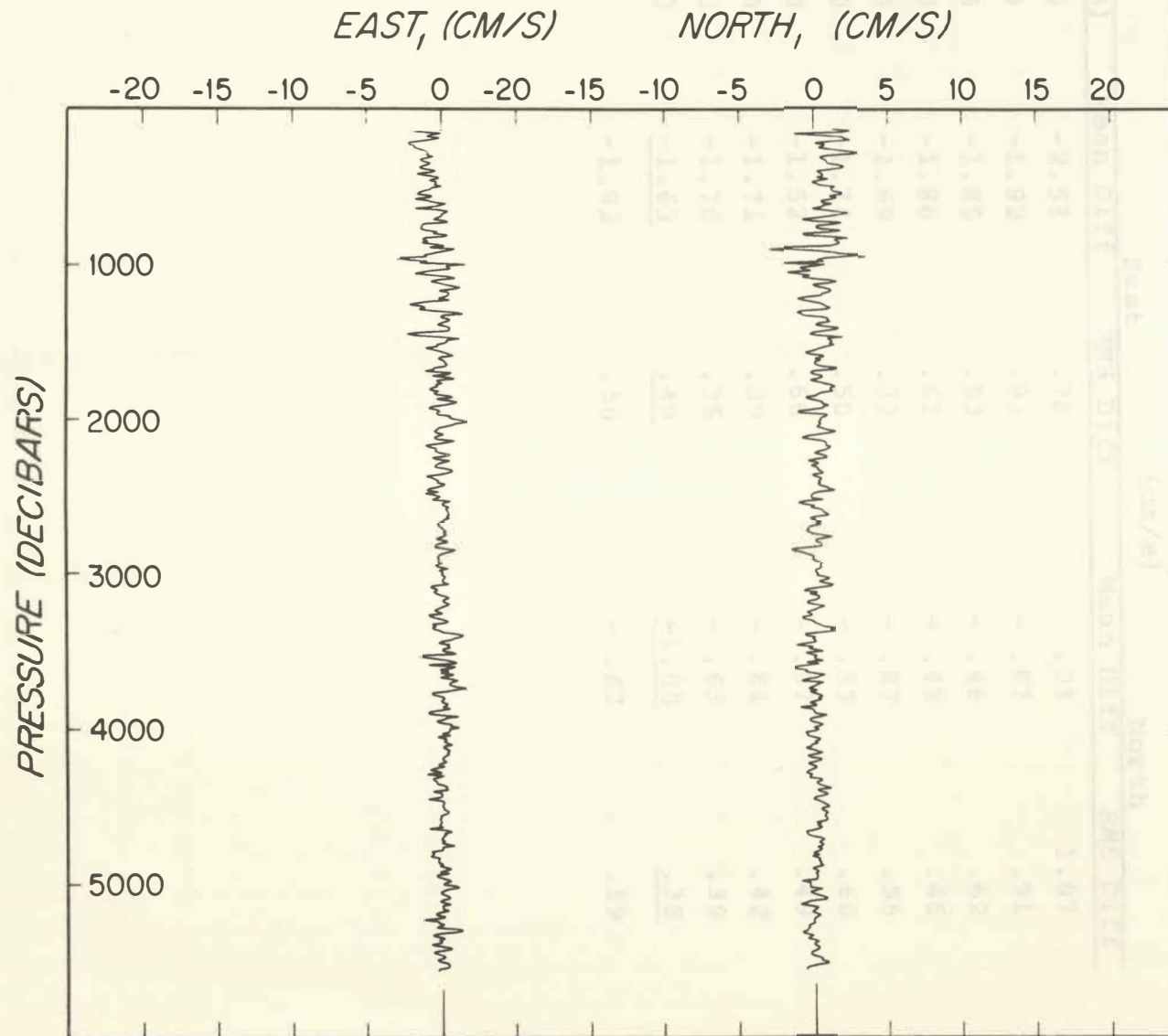


Figure V-10. Profiles of the Velocity Difference Measured between 213D and 214D

Table V-6

213D MINUS 214D STATISTICS

Pressure Span (decibars)	(cm/s)			
	East		North	
	Mean Diff	RMS Diff	Mean Diff	RMS Diff
500-1000	-2.53	.78	.03	1.07
1000-1500	-1.92	.93	-.67	.91
1500-2000	-1.85	.53	-.46	.62
2000-2500	-1.86	.61	-.48	.46
2500-3000	-1.69	.33	-.87	.55
3000-3500	-1.74	.50	-.83	.60
3500-4000	-1.52	.66	-.97	.49
4000-4500	-1.71	.39	-.84	.42
4500-5000	-1.70	.36	-.63	.39
5000-5500	<u>-1.63</u>	<u>.49</u>	<u>-1.00</u>	<u>.38</u>
Averages	-1.82	.56	-.67	.59

Figure Summary

This section has analyzed the origin and possible significance of the errors in the comparison of the two sets of data listed in Table V-1. It is pointed out that the errors are not independent, but are correlated. The errors are not random, but are systematic. Comparisons with other profiles or direct methods suggest errors of about 1 cm/s. Comparisons

differences to be larger in the thermocline is probably due to small errors in the measurement of depth between the two instruments (~ 5 -10 dbar). Since the velocity changes most rapidly with depth in the thermocline, an error in depth between measurements will lead to larger velocity differences than in the deep water. Therefore, an RMS difference of .4-.6 cm/s is taken as being typical for this comparison. The mean differences over 500 dbar intervals appear to change by about 1 cm/s from the top level to the bottom. Below 1000 dbar the mean differences change by only about .5 cm/s while the value between 500-1000 dbar is most different. It is interesting to note that the mean difference for u decreases by 1 cm/s while that for v increases by 1 cm/s. This change is suggestive of an error in the determination of current direction on one or the other of the profiles.

Error Summary

This section has evaluated the origin and possible significance of many errors affecting the performance of the method. If the errors listed in Table V-3 are considered to be acting independently, then the predicted RMS variabilities are .4 cm/s for the east and .7 cm/s for the north components. Comparisons with other profiles or float methods suggest errors of about 1 cm/s. Comparisons

between EMVP data indicate RMS errors of .4 to .7 cm/s for both velocity components. On the basis of this evidence it appears that velocity uncertainties on small scale (<500 dbar) are about $\pm .5$ cm/s. On larger vertical scales, up to the water depth, the uncertainties increase to about 1 cm/s.

The series 202 through 206 and the other data used have been processed in the routine manner. A further reduction in the mean and RMS differences might be achieved with some special handling. By varying some parameters the processing system can be manipulated to reduce some of these differences on each profile or pair of profiles. However, such special processing has not been carried out in order to obtain results typical of routine performance and analysis.

Yet it should be emphasized that this level of typical performance is not assured under all circumstances. A degradation in performance would be expected from increased electronic noise or during geomagnetic disturbances, for example. Careful attention to the performance of each element of the instrumentation and analysis method must be maintained in order to assure the present level of performance.

SECTION VI

Launch and Recovery Procedures

Prior to launch, the short electronics rack with acoustic projector attached is brought into the lab. The vehicle and major electronics remains on deck in a movable rack or carriage. The recorder is cleaned and new tape is loaded. The recorder, sealed in a rigid plastic case, is then purged with FREON to remove damp air. Usually, a freshly charged battery is installed and the internal oscillator synchronized with the master oscillator in the lab. Thumb wheel switches are set to identify the drop and instrument numbers and to determine the amount of delay until surface release and instrument shut-off. The recorder end of the vehicle is purged with FREON; then the electronics is inserted into vehicle and attached with V-channel clamp torqued to a set amount. A plug providing stand-by power can be inserted if launch is delayed. The surface release solenoid is test-fired, then plugged in with a balloon attached to the release mechanism. The radio beacon and Xenon flasher unit is installed on the forward end. The weights are made up and set aside near the launch station.

When ready to launch, the reset and stand-by power plugs are removed and replaced by open plugs. The time when the reset plug is removed is recorded. A line is looped through the projector guard, doubled with ends together. The instrument is raised, using a quick-release hook, by the projector

guard while the forward guard is lifted and guided manually. Once vertical the instrument is swung over the rail, steadied by hand, ready for attachments of weights. After the weights are attached, the instrument is lowered into the water. The surface float supports the weight and the hook is released. The behavior of the instrument is closely watched to detect any problems such as leaking and a check is made of the acoustic signals received via the shipboard hydrophone. When all appears to be ready, the looped retaining line is released and brought aboard. The ship gets underway to remove its electric field from the vicinity of the now-free instrument. The instrument is listened to using either hull-mounted hydrophones or a pair of phones on a cable put over the side. If not engaged in other work, the ship stands off several hundred meters until the surface float is released. Otherwise, the ship may pursue other tasks such as STD or hydro work until time to recover the free instrument.

While the instrument is profiling, the depth and slant range are monitored. Occasionally the horizontal range is calculated. At some point, depending on other commitments, the ship gets underway and returns to the vicinity of the launch point. Usually, the return is guided by the real-time analysis of the range information. An attempt is made to reduce the range to less than 1 km as the instrument nears

the surface. Near-surface sound refraction sometimes produces a shadow zone for a shallow hydrophone, starting several hundred meters to a kilometer from the surfaced instrument. If acoustic contact is lost at this stage using a hull-mounted hydrophone, the towed set may be deployed. Also the ship can be guided by the radio direction finder using the radio beacon signal. At night the Xenon flasher is quite effective in moderate seas.

After the bridge sights the instrument, final preparations for recovery are begun. At night a strong hand-held spotlight is directed on the instrument at all times. As the ship maneuvers for an approach into the wind (and sea), long aluminum poles supporting hooks attached to light lines are manned. As the instrument passes alongside, the poles are maneuvered so that a hook catches on one of the bars of the forward guard cage. As the pole is withdrawn, the hook remains and a safety bar is released to close the bail. The hook is now securely attached allowing the instrument to be slowly pulled alongside. The instrument can be raised by the snap hook and its line or another rig can be used now.

Once back in its carriage, the probe is washed with fresh water, the reset plug replaces the open and the solenoid and projector are unplugged. After drying the seal area, the projector end with tape recorder is removed and taken into the lab. The now-open end is capped with another end cap or plastic bag.

In the lab the magnetic tape and battery are removed. The battery is returned to the charger. The projector end is either made ready for another drop or secured in the overhaul rack for storage or repair.

Chapman, S. and Bartels, J. Geomagnetism, Vol. 1, The University Press, Oxford (1940), 342 pp.

Coat, C. S., Willcox, J. W., and Lyndon, J. C. "Electromagnetic Studies of Ocean Currents and Electrical Conductivity Below the Ocean Floor." In: A. Maxwell (Editor), The Sea, Vol. 4, Part I (1971), pp. 627-633.

Dreyer, W. G. and Sanford, T. B. "A Free-Fall Electromagnetic Current Meter-Instrumentation." In: Proceedings of the IEEE Conference on Electronics Engineering in Ocean Technology, I.E.E.E. London (1970), pp. 153-176.

Gilling, W. and Johnson, G. "High Resolution Current Profiling in the Straits of Florida." Deep-Sea Res. 19 (1972), pp. 255-274.

Ponarev, G. A. "The Effect of Ocean Vortex Currents on the Operation of the CEX Current Meter." Oceanology 8 (1968), pp. 579-586.

Malkus, W. V. R., "A Portable Bathythermograph." J. Mar. Res., 12 (1954), pp. 34-37.

Meltz, John A. "A Nine-Channel Digital Magnetic Tape Format for Storing Meteorographic Data," Ref. No. 69-55 Honda Hole Oceanographic Expedition (unpublished manuscript), 11 pp.

Mangelsdorf, V. C. "The world's Longest Salt Bridge." In: Marine Sciences Expedition, Vol. 1, Plenum Press, New York (1962), pp. 173-183.

McNary, J. E. "Determination of Current Velocity Profile Using an Inclined-tube flow," University of Miami Report ML 58371 (1960), 90 pp.

Morse, D. M. and Feshbach, H. Methods of Theoretical Physics, Vol. 1, McGraw-Hill, New York (1953), 747 pp.

References

Bowden, K. F. "The Direct Measurement of Subsurface Currents In the Oceans," Deep-Sea Res. 2, 1954, pp. 33-47.

Chapman, S. and Bartels, J. Geomagnetism, Vol. I, The University Press, Oxford (1940), 542 pp.

Cox, C. S., Filloux, J. H., and Larsen, J. C. "Electromagnetic Studies of Ocean Currents and Electrical Conductivity Below the Ocean Floor." In: A. Maxwell (Editor), The Sea, Vol. 4, Part I (1971), pp. 637-693.

Drever, R. G. and Sanford, T. B. "A Free-Fall Electromagnetic Current Meter-Instrumentation." In: Proceedings of the IEEE Conference on Electronic Engineering In Ocean Technology, I.E.R.E. London (1970), pp. 353-370.

Düing, W. and Johnson, D. "High Resolution Current Profiling In the Straits of Florida." Deep-Sea Res. 19 (1972), pp. 259-274.

Fonarev, G. A. "The Effect of Ocean Telluric Currents on the Operation of the GEK Current Meter," Oceanology 8 (1968), pp. 579-586.

Malkus, W. V. R., "A Recording Bathypitotometer," J. Mar. Res., 12 (1953), pp. 51-59.

Maltais, John A. "A Nine-Channel Digital Magnetic Tape Format for Storing Oceanographic Data," Ref. No. 69-55 Woods Hole Oceanographic Institution (unpublished manuscript), 11 pp.

Mangelsdorf, P. C. "The World's Longest Salt Bridge," In: Marine Sciences Instrumentation, Vol. 1, Plenum Press, New York (1962), pp. 173-185.

McNary, J. F. "Determination of Current Velocity Profile Using an Inclinator Line," University of Miami Report ML 68371 (1968), 90 pp.

Morse, P. M. and Feshbach, H. Methods of Theoretical Physics, Vol. I, McGraw-Hill, New York (1953), 997 pp.

Plaisted, R. O. and Richardson, W. S. "Current Fine Structure In the Florida Current," J. Mar. Res. 28 (1970), pp. 359-363.

Pochapsky, T. E. and Malone, F. D. "A Vertical Profile of Deep Horizontal Current Near Cape Lookout, North Carolina." J. Mar. Res., 30 (1972), pp. 163-167.

Richardson, W. S., Stimson, P. B. and Wilkins, C. H. "Current Measurements from Moored Buoys." Deep-Sea Res. 10 (1963), pp. 369-388.

Richardson, W. S. and Schmitz, W. J., Jr. "A Technique for the Direct Measurement of Transport with Application to the Straits of Florida," J. Mar. Res. 23 (1965), pp. 172-185.

Rossby, H. T. "A Vertical Profile of Currents Near Plantagenet Bank," Deep-Sea Res. 16 (1969), pp. 337-385.

Sanford, T. B. "Motionally Induced Electric and Magnetic Fields In the Sea." J. Geophys. Res. 76 (1971), pp. 3476-3492.

Siedler, G. and Krause, G. "Ein system zur kontinuierlichen Messung physikalischer Grossen in Meere. Kieler Meeresforschungen, 20 (1964), pp. 130-135.

Swallow, J. C. "A Neutral Buoyancy Float for Measuring Deep Currents," Deep-Sea Res. 3 (1955), pp. 74-81.

von Arx, W. S. An Introduction to Physical Oceanography, Addison-Wesley, Reading, Massachusetts (1962), 422 pp.

Young, G. A. and Kantis, A. L. "A Study of Aeomagnetic Component Data Plantagenet Bank," TR-144, U. S. Naval Oceanographic Office (1964), 18 pp.

MANDATORY DISTRIBUTION LIST
FOR UNCLASSIFIED TECHNICAL REPORTS, REPRINTS, & FINAL REPORTS
PUBLISHED BY OCEANOGRAPHIC CONTRACTORS
OF THE OCEAN SCIENCE & TECHNOLOGY DIVISION
OF THE OFFICE OF NAVAL RESEARCH
(REVISED FEBRUARY, 1974)

1	<p>Director of Defense Research and Engineering Office of the Secretary of Defense Washington, D. C. 20301 ATTN: Office, Assistant Director (Research)</p>	<p>Commander Naval Oceanographic Office Washington, D. C. 20390 ATTN: Code 1640 (Library) 1 ATTN: Code 70 1</p>
12	<p>Defense Documentation Center Cameron Station Alexandria, Virginia 22314</p> <p>Office of Naval Research Department of the Navy Arlington, Virginia 22217</p>	<p>National Oceanographic Data Center National Oceanic & Atmospheric Administration U.S. Department of Commerce 1 Rockville, Maryland 20852</p>
3	<p>ATTN: Ocean Science & Technology Division, Code 480</p>	
1	<p>ATTN: Naval Applications & Analysis Division, Code 460</p>	
1	<p>ATTN: Code 102-OS</p>	
1	<p>Office of Naval Research Branch Office 495 Summer Street Boston, Massachusetts 02210</p>	
1	<p>LCDR David Cacchione, (USN) ONR Representative Woods Hole Oceanographic Institution Woods Hole, Massachusetts 02543</p> <p>Director Naval Research Laboratory Washington, D. C. 20390</p>	
6	<p>ATTN: Library, Code 2029 (ONRL)</p>	
6	<p>ATTN: Library, Code 2620</p>	

Woods Hole Oceanographic Institution
WHOI-74-46

THE DESIGN AND PERFORMANCE OF A FREE-FALL ELECTRO-MAGNETIC VELOCITY PROFILER (EMVP) by Thomas B. Sanford, Robert G. Drever, and John H. Dunlap. 122 pages. July 1974.. Contract No. N00014-66-C0241; NR 083-004.

The principles of operation, the construction and the performance are described for a free-fall Electro-Magnetic Velocity Profiler (EMVP). The device measures and records weak electric currents produced by the motion of the sea through the geomagnetic field. The electric current measurements as a function of depth are interpreted in terms of the depth variable, horizontal velocity field. A complete velocity profile in 6000 m of water is achieved in about 1-1/2 hours with an accuracy of about 1 cm/s at a vertical resolution of 10 m. In addition to velocity, temperature, electrical conductivity and pressure are recorded once per second for a vertical resolution of about 1 m. The velocity and density data are processed at sea immediately after the drop. Real-time acoustic telemetry is used to monitor performance during a drop and to navigate the ship relative to the free instrument. The EMVP has been used extensively (171 drops) in several experiments including MODE-1.

1. EMVP
2. Velocity Profiles
3. Current Meter

- I. Sanford, Thomas B.
- II. Drever, Robert G.
- III. Dunlap, John H.
- IV. N00014-66-C0241; NR 083-004

This card is UNCLASSIFIED

Woods Hole Oceanographic Institution
WHOI-74-46

THE DESIGN AND PERFORMANCE OF A FREE-FALL ELECTRO-MAGNETIC VELOCITY PROFILER (EMVP) by Thomas B. Sanford, Robert G. Drever, and John H. Dunlap. 122 pages. July 1974. Contract No. N00014-66-C0241; NR 083-004.

The principles of operation, the construction and the performance are described for a free-fall Electro-Magnetic Velocity Profiler (EMVP). The device measures and records weak electric currents produced by the motion of the sea through the geomagnetic field. The electric current measurements as a function of depth are interpreted in terms of the depth variable, horizontal velocity field. A complete velocity profile in 6000 m of water is achieved in about 1-1/2 hours with an accuracy of about 1 cm/s at a vertical resolution of 10 m. In addition to velocity, temperature, electrical conductivity and pressure are recorded once per second for a vertical resolution of about 1 m. The velocity and density data are processed at sea immediately after the drop. Real-time acoustic telemetry is used to monitor performance during a drop and to navigate the ship relative to the free instrument. The EMVP has been used extensively (171 drops) in several experiments including MODE-1.

1. EMVP
2. Velocity Profiles
3. Current Meter

- I. Sanford, Thomas B.
- II. Drever, Robert G.
- III. Dunlap, John H.
- IV. N00014-66-C0241; NR 083-004

This card is UNCLASSIFIED

Woods Hole Oceanographic Institution
WHOI-74-46

THE DESIGN AND PERFORMANCE OF A FREE-FALL ELECTRO-MAGNETIC VELOCITY PROFILER (EMVP) by Thomas B. Sanford, Robert G. Drever, and John H. Dunlap. 122 pages. July 1974.. Contract No. N00014-66-C0241; NR 083-004.

The principles of operation, the construction and the performance are described for a free-fall Electro-Magnetic Velocity Profiler (EMVP). The device measures and records weak electric currents produced by the motion of the sea through the geomagnetic field. The electric current measurements as a function of depth are interpreted in terms of the depth variable, horizontal velocity field. A complete velocity profile in 6000 m of water is achieved in about 1-1/2 hours with an accuracy of about 1 cm/s at a vertical resolution of 10 m. In addition to velocity, temperature, electrical conductivity and pressure are recorded once per second for a vertical resolution of about 1 m. The velocity and density data are processed at sea immediately after the drop. Real-time acoustic telemetry is used to monitor performance during a drop and to navigate the ship relative to the free instrument. The EMVP has been used extensively (171 drops) in several experiments including MODE-1.

1. EMVP
2. Velocity Profiles
3. Current Meter

- I. Sanford, Thomas B.
- II. Drever, Robert G.
- III. Dunlap, John H.
- IV. N00014-66-C0241; NR 083-004

This card is UNCLASSIFIED

Woods Hole Oceanographic Institution
WHOI-74-46

THE DESIGN AND PERFORMANCE OF A FREE-FALL ELECTRO-MAGNETIC VELOCITY PROFILER (EMVP) by Thomas B. Sanford, Robert G. Drever, and John H. Dunlap. 122 pages. July 1974. Contract No. N00014-66-C0241; NR 083-004.

The principles of operation, the construction and the performance are described for a free-fall Electro-Magnetic Velocity Profiler (EMVP). The device measures and records weak electric currents produced by the motion of the sea through the geomagnetic field. The electric current measurements as a function of depth are interpreted in terms of the depth variable, horizontal velocity field. A complete velocity profile in 6000 m of water is achieved in about 1-1/2 hours with an accuracy of about 1 cm/s at a vertical resolution of 10 m. In addition to velocity, temperature, electrical conductivity and pressure are recorded once per second for a vertical resolution of about 1 m. The velocity and density data are processed at sea immediately after the drop. Real-time acoustic telemetry is used to monitor performance during a drop and to navigate the ship relative to the free instrument. The EMVP has been used extensively (171 drops) in several experiments including MODE-1.

1. EMVP
2. Velocity Profiles
3. Current Meter

- I. Sanford, Thomas B.
- II. Drever, Robert G.
- III. Dunlap, John H.
- IV. N00014-66-C0241; NR 083-004

This card is UNCLASSIFIED

UNCLASSIFIED

7/8/74

SECURITY CLASSIFICATION OF THIS PAGE (When Data Entered)

REPORT DOCUMENTATION PAGE		READ INSTRUCTIONS BEFORE COMPLETING FORM
1. REPORT NUMBER WHOI-74-46	2. GOVT ACCESSION NO.	3. RECIPIENT'S CATALOG NUMBER
4. TITLE (and Subtitle) THE DESIGN AND PERFORMANCE OF A FREE-FALL ELECTRO-MAGNETIC VELOCITY PROFILER (EMVP)		5. TYPE OF REPORT & PERIOD COVERED Technical
		6. PERFORMING ORG. REPORT NUMBER
7. AUTHOR(s) Thomas B. Sanford, Robert G. Drever, and John H. Dunlap		8. CONTRACT OR GRANT NUMBER(s) N00014-66-C0241
9. PERFORMING ORGANIZATION NAME AND ADDRESS Woods Hole Oceanographic Institution Woods Hole, MA 02543		10. PROGRAM ELEMENT, PROJECT, TASK AREA & WORK UNIT NUMBERS NR 083-004
11. CONTROLLING OFFICE NAME AND ADDRESS Office of Naval Research Code 480		12. REPORT DATE July 1974
		13. NUMBER OF PAGES 122
14. MONITORING AGENCY NAME & ADDRESS (if different from Controlling Office)		15. SECURITY CLASS. (of this report) Unclassified
		15a. DECLASSIFICATION/DOWNGRADING SCHEDULE
16. DISTRIBUTION STATEMENT (of this Report) Approved for public release; distribution unlimited.		
17. DISTRIBUTION STATEMENT (of the abstract entered in Block 20, if different from Report)		
18. SUPPLEMENTARY NOTES		
19. KEY WORDS (Continue on reverse side if necessary and identify by block number) 1. EMVP 2. Velocity Profiles 3. Current Meter		
20. ABSTRACT (Continue on reverse side if necessary and identify by block number) The principles of operation, the construction and the performance are described for a free-fall Electro-Magnetic Velocity Profiler (EMVP). The device measures and records weak electric currents produced by the motion of the sea through the geomagnetic field. The electric current measurements as a function of depth are interpreted in terms of the depth variable, horizontal velocity field. A complete velocity profile in 6000 m of water is achieved in about 1-1/2 hours with an accuracy of about 1 cm/s at a vertical resolution of		

20. cont.

10 m. In addition to velocity, temperature, electrical conductivity and pressure are recorded once per second for a vertical resolution of about 1 m. The velocity and density data are processed at sea immediately after the drop. Real-time acoustic telemetry is used to monitor performance during a drop and to navigate the ship relative to the free instrument. The EMVP has been used extensively (171 drops) in several experiments including MODE-1.